ATOMIC DATA AND NUCLEAR DATA TABLES **60,** 177–285 (1995)

NUCLEAR GROUND STATE CHARGE RADII FROM ELECTROMAGNETIC INTERACTIONS

G. FRICKE and C. BERNHARDT

Institut für Kernphysik, Universität Mainz
J.-J.-Becher-Weg 45, D-55099 Mainz, Germany

K. HEILIG

Institut für Atom- und Molekülphysik, Universität Hannover
Appelstrasse 2, D-30167 Hannover, Germany

L. A. SCHALLER and L. SCHELLENBERG

Institut de Physique, Université de Fribourg
Pérolles, CH-1700 Fribourg, Switzerland

E. B. SHERA

Los Alamos National Laboratory
Los Alamos, New Mexico 87545

and

C. W. DE JAGER

National Institute for Nuclear Physics and High Energy Physics
P.O. Box 41882, 1009 DB Amsterdam, The Netherlands

The Tables summarize experimental results from muonic atom transition energies, nuclear charge parameters from elastic electron scattering, and K x-ray isotope shifts in so far as they provide information on nuclear ground-state charge radii. Numerous experimental results for optical isotope shifts have been published elsewhere; for eight elements the relevant information is condensed ("projected") here to one optical line per element. A model-independent analysis which combines data from all three experimental methods is applied to these elements and is presented as an illustration of the improved accuracy for the rms radii and Barrett radii which result from this analysis.

0092-640X/95 $12.00

CONTENTS

INTRODUCTION

1. Preface

This compilation contains nuclear ground-state charge radii from measurements probing the nucleus with the well-understood electromagnetic interaction. Methods using strong forces to determine nuclear radii are not included. Since the previous compilations of results from

four electromagnetic methods, namely measurements of optical transitions[1] and K x rays,[2] determination of transition energies in muonic atoms,[3] and elastic electron scattering experiments,[4] a vast amount of new experimental information on the electromagnetic structure of the nuclear ground state of many isotopes has become available, and the accuracies have been improved. So it seems useful to give an up-to-date summary.

Muonic atom and electron scattering investigations require at least tens of milligrams of target material. So far only the optical method is capable of measuring unstable isotopes when only tiny amounts of material are available. Modern laser-spectroscopic techniques for optical isotope shift measurements have made it possible to reach even short-lived (down to 1 s) unstable isotopes.[5] Hence, many experimental and theoretical optical isotope shift investigations are still in progress.[6] The main goal of most of the publications today is no longer the determination of radii differences but the search for more subtle effects in the electron shells of the atom. So the time has come to make a resumé of our present knowledge on nuclear charge sizes. For this purpose, the input from muonic atom and electron scattering data is vital.

The muon factories at Los Alamos (LAMPF) and at Villigen (PSI, formerly SIN) started their operation in 1974. They delivered orders of magnitude higher muon-beam fluxes than before achieved elsewhere, yielding results for muonic x-ray transition measurements with higher precision. Therefore, systematic effects of *isotope* and *isotone* shifts could be determined. Up to now isotone shifts of high accuracy could be deduced only from muonic atoms. The precision of the nuclear charge radii deduced from muonic atoms is in most cases limited by the error in the calculation of the nuclear polarization corrections rather than by counting statistics or other uncertainties. Almost all stable isotopes have now been measured by the muonic x-ray transition technique. This provides another reason for a new nuclear ground-state charge radii compilation.

The four electromagnetic methods are sensitive to different properties of the nuclear ground-state charge distributions. The optical transitions and the K x rays are sensitive to the differences of the mean-square charge radii $\delta\langle r^2\rangle$ between isotopes, with small contributions from higher radial moments $\delta\langle r^4\rangle$ and $\delta\langle r^6\rangle$. The radial moments are defined by

$$\langle K(r)\rangle = \frac{1}{Ze}\int \rho_N(r)K(r)\,d\tau. \tag{1.1}$$

Specifically,

$$\langle r^2\rangle = \frac{1}{Ze}\int \rho_N(r)r^2\,d\tau \tag{1.2}$$

and

$$\langle r^n\rangle = \frac{1}{Ze}\int \rho_N(r)r^n\,d\tau, \tag{1.3}$$

where $\rho_N(r)$ is the nuclear charge density distribution and $\int \rho_N(r)d\tau = Ze$.

The transition energies in muonic atoms are sensitive to the Barrett equivalent radius[7] $R_{k\alpha}$, with

$$K(r) = r^k e^{-\alpha r}. \tag{1.4}$$

(Throughout this paper $R_{k\alpha}$ always denotes the Barrett equivalent radius.) On the other hand, the charge distribution $\rho_N(r)$ can be deduced from elastic electron scattering cross sections. A combination of the data from different experimental methods generally yields more detailed and accurate knowledge of the nuclear radii than is available from any single method. Because of the different quantities determined by each method, one has to be careful that no model-dependent bias is introduced when the data are combined. However, in the following it will be shown that with the help of a combined analysis of elastic electron scattering data, muonic transition energies, and optical and K x-ray measurements, nearly model-independent values for the root-mean-square (rms) charge radii of stable nuclei and at least the λ values (see Eq. (2.7)) for the chains of unstable isotopes can be deduced with high precision.

In addition, two important factors for optical transitions between different electronic states can be evaluated by such a combined analysis, namely the change of the electron density at the nucleus, represented by F_i, and the mass shift, described by the factor M_i (see Section 2). The factors F_i and M_i can thus be determined from experimental data, making it possible to derive $\delta\langle r^2\rangle$ without any knowledge of the electron shell properties. Moreover, the factor F_i is a valuable experimental input for the testing of calculations of electronic wave functions.

In the next four sections a short survey of the four different electromagnetic techniques for the determination of nuclear charge radii is given. The information contained in the measured quantities is discussed and the particular advantages of each method are emphasized. The general ideas and the procedure of a combined model-independent analysis and the results are discussed in the concluding Section 6.

2. Optical Spectroscopy

Outer atomic electrons may serve as a probe of the nuclear structure. The isotope shift (IS) of optical transitions is observed as a small energy shift of the centers of gravity of the spectral components of different isotopes in optical transitions. It is well known[1,8,9] that the IS has two causes. These are distinct isotope-dependent nuclear properties that interact with the electrons of the shells, the nonzero nuclear size and the finite nuclear mass, giving rise, respectively, to the field (or volume) shift (FS) and the mass shift (MS). The observed shift $\delta\nu_i^{AA'}$ between two

isotopes with mass numbers A and A' in an atomic spectral line i of wavenumber or frequency ν is the sum of FS and MS; i.e.,

$$\delta\nu_i^{AA'} = \delta\nu_{i,\mathrm{FS}}^{AA'} + \delta\nu_{i,\mathrm{MS}}^{AA'}. \tag{2.1}$$

It is customary to split the observed mass shift into two contributions, the trivial normal mass shift (NMS; reduced mass) and the very difficult to calculate specific mass shift (SMS; correlations between electrons):

$$\delta\nu_{i,\mathrm{MS}}^{AA'} = \delta\nu_{i,\mathrm{NMS}}^{AA'} + \delta\nu_{i,\mathrm{SMS}}^{AA'}. \tag{2.2}$$

These shifts depend in the same way on the atomic masses A and A',

$$\delta\nu_{i,\mathrm{MS}}^{AA'} = M_i \frac{A - A'}{AA'}, \tag{2.3}$$

$$\delta\nu_{i,\mathrm{NMS}}^{AA'} = \frac{\nu_i}{1822.9} \frac{A - A'}{AA'}, \tag{2.4}$$

where the factor M_i is the mass shift factor containing contributions of NMS and SMS.[8,9] The NMS always shifts the heavier isotopes toward larger energies (or wavenumbers). By convention this is called a positive IS in the line. Thus, the MS decreases with increasing A, and the relative MSs for isotopes A, $A^* = A + 2$, and $A^{**} = A + 4$ are related through

$$\delta\nu_{i,\mathrm{MS}}^{AA^*} : \delta\nu_{i,\mathrm{MS}}^{A^*A^{**}} = A^{**} : A. \tag{2.5}$$

Good theoretical calculations of the SMS exist only for a few elements, for example, for Ca.[10] In all other cases rather rough estimates (for example, by comparison with results in light elements) have to be used for the SMS,[8] if no information from other than optical investigations is available.

The FS reflects the isotopic variation of the mean-square nuclear charge radius $\delta\langle r^2\rangle$. Traditionally the FS in a transition i is written as

$$\delta\nu_{i,\mathrm{FS}}^{AA'} = F_i \lambda^{AA'}, \tag{2.6}$$

where

$$\lambda^{AA'} = \delta\langle r^2\rangle^{AA'} + (C_2/C_1)\delta\langle r^4\rangle^{AA'} + (C_3/C_1)\delta\langle r^6\rangle^{AA'} + \cdots, \tag{2.7}$$

with the convention that $\delta\langle r^2\rangle^{AA'} = \langle r^2\rangle^{A} - \langle r^2\rangle^{A'}$. This parameterization was introduced in 1965 by Seltzer; the C coefficients were tabulated in Refs. 2 and 11, and corrections were added in Ref. 12 (for further explanations see also Refs. 1, 9, and 13). F_i is the electronic factor, which is proportional to the change of the electronic charge density at the nucleus in the transition i under investigation. The FS percentage is largest in transitions that involve s electrons. In order to determine $\lambda^{AA'}$ from the FS, the electronic factor F_i has to be known. Different procedures have been used so far for its determination, as discussed below.

(i) Semiempirical methods (Goudsmit–Fermi–Segrè; see, for example, Refs. 1, 8, and 9). For alkali-like ns–np transitions the following expressions hold:

$$F_i = E_i f(Z), \quad E_i = \beta E_{ns}, \quad E_{ns} = \pi a_0^3 |\psi(0)|^2_{ns}/Z, \quad \beta = \frac{\Delta|\psi(0)|^2_{ns-np}}{|\psi(0)|^2_{ns}}. \tag{2.8}$$

In these expressions, $f(Z)$ is the correction factor for the finite size of the nucleus and for relativistic effects,[14–16] β is a screening factor caused by the screening of lower, closed shells,[1] a_0 is the Bohr radius, and $\Delta|\psi(0)|^2_{ns-np}$ is the nonrelativistic change of the electron charge density in an ns–np transition at the nucleus. The probability density $|\psi(0)|^2_{ns}$ is calculated either from the fine structure (ns series) or from the hyperfine structure (a_s factor). Similar procedures are in principle possible with other kinds of transitions.[1]

(ii) *Ab initio* calculations made with self-consistent-field procedures. For many elements calculations with a multiconfigurational Dirac–Fock method have been done or are in progress.[17,18]

(iii) A rather new procedure utilized in the present paper, wherein only measured values enter into the determination of F_i and M_i. No information is needed about $\Delta|\psi(0)|^2$, the purity of configurations, or mass shifts. The procedure makes use of a special King plot, in which the so-called *scaled* IS (see Appendix A) of a selected optimal line is plotted versus the scaled λ values for the same isotope pairs. The λ values are evaluated in a combined analysis of muonic atoms and elastic electron scattering data (see Section 6).

From Eq. (2.3) it follows that the relative mass shifts for a chain of isotopes are exactly the same in all optical lines. The relative field shifts—differing from the mass shift ratios—are also the same in all lines; see Eq. (2.6). The ratio of mass shift to field shift varies—often strongly—from line to line. These correlations are used to connect the measurements in different lines.

To explain the procedure, let us assume as a very simple case that three isotope pairs have been investigated in two optical lines. The evaluation will be done by a (two-dimensional) King plot (see Appendix A). The proper projection onto the regression line in this plot gives improved IS values for each of both lines. Naturally, it would be even more reliable to use many more lines for this procedure. The result is a so-called multidimensional King plot[19] (variance–covariance matrix). Any of the lines in that plot may in principle be taken as the line to be projected. For the projection, the desired characteristic in the selected line is that the observed relative total ISs differ as much as possible from the relative MSs (Eq. (2.3)) and that the accuracy of the measurements is adequate.

Electrons with nonzero orbital angular momentum have a very small or negligible charge density at the nucleus. Nevertheless, due to screening factors similar to β, large FSs may also occur in some non s–p transitions. Furthermore, in alkali-like electronic transitions the $s_{1/2}$–$p_{1/2}$ FS is often nearly the same as the $s_{1/2}$–$p_{3/2}$ FS. The MS happens to be also the same for both $p_{1/2}$ and $p_{3/2}$ electrons.[20]

A number of elements were selected to illustrate the procedure of the combined analysis (Section 6). The corrected shifts for the projected lines of these elements are given in Table I. They are used together with the combined results from elastic electron scattering and muonic x rays to evaluate the optical factors F_i and M_i by a special King plot. By means of ordinary (two dimensional) King plots, the F_i and M_i values for all other investigated optical lines can then be determined easily. This will be explained in detail in the next sections. For optical IS measurements no nuclear polarization corrections[21] have been applied. Why this might be permitted is explained in Appendix A.

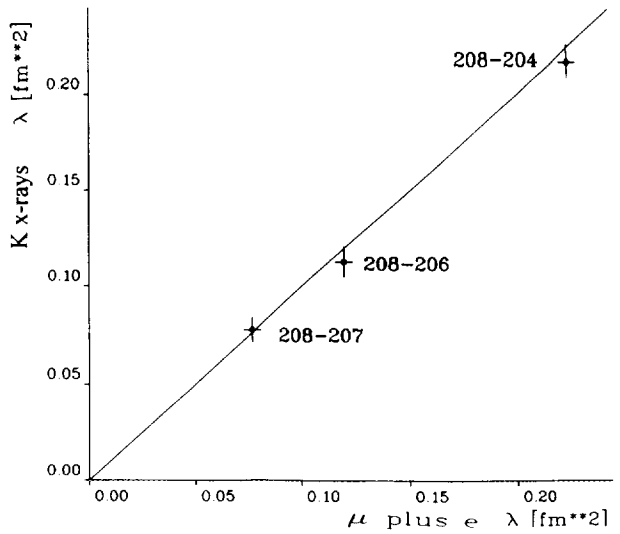

Figure 1. Values of $\lambda^{AA'}$ (in fm^2) from K x rays versus those from the combined results of muonic x-ray spectroscopy and elastic electron scattering for the stable Pb isotopes. Numbers beside the data points refer to isotope pairs. The 45° line is added for convenience.

3. *K* X-Ray Spectroscopy

The isotope shift of K x-ray transitions has the same two origins as the IS in optical transitions: field effect and mass effect. In contrast to optical shift effects from outer electrons, the calculation of the electronic factors F_i and M_i is much easier and more reliable for the inner-shell x-ray transitions (see Refs. 2 and 22).

The difficulties of x-ray isotope shift measurements lie in experimental restrictions: no x-ray interferometers and no tunable, narrowband x-ray lasers exist hitherto. The measurements thus have had to be performed with curved crystal spectrometers. Therefore, the relative experimental errors range from a few to about 50%. In modern optical laser-spectroscopic measurements, on the other hand, the errors are in most cases smaller by at least one order of magnitude.

The nuclear parameter $\lambda^{AA'}$ (Eq. (2.7)) can be determined analogously as in optical spectroscopy: Eqs. (2.1) to (2.7) also hold for K x-ray isotope shifts. Most of the experimental results date back to before 1974. They are listed in Ref. 2 and are included in Table II together with the only measurement since 1974, the shift of the Pb isotopes.[23] This new measurement together with the data from Lee and Boehm[24] yields absolute and accurate values for the radii differences of the Pb isotopes, which can be compared with the combined results from muonic x rays and elastic electron scattering (see Fig. 1). Here the $\lambda^{AA'}$ values derived from the three experimental methods are plotted; a diagonal line at 45° is added for convenience. The excellent agreement of these results shows the reliability for each of the three independent methods and suggests the reliability of the combined analysis of optical, muonic x-ray, and electron scattering data (see Section 6) for absolute calibration of optical isotope shift measurements from experimental data only, without model assumptions. Details will be given in the next sections.

4. Muonic Atom Spectroscopy

A compilation entitled "Charge-Distribution Parameters, Isotope Shifts, Isomer Shifts, and Magnetic Hyperfine Constants from Muonic Atoms," by Engfer et al.,[3] appeared in 1974 in ATOMIC DATA AND NUCLEAR DATA TABLES. Subsequent to that date the muon factories LAMPF and PSI came into operation and delivered muon beams with much higher intensities. As a result, a wealth of new and more precise data has been obtained. The investigation of almost all stable isotopes became possible. From the muonic $2p$–$1s$ transition energies given in Ref. 25, nuclear charge radii are deduced in the present work. The accuracy of almost all but the lightest nuclear radii is limited no longer by the experimental error but by the uncertainty of the calculated nuclear polarization correction.

The procedure for deducing a nuclear charge radius from the measured transition energies has been described in detail in the above referenced summary.[3] Hence, only a short description for such an analysis is given in the following.

The transition energies in muonic atoms are strongly affected by the size of the nucleus. In first-order perturbation theory the energy shift of a muonic transition between levels i and f due to this "finite size" effect is given by[3]

$$\delta E_{if} = 4\pi \int_0^\infty \delta\rho_N(r)[V_\mu^i(r) - V_\mu^f(r)]r^2 dr. \quad (4.1)$$

Here $V_\mu^i(r)$ and $V_\mu^f(r)$ are the potentials generated by the bound muon in the states i and f, respectively, and $\delta\rho_N(r)$ denotes a variation of the spherical charge distribution of the nucleus.

In the region where $\rho_N(r)r^2$ is large, the difference $V_\mu^i - V_\mu^f$ can be approximated well by the analytic expression $Br^k e^{-\alpha r}$, as has been suggested by Barrett.[7] Thus, perturbation theory implies that a Barrett moment

$$\langle r^k e^{-\alpha r}\rangle = \frac{4\pi}{Ze}\int_0^\infty \rho_N(r) r^k e^{-\alpha r} r^2 dr \quad (4.2)$$

may be deduced model-independently from the experimental transition energy E_{if}. With this moment an equivalent radius $R_{k\alpha}$, which has a dimension of a length, can be defined by the implicit equation

$$3[R_{k\alpha}]^{-3}\int_0^{R_{k\alpha}} r^k e^{-\alpha r} r^2 dr = \langle r^k e^{-\alpha r}\rangle. \quad (4.3)$$

$R_{k\alpha}$ is thus the radius of a sphere with constant charge density which yields the same moment $\langle r^k e^{-\alpha r}\rangle$ as the actual nuclear charge distribution. Throughout this compilation, $R_{k\alpha}$ always denotes the Barrett equivalent radius and $R_{k\alpha}^\mu$ the one deduced from the muonic atom $2p$–$1s$ transitions.

For an exact analysis, the eigenvalues of the Dirac equation with an analytic parametrization of $\rho_N(r)$ are determined numerically by fitting the free parameters of the charge distribution used to the experimental transition energies. As usual, for spherical nuclei the two-parameter Fermi charge distribution (Fermi II) was used,

$$\rho_N(r) = \rho_0(1 + \exp[(r - c)/a])^{-1}, \quad (4.4)$$

where c is the half-density radius. The surface thickness t of the distribution is

$$t = 4a \ln 3 = 4.394a. \quad (4.5)$$

For deformed nuclei the half-density radius is written as

$$c = R_0[1 + \beta_2 Y_{20}(\theta, \phi)]. \quad (4.6)$$

Here, $\beta_2 Y_{20}$ gives the angular variation of c, β_2 is the quadrupole deformation parameter, and R_0 is the monopole radius. From the fitted charge distributions, a mean-square charge radius is calculated using Eq. (1.2).

In the next step the parameters B, k, and α of the Barrett moment were fitted to reproduce the muon potential difference $V_\mu^i(r) - V_\mu^f(r)$ (see Eq. (4.1)). To optimize the model independence, this was done separately for every transition to every numerically calculated muon potential difference. Then the Barrett moments $\langle r^k e^{-\alpha r}\rangle$ and the corresponding equivalent radii $R_{k\alpha}^\mu$ were calculated from $\rho_N(r)$.

The degree of model independence of the $R_{k\alpha}^\mu$ compared to the rms radii is illustrated with ^{40}Ca and ^{208}Pb in Fig. 2 using a two-parameter Fermi distribution for $\rho_N(r)$. By adjusting the half-density radius c to the measured transition energy with a given surface parameter, a change in the assumed surface thickness from t = 1.8 fm to t = 2.8 fm results in a change in the rms radius of 20 am (1 am = 10^{-18} m) for ^{40}Ca and 50 am for ^{208}Pb, whereas the corresponding change in the Barrett radius $R_{k\alpha}^\mu$ amounts to an impressively small value[26] of just 0.2 am for ^{208}Pb. This shows the model independence of $R_{k\alpha}^\mu$, since the nuclear polarization uncertainty or the experimental error is always larger than 0.2 am, as can easily be verified with the help of the factor C_z (see Tables IIIA and IIIC): C_z converts a small change in the transition energy into a small change of the $R_{k\alpha}^\mu$ radius.

Table IIIA presents results for $Z < 60$ and $Z > 77$, namely the experimental $2p$–$1s$ energies, the fitted energies, the nuclear polarization correction, the adjusted half-density radius c, the model-dependent rms radius, the Barrett parameters α and k, the factor C_z, and finally $R_{k\alpha}^\mu$. The error given for the $2p$–$1s$ energies is statistical

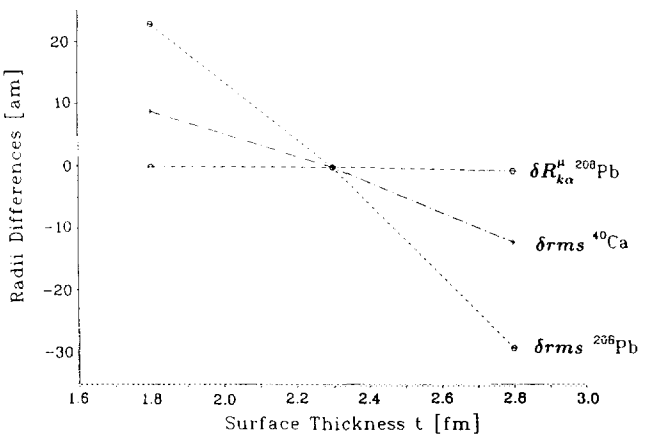

Figure 2. Illustration of the model independence of the Barrett radii $R_{k\alpha}^\mu$ compared to the model-dependent rms radii. Plotted is $\delta R_{k\alpha}^\mu(t) = R_{k\alpha}^\mu(t = 2.3\text{ fm}) - R_{k\alpha}^\mu(t)$ for ^{208}Pb and $\delta\text{rms}(t) = \text{rms}(t = 2.3\text{ fm}) - \text{rms}(t)$ for ^{40}Ca and ^{208}Pb, where t is the surface thickness of a two-parameter Fermi charge distribution (Eq. (4.4)). The variation of $R_{k\alpha}^\mu$ between t = 1.8 fm and t = 2.8 fm for Pb is less than 0.2 am (1 am = 10^{-18} m), whereas the model-dependent rms radius decreases by 50 am.

only and is computed using a weighted least-squares adjustment procedure which includes all elements from oxygen to samarium.[25] The χ^2 value per degree of freedom of this adjustment was 1.93. No systematic error like the nonlinearity in the electronics is included. The first error on the $R^{\mu}_{k\alpha}$ is obtained by multiplying the statistical error of the $2p$–$1s$ energies by the sensitivity factors $C_z = dR^{\mu}_{k\alpha}/dE$. The second error is due to the uncertainty in the calculation of the nuclear polarization corrections. This error was conservatively estimated by Rinker[27] to be 30% of the total nuclear polarization value. The nuclear data for the calculation of the nuclear polarization corrections (excitation energies and $B(E2)$ values) are taken from the latest Nuclear Data Sheets. The rms radii $\langle r^2\rangle^{1/2}_{\text{model}}$ (no error assigned) given in Tables IIIA and IIIC have the suffix "model" to point out that this value is based on the Fermi two-parameter charge distribution and is model-dependent as can be seen from Fig. 2. Nevertheless, a reasonable systematic error for the $\langle r^2\rangle^{1/2}_{\text{model}}$ values, which are calculated with the skin thickness $t = 2.3$ fm, may be obtained from this figure by varying the skin thickness parameter by ±10%. This is supported by a direct comparison of the rms values in Tables III and XII. Note that the relative statistical error of the $\langle r^2\rangle^{1/2}_{\text{model}}$ values is the same as that of the $R^{\mu}_{k\alpha}$ values from Tables III.

For deformed nuclei with $60 \leq Z \leq 77$ (see Table IIIB), in addition to the static quadrupole interaction, there is a strong dynamic $E2$ interaction between nuclear and muonic levels also for even–even nuclei.[3,28] For odd nuclei, the observed spectra can become rather complex. As an example, the observed splitting in the ^{181}Ta $2p$–$1s$ transition into more than 30 components[29] is shown in Fig. 3. The literature contains further fitted parameters like quadrupole deformation and so forth. All components could be fitted remarkably well with a χ^2 per degree of freedom of 1.2. In Table IIIB, up to 10 (20) of the strongest components for the $2p_{3/2}$–$1s_{1/2}$ and $2p_{1/2}$–$1s_{1/2}$ complex are listed for even (odd) deformed nuclei. Table IIIC shows, besides the nuclear polarization values for the center of gravity of the hyperfine components, the model parameters of the deformed Fermi-type charge density distribution and the fitted Barrett parameters. More details are found in the references.

Table IV contains in matrix form the energy differences between isotopes for the two $2p$–$1s$ transitions together with the experimental errors. For the small energy shifts between neighboring isotopes (≈20 keV) or isotones (≈200 keV), no energy calibration error is expected; so, the experimental error is determined mainly by statistics and to a minor part by the subtraction of the background of the spectrum. The related differences for the Barrett radii $\Delta R^{\mu}_{k\alpha}$ are given in Table V. There, the second error is the nuclear polarization uncertainty. As an upper limit, this error was estimated to be 10% of the larger of the

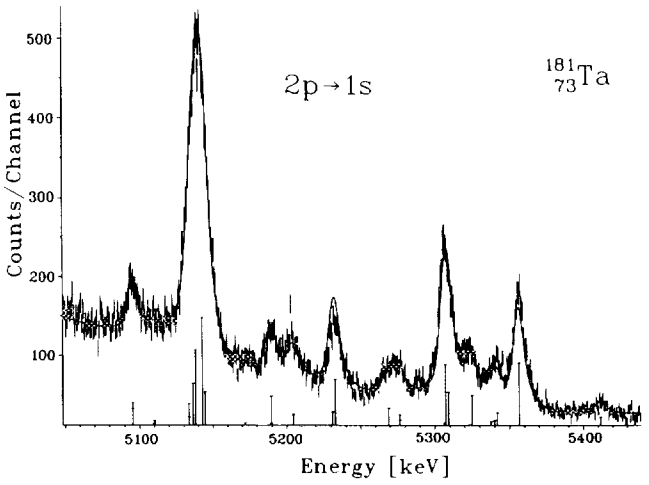

Figure 3. Energy spectrum in the region of the $2p$–$1s$ muonic atom transition complex for ^{181}Ta shown with the calculated components of the fitted curve (solid line). The fit gives $\chi^2 = 1.2$ per degree of freedom. The dynamic hyperfine interaction results in more than 30 components.

nuclear polarization values for the two isotopes. For deformed nuclei, ½ of the larger error of the two isotopes—as assigned to the absolute values of $R^{\mu}_{k\alpha}$—is given. Tables VI and VII give the corresponding data for isotones.

All $\Delta R^{\mu}_{k\alpha}$ values for even–even isotope pairs with $\Delta N = 2$ are displayed in Figs. 4a–4c. The $\Delta R^{\mu}_{k\alpha}$ values for even–even isotone pairs with $\Delta Z = 2$ are shown in Figs. 5a and 5b. So far only muonic atoms can measure shifts accurately enough to show that the systematic behavior is similar for isotopes and isotones. There are strong shell effects: the differences in radii are largest at the beginning of a neutron or proton shell and decrease almost linearly from there. Toward the end of a shell the values may become constant (see, for example, Fig. 4c for isotopes and Fig. 5b for isotones). Exceptions to the linear behavior are the s–d shell and the europium region, where the behavior is modified by strong deformation changes of the nuclei.[29,30] A more detailed discussion of the systematics of the radii differences can be found in Refs. 30–32. Since the Barrett parameters k and α are fitted for each nucleus separately, different radial moments are compared. The model error introduced hereby has been evaluated by Bernhardt.[29] It is less than 0.2 am for isotopes ($\Delta N = 2$) and less than 1.0 am for isotones ($\Delta Z = 2$). For a detailed error discussion, see the relevant literature.

In spite of all these corrections, the total error in the Barrett radius $R^{\mu}_{k\alpha}$ deduced from muonic atoms is much smaller than the error of the same quantity calculated from the charge distribution resulting from an elec-

tron scattering experiment. At present the finite size shift of muonic atom transitions is the most precise method for determining absolute nuclear radial moments.

5. Elastic Electron Scattering Measurements

In elastic electron scattering experiments the measured quantity is the differential cross section $d\sigma(E, \theta)/d\Omega$ for the elastic scattering of an electron of energy E through an angle θ.

Although a careful analysis of the experimental cross sections must be performed with a phase shift code,[33] the information contained in the cross section data can be discussed in the framework of the first Born approximation.[34] In the case of a nucleus with spin $I = 0$, where only spherical charge scattering contributes to the elastic cross section, $d\sigma/d\Omega$ can be factorized into $(d\sigma/d\Omega)_{\text{Mott}}$ for a point-like nucleus and a structure function, the form factor $F(q)$, which depends only on the momentum transfer $q = (2E/\hbar c) \cdot \sin(\theta/2)$, under the condition $m_e c^2 \ll E$:

$$\left.\frac{d\sigma}{d\Omega}\right|_{\text{exp}} = \left.\frac{d\sigma}{d\Omega}\right|_{\text{Mott}} |F(q)|^2,$$

$$\text{with } \left.\frac{d\sigma}{d\Omega}\right|_{\text{Mott}} = \frac{Z^2 e^4}{4E^2} \frac{\cos^2\theta/2}{\sin^4\theta/2}. \quad (5.1)$$

The form factor $F(q)$ is related to the nuclear charge distribution $\rho_N(r)$ through a Fourier–Bessel transformation:

$$F(q) = \int \rho_N(r) j_0(qr) d\tau, \quad 0 < q < \infty. \quad (5.2)$$

The model-independent Fourier–Bessel analysis, introduced by Dreher et al.,[35] uses an expansion of the nuclear charge density distribution with the limitation $\rho_N(r) = 0$ for $r > R_{\text{cut}}$,

$$\rho_N(r) = \sum_{\nu=1}^{\infty} a_\nu j_0(q_\nu r), \quad (5.3)$$

where $j_0(qr) = (\sin qr)/(qr)$ denotes the spherical Bessel function of order zero. The coefficients a_ν for $\nu = 1 \cdots N$ are related directly to the form factor value at $q_\nu = \nu\pi/R_{\text{cut}}$ by

$$a_\nu = \frac{q_\nu^2}{2\pi R_{\text{cut}}} F_{\text{exp}}(q_\nu), \quad (5.4)$$

with R_{cut} being the cutoff radius. The maximum value of the momentum transfer q_{max} is given by the experimental conditions. It determines the number of measured Fourier–Bessel coefficients

$$N = \frac{R_{\text{cut}} q_{\text{max}}}{\pi}. \quad (5.5)$$

Beyond the cutoff radius, the nuclear charge distribution $\rho_N(r)$ is assumed to be zero. The behavior of the form factor $F(q)$ in the region $q > q_{\text{max}}$ where no data were measured is assumed to be bounded by a $q^{-4}\exp(-q^2\langle r^2\rangle_p)$ dependence, where $\langle r^2\rangle_p^{1/2}$ is the rms radius of the proton. These assumptions originate from expectations for the distribution of the nucleons inside the nucleus and for the finite size of the nucleons, respectively. They yield an upper limit for the contributions from the higher Fourier–Bessel components a_ν with $\nu > N$, which are not determined directly. This method[35] has the advantage that uncertainties in the charge distribution originating from the experimental errors and from the lack of knowledge about the form factor for $q > q_{\text{max}}$ can be determined separately. For the normalization we have adopted the convention that the integral over the nuclear charge density distribution equals the nuclear charge Ze. By using the Fourier–Bessel expansion technique, realistic charge distribution error bands can be derived which reflect both the statistical error and the error due to the limited range of the experimentally accessible momentum transfer.[35]

Another parametrization, which is often used and was first introduced by Sick,[36] is the "sum of Gaussians." More about this procedure can be found in the original literature or in the compilation by de Vries et al.[4]

Tables VIII and IX show elastic electron scattering results published in the time period from that last compilation[4] up to 1993. The same notation as in the 1987 compilation is used. In Table VIII we present charge density distribution parameters and in Table IX the Fourier–Bessel coefficients a_ν according to Eq. (5.4) and the value of the cutoff radius used. The coefficients' errors are not given in the Table. Because these errors are strongly correlated, the uncertainties in the nuclear charge density distribution can be determined only from the full error-correlation matrices, which are not published in the literature. In the following the Fourier–Bessel coefficients are used without errors. A justification will be given in Section 6 and illustrated with the example of samarium. In addition, the values for $\langle r^n\rangle_e^{1/n}$, $n = 2, 4, 6$, and $R_{k\alpha}^e$ are given. This allows the computation of V_n^e factors, with $n = 2, 4, 6$, which will be used in the combined analysis in Section 6.

Figure 4. Isotope shifts of Barrett radii for stable nuclei deduced from muonic atoms. The differences of the model-independent equivalent charge radii $R_{k\alpha}^e$ between even–even neighboring isotopes (that is, nuclides with N and $N + 2$) are plotted at the neutron numbers $N + 1$. Each symbol is used several times, but in the vicinity of a certain N it always represents one particular element. The lines are drawn to guide the eye. Radii differences are taken from Table V.

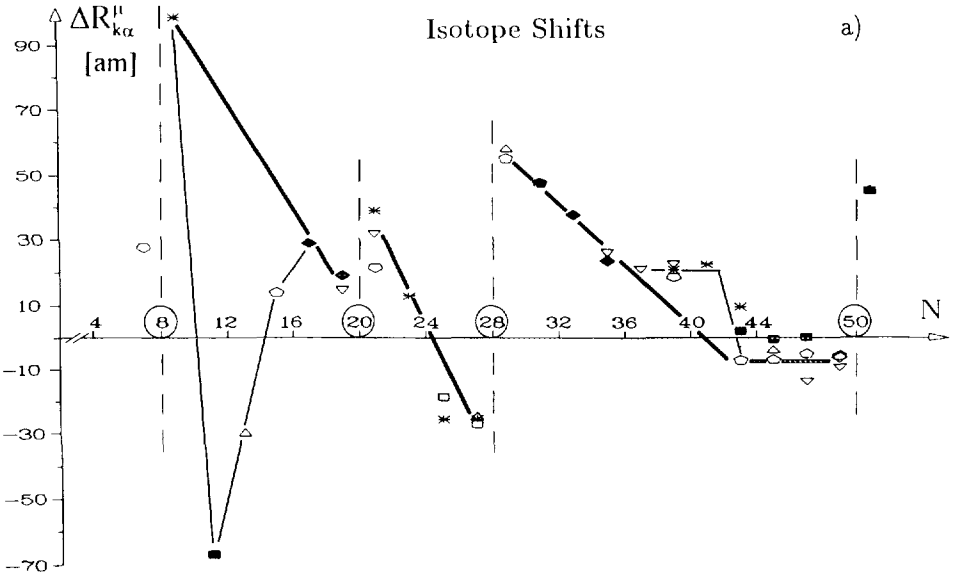
Isotope Shifts
a)
$\Delta R^{\mu}_{k\alpha}$ [am]
90
70
50
30
10
−10
−30
−50
−70
4
8
12
16
20
24
28
32
36
40
44
50
N

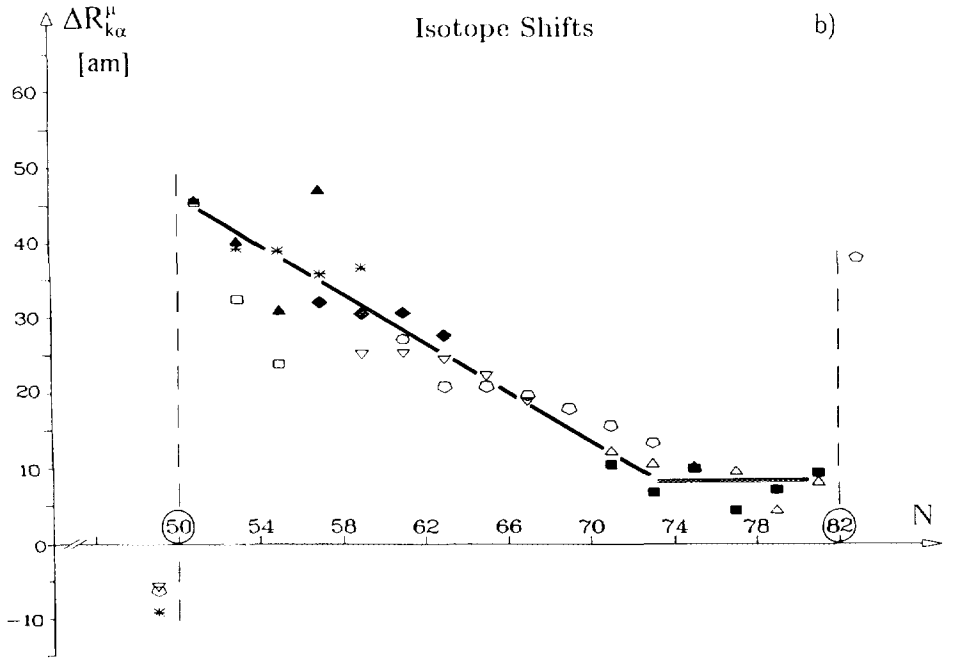
Isotope Shifts
b)
$\Delta R^{\mu}_{k\alpha}$ [am]
60
50
40
30
20
10
0
−10
50
54
58
62
66
70
74
78
82
N

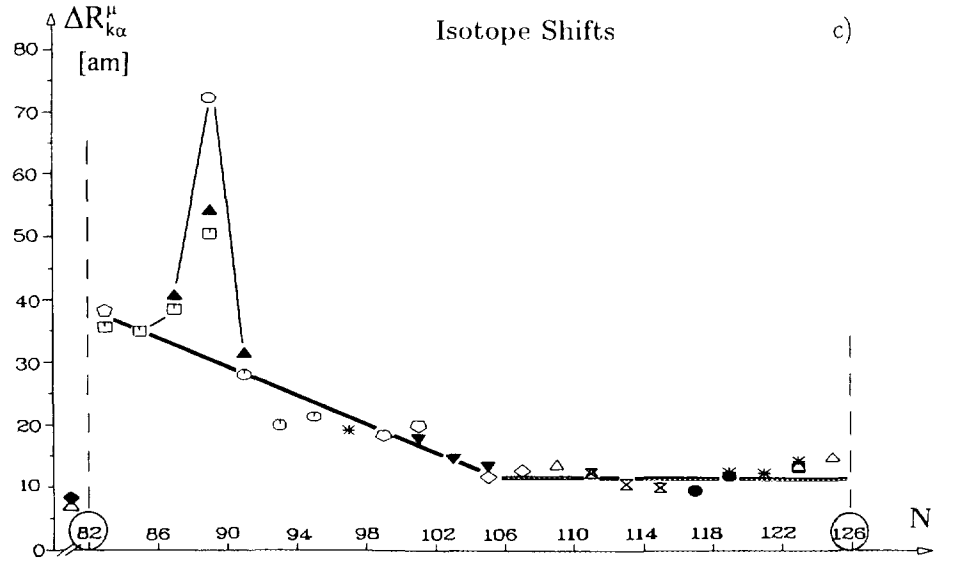
Isotope Shifts
c)
$\Delta R^{\mu}_{k\alpha}$ [am]
80
70
60
50
40
30
20
10
0
82
86
90
94
98
102
106
110
114
118
122
126
N

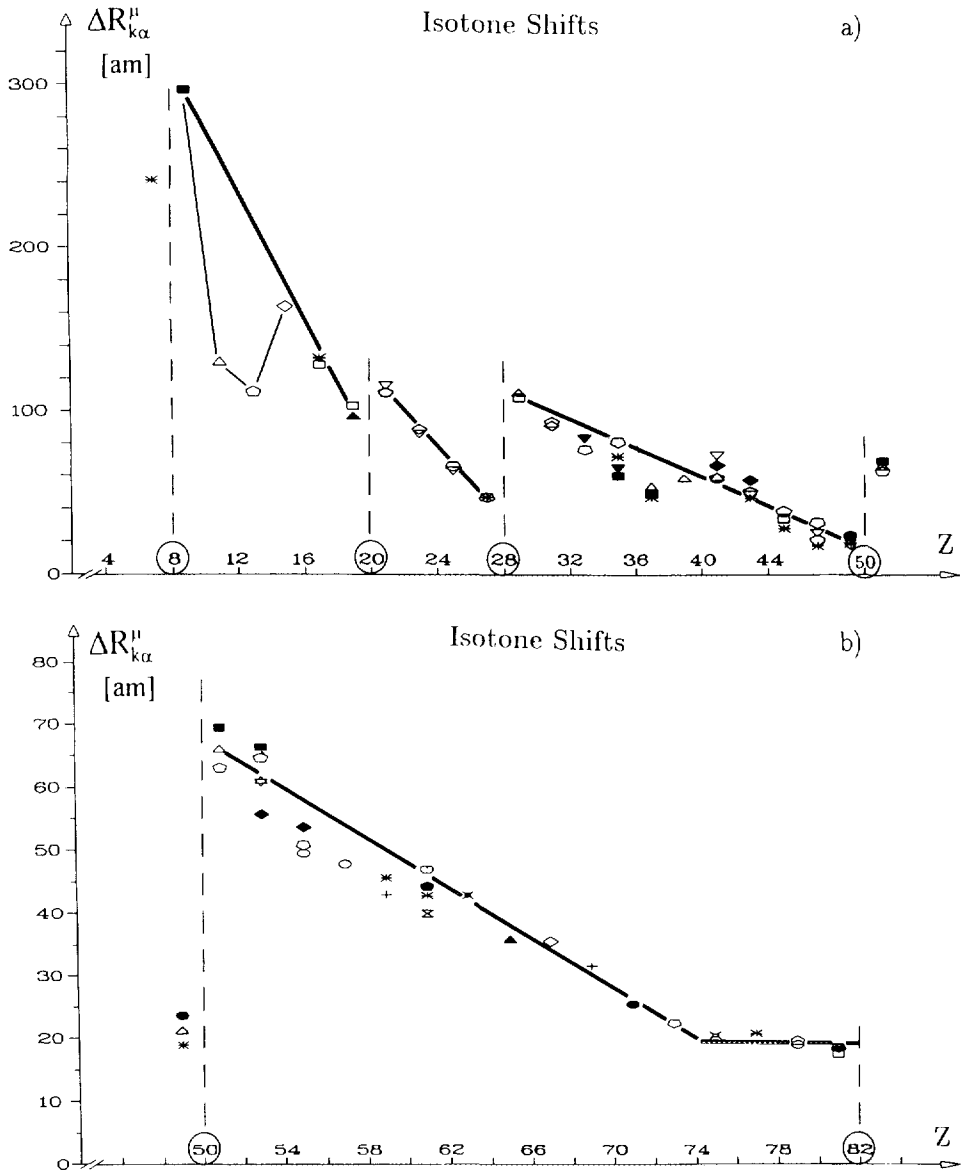

Figure 5. Isotone shifts of Barrett radii deduced from muonic atoms for stable nuclei. The differences of the model-independent equivalent charge radii $R^{\mu}_{k\alpha}$ between even-even neighboring isotones (that is, nuclides with Z and $Z + 2$) are plotted at the proton numbers $Z + 1$. Each shift in the vicinity of a certain Z is marked by a different symbol. The lines are drawn to guide the eye. Radii differences are taken from Table VII.

The accuracy of elastic electron scattering experiments is limited for several reasons:

1. The influence of systematic error sources in elastic electron scattering experiments is relatively large compared to the precision of the other methods as discussed in the following chapter. An error of less than 1% in the overall normalization of the measured cross sections is difficult to obtain experimentally.

2. An additional error is introduced by the restricted q range accessible to the experiment. The resulting "completeness error" can be estimated by an asymptotic expansion of $F(q)$ for high-q values.

3. The charge distributions might be affected by dispersion corrections which take into account virtual excitations of the nucleus during the scattering process.[37] By investigating a possible energy dependence of the form factor, the dispersion corrections were studied recently by

Offermann et al.[38] at NIKHEF and at MIT. They found that at present the corrections cannot be calculated reliably (see also Friar and Rosén[37]). In addition, the assumption made for the value of the cutoff radius R_{cut} also contributes to the error in the charge distribution $\rho_N(r)$.[35]

Because of these errors, especially the relatively large systematic uncertainties, the typical accuracy of an rms radius determined by an elastic electron scattering experiment is limited to approximately 0.2%. The electron scattering measurements—as well as the muonic atom investigations—can be applied only for those nuclei for which a sufficient amount of target material is available (at least tens of milligrams). Thus, elastic electron scattering experiments are essentially feasible only for stable isotopes.

On the other hand, electron scattering offers the unique possibility of determining the radial dependence of a charge distribution $\rho_N(r)$, whereas all other electromagnetic techniques determine only integral quantities of $\rho_N(r)$. Therefore, the charge distribution can be used to connect the different characteristic radial moments determined by different methods. This will be achieved via the ratio of the different radial moments

$$V_n^e = \frac{R_{k\alpha}^e}{\langle r^n \rangle_e^{1/n}}, \tag{5.6}$$

which can be calculated approximately one order of magnitude more precisely than the absolute radial moments. As an example, the V_n^e factors for the stable lead isotopes have been recently calculated by Mazanek,[39] which results in a relative error for V_2^e of $\delta V_2^e/V_2^e = 1 \times 10^{-4}$. This makes it possible to convert $R_{k\alpha}^\mu$ ($\delta R_{k\alpha}^\mu/R_{k\alpha}^\mu = 2 \times 10^{-4}$) to the rms radius with almost no loss of accuracy. Thus, elastic electron scattering experiments provide a valuable tool to correlate the precise information obtained by muonic, optical, and K x-ray isotope shift measurements (see Section 6).

6. Combined Analysis

The aim of the common analysis of the four methods described above is the determination of the rms radius $\langle r^2 \rangle^{1/2}$ and the optical factors F_i and M_i. This is possible in a model-independent way as will be shown below. The four methods are sensitive to different radial moments: optical (abbreviated o) and K x-ray (K-x) isotope shifts to $\lambda^{AA'}$ (Eq. (2.7)), transitions in muonic atoms (μ) to the Barrett radius $R_{k\alpha}^\mu$ (Eq. (4.3)), and elastic electron scattering (e) to the charge distribution $\rho_N(r)$.

It has been demonstrated in Section 4 that the most precise radius—the Barrett radius $R_{k\alpha}^\mu$—can be deduced from muonic atoms. The Barrett radius can be related to the different radial moments $\langle r^n \rangle^{1/n}$, with $n = 2, 4, 6$, via the ratio $V_n^e = R_{k\alpha}^e/\langle r^n \rangle_e^{1/n}$ calculated from elastic electron scattering data. The integrand $\rho_N(r) r^{k+2} e^{-\alpha r}$ for the Barrett radius and the integrands $\rho_N(r) r^{n+2}$ for the different radial moments are shown for calcium in Fig. 6. The integrand with $n = 2$ and the integrand for the Barrett moment show a very similar radial dependence. Therefore it is not astonishing that the values for the Barrett equivalent radius $R_{k\alpha}$ and the rms equivalent radius $(5/3)^{1/2}\langle r^2 \rangle^{1/2}$ are nearly the same. While for lighter nuclei, where $k \approx 2$ and $\alpha \approx 0$, such a behavior is expected, even for lead the deviation for the different radii is only 1% (see Fig. 7). Specifically, for ^{208}Pb, $(5/3)^{1/2}\langle r^2 \rangle_{model}^{1/2} = 7.106$ and $R_{k\alpha}^\mu = 7.031$. Evidently most of the systematic errors of an elastic electron scattering experiment will cancel in the ratios V_n^e. As a consequence, the accuracy of the $\langle r^n \rangle_{\mu e}^{1/n} = R_{k\alpha}^\mu/V_n^e$ values is much better than the precision of the corresponding radial moments deduced from elastic electron scattering data alone. The relative accuracy of both $R_{k\alpha}^\mu$ and V_2^e is[26] about 10^{-4}. Thus, combining the muonic $R_{k\alpha}^\mu$ value with the V_2^e ratio yields an rms radius with an error less than twice the error of the Barrett moment. For a detailed error discussion see Refs. 29 and 40.

Once the radial moments of the stable isotopes are determined by such a combined analysis of μ and e data, the calculation of the parameters $\lambda_{\mu e}^{AA'} = \delta\langle r^2 \rangle^{AA'} + (C_2/C_1)\delta\langle r^4 \rangle^{AA'} + (C_3/C_1)\delta\langle r^6 \rangle^{AA'} + \cdots$ for these nuclei is straightforward. The resulting $\lambda_{\mu e}^{AA'}$ values can be compared with the $\lambda_{K\text{-}x}^{AA'}$ values derived from K x-ray experiments. The impressive consistency of the two meth-

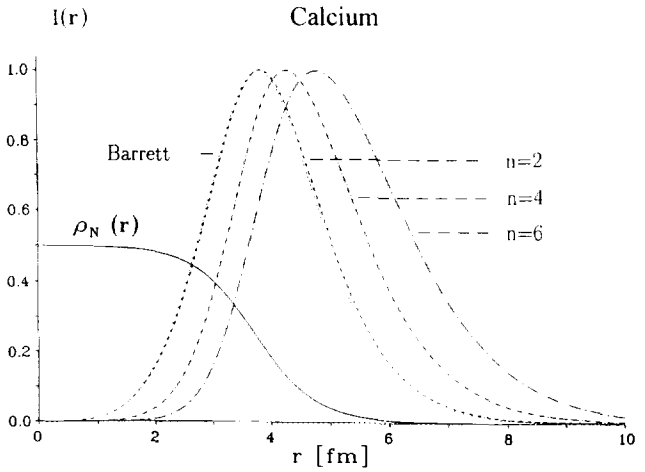

Figure 6. Integrands of the different radial moments $\rho_N(r) r^{n+2}$ and $\rho_N(r) r^{k+2} e^{-\alpha r}$ for calcium. The integrands are normalized to one at the maximum. For comparison the shape of the nuclear charge distribution (solid line) is also shown.

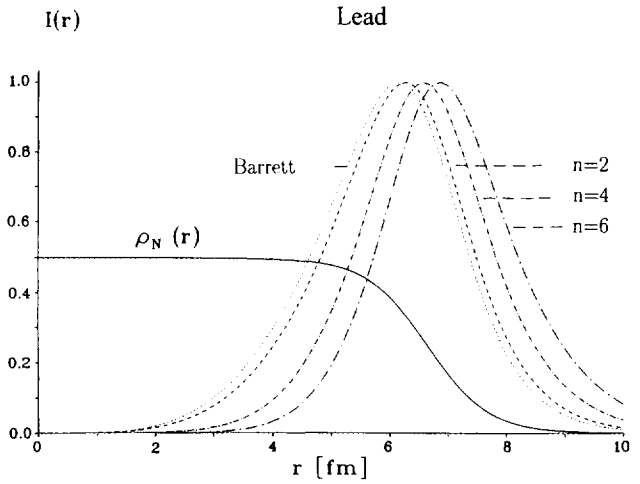

Figure 7. Same as Fig. 6, but for lead.

ods, i.e., K-x and μ plus e, is shown for the lead isotopes in Fig. 1. This supports the concept of calculating $\lambda_{\mu e}$ from measured data only without any model assumptions. If $\lambda^{AA'}$ parameters for at least two isotope pairs are available, either from μ plus e or from K-x experiments, the optical factors F_i and M_i can be determined by a King plot, using the experimental optical frequency shifts $\delta\nu_i^{AA'}$ and applying the equation (see Eqs. (2.1–2.7))

$$\delta\nu_i^{AA'} = F_i\lambda^{AA'} + M_i\frac{A-A'}{AA'}. \qquad (6.1)$$

In the King plot diagrams in Table X the *reduced* IS (see Eq. (7.3)) is plotted on the y axis versus the *reduced* $\lambda_{\mu e}^{AA'}$ values (see Eq. (7.4)) on the x axis. The reduced IS follows from multiplying Eq. (6.1) by two mass-dependent factors and is given by

$$\frac{A_{\rm std}-A'_{\rm std}}{A_{\rm std}A'_{\rm std}}\frac{AA'}{A-A'}\delta\nu_{\rm exp}^{AA'} = \frac{A_{\rm std}-A'_{\rm std}}{A_{\rm std}A'_{\rm std}}\frac{AA'}{A-A'}F_i\lambda^{AA'} + \frac{A_{\rm std}-A'_{\rm std}}{A_{\rm std}A'_{\rm std}}M_i. \qquad (6.2)$$

The multiplication by the factor containing $A_{\rm std}$ facilitates the reading of the King plot: the intersection of the regression line with the y axis gives the mass shift of the standard pair in the line i.

After the factors F_i and M_i have been determined, the optical experimental frequency shifts of other stable and unstable isotopes can be converted to precise $\lambda^{AA'}$ values for the whole isotopic chain. The errors of F_i and M_i are correlated, as Eq. (6.1) shows. Therefore the $\lambda^{AA'}$ values are determined more precisely if the correlation is large. This is the case in the examples given. In order to obtain $\delta\langle r^2\rangle^{AA'}$, the $\lambda^{AA'}$ parameters must be corrected for the contribution of the differences in the higher radial moments ($\delta\langle r^4\rangle$, $\delta\langle r^6\rangle$). For isotopes where no experimental data on V_n factors exist, one can either extrapolate the unknown V_n factors from the values of the stable isotopes, or one can use theoretical model calculations[41–43] or a parametrized charge distribution (Fermi II, Eq. (4.4)). If the $2p$–$1s$ *and* the $3d$–$2p$ transitions in muonic atoms have been measured, the two parameters of the Fermi II charge distribution, c and t, can be determined experimentally (see, for example, Ref. 44). This allows the calculation of V_n^{μ} factors from muonic data alone. The method still uses the Fermi II charge distribution but with both parameters c *and* t measured. The averaged contribution of the higher radial moments to $\lambda^{AA'}$ is given in Fig. 8 (see also Table X). Finally, with the absolute rms values of the stable isotopes deduced from μ and e measurements in connection with the $\delta\langle r^2\rangle_{o\mu e}^{AA'}$ values derived from a combined analysis in a King plot, the rms radii of the whole isotope chain can be calculated.

Before giving an example it is useful to recall the conditions for an effective combined analysis:

(i) Precise experimental results for optical isotope shift measurements (with a high percentage of FS) and Barrett radii $R_{k\alpha}^{\mu}$ from muonic atom $2p$–$1s$ transition energies. These data are now available for most isotopes.

(ii) Nuclear charge distributions from elastic electron scattering experiments to calculate the V_n^{e} factors,

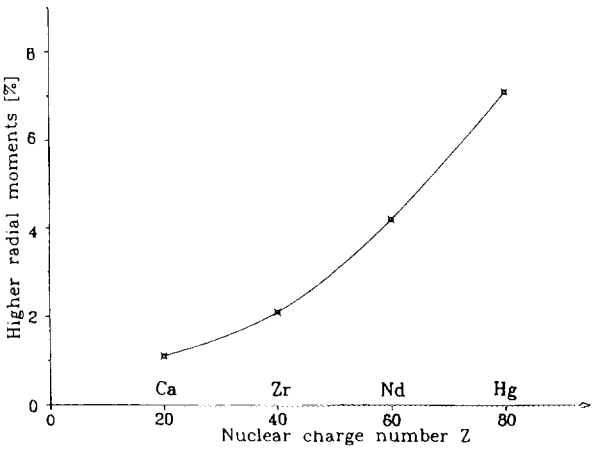

Figure 8. Averaged contribution (in percent) of higher radial moments $\delta\langle r^4\rangle$ and $\delta\langle r^6\rangle$ to the λ factor (see Eq. (2.7)). The contribution is always negative, that is, $\lambda < \delta\langle r^2\rangle$.

which correlate the different radial moments. About half of the stable even isotopes have been measured by the elastic electron scattering method. For odd isotopes, however, only a few data are available because of difficulties caused by contributions from magnetic and/or electric moments and the experimental difficulties of resolving the elastically scattered from the inelastically scattered electrons. This makes it necessary to interpolate the unknown V_n^e from values in neighboring isotopes and sometimes between neighboring elements.[29] A justification for this procedure is given below. If the V_n^e factor has been measured for one isotope only, that same factor may be used for all isotopes. In the cases of the even molybdenum and zirconium isotopes, electron scattering results have shown that the variation of the V_2^e factors within a chain of isotopes is less than their limits of error (about 10^{-4}).[26]

The input values for $\delta\nu_{proj}$ and the $R_{k\alpha}^{\mu}$, the $\Delta R_{k\alpha}^{\mu}$, and the V_n values are listed in Tables I, III, V, and X, respectively ($\delta\nu_{proj}$ is introduced in Section 2). The procedure and additional assumptions (for V_n factors, for example) used for the King plots and the results (Table X) are demonstrated below for samarium.

In samarium, elastic electron scattering data are available only for the isotopes A = 148, 152, and 154 (Refs. 45, 46). For these isotopes, the V_n^e factors and their errors were calculated by Mazanek,[39] using the model-independent Fourier–Bessel analysis. For the other stable isotopes, 144, 147, 149, and 150, where no electron scattering data exist, the V_n^e values have been interpolated. This seems to be adequate, because the V_n^e factors show only a small variation within the isotopes of one element[26] and because the consistency of the data is excellent (see the samarium King plot in Fig. 9). All points lie almost perfectly on a straight line, resulting in a χ^2 per degree of freedom of 0.08. This small value indicates that the reported error for the combined μ plus e data is too large. The error of the V_n^e factors depends mostly on systematic uncertainties in the elastic scattering data, like normalization, scattering energies, or angles, which are not easy to determine. Also, no correlation between the different isotopes has been taken into account when determining the error of the V_n^e factors. On the other hand, there is no error matrix available for most of the reported a_ν coefficients. The V_n^e can be calculated from the Fourier–Bessel coefficients a_ν (see Table IX) but without the proper error. Therefore it is customary and reasonable to use the King plot parameters $\lambda_{\mu e}$ deduced assuming no error for the V_n^e factors. The result for samarium is given in Fig. 10, which still demonstrates an excellent agreement between the o and μ plus e data, with a χ^2 value per degree of freedom close to one. This result also indicates that the error assigned to the $\Delta R_{k\alpha}^{\mu}$ differences due to uncertainties in the nuclear polarization corrections (nuclear polarization; see Section 4) might be regarded as an upper limit

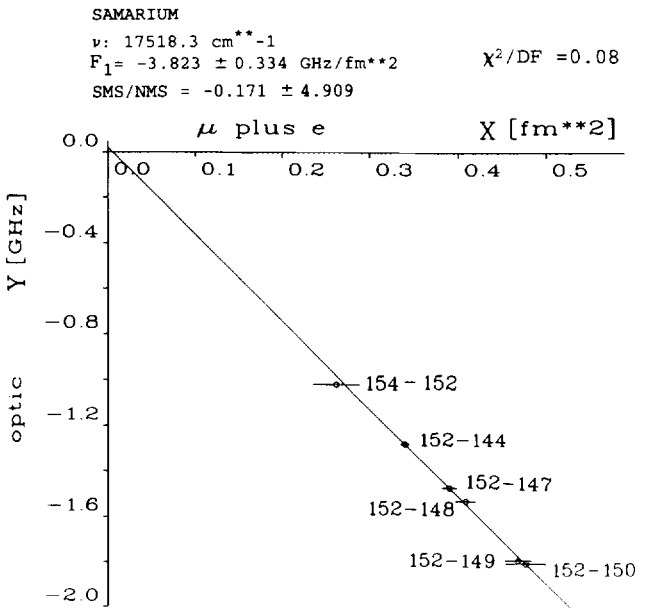

Figure 9. King plot of optical isotope shift measurements against muonic x-ray and elastic electron scattering data for Sm. The error of the V_n^e factors (Eq. (5.6)) is included. This results in a too small χ^2 of 0.08 per degree of freedom. For definitions of X and Y, see Explanation of Table X.

and that, as mentioned, the interpolation for the unknown V_n^e values seems to be justified. The results of this combined analysis are the optical factors F_i and M_i, which can be compared to values from theoretical calculations (Table XI), and the rms radii (Table XII).

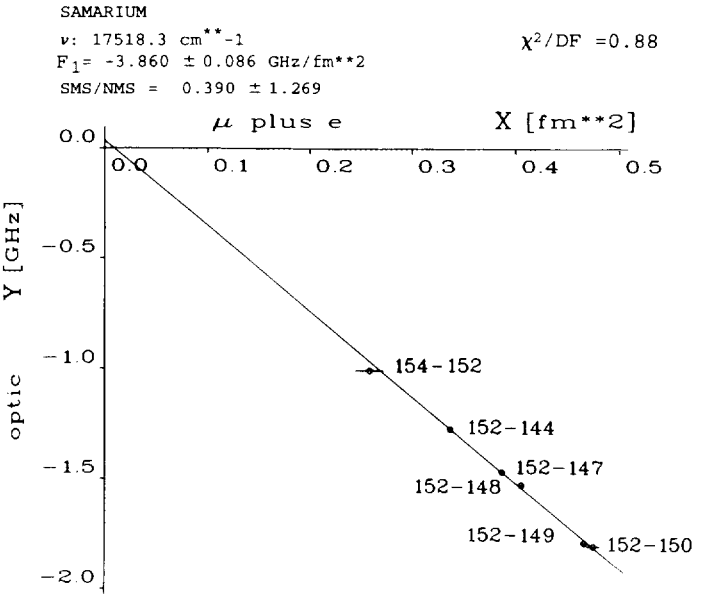

Figure 10. Same as Fig. 9, but without including any error for the V_n^e factors. The result is a more reasonable χ^2 of 0.88 per degree of freedom.

The final results of the combined analysis are shown in King plots (Table X) which illustrate the consistency between the input data from the different experimental methods. Supplementary remarks are given for each element—for example, on the origin of the V_n's—in order to reveal the method of our calculations and to facilitate checks. Many radioactive isotopes have been investigated by optical spectroscopy. As an example, we give in Table X mean-square radii differences of the unstable lead isotopes as deduced from the regression line established by the stable isotopes. The corresponding mean-square radii are listed in Table XII in order to give an impression for the errors of the radii of the isotopes far from stability. The examples given in this paper should stimulate further experimental and theoretical investigations on the subject. Work on a combined analysis of other elements than those given in Table X is in progress.

7. Appendix A: King Plot

Terminology used in this paper is summarized as follows:

observed IS: $\delta\nu_i^{AA'} = \nu_i^A - \nu_i^{A'}$ (7.1)

projected IS: the IS in a selected line, evaluated from the IS shifts in all relevant lines by means of a variance–covariance matrix

scaled (≡ modified) IS: $\delta\nu_i^{AA'}\dfrac{AA'}{A-A'} = \delta\nu_i^{AA'}S$ (7.2)

reduced IS: $\delta\nu^{AA'}S\dfrac{A_{\rm std}-A'_{\rm std}}{A_{\rm std}A'_{\rm std}}$ (7.3)

reduced λ: $\lambda^{AA'}S\dfrac{A_{\rm std}-A'_{\rm std}}{A_{\rm std}A'_{\rm std}}$, (7.4)

where $A_{\rm std}$, $A'_{\rm std}$ is an arbitrarily chosen standard isotope pair. Projected IS is IS in a selected line, evaluated from IS shifts in all relevant lines by means of a variance–covariance matrix. For sign conventions, see also Appendix B.

A (two-dimensional) King plot is a diagram where the scaled IS of a line i is plotted on the y axis versus the scaled IS of another line j on the x axis. From Eqs. (2.1), (2.3), and (2.4) follows Eq. (6.1):

$$\delta\nu_i^{AA'} = F_i\lambda^{AA'} + M_i\frac{A-A'}{AA'}.$$

As a consequence,

(i) the plotted points (= scaled IS$^{AA'}$) must lie on a straight line,

(ii) the slope of the regression line is

$$F_i/F_j, \quad (7.5)$$

(iii) the intersection of the regression line with the y axis is

$$y = M_i - M_jF_i/F_j. \quad (7.6)$$

These equations—and consequently the following discussion—imply that the IS is caused by FS and MS only and that any additional isotope-dependent influence on the measured IS has been accounted for. For example, care has to be taken to include second-order hyperfine perturbations.[47] Another effect is a possible nuclear polarization by the electron. In samarium, the following changes for $\lambda^{AA'}$ have been calculated:[21] ^{150}Sm–^{148}Sm, 2%; ^{152}Sm–^{150}Sm, 6%; ^{154}Sm–^{152}Sm, 6%. The excellent agreement between the optical IS measurements (not corrected for nuclear polarization) versus μ plus e data in the samarium King plot (see Fig. 10) indicates, however, that the nuclear polarization correction for optical transitions may not be in accordance with the calculated values. For other nuclides that are not so heavily deformed as those in the Sm region, a much smaller influence on the IS is expected from theoretical considerations.[21]

Which reference isotope should be used for the plot? As an example, we discuss strontium, an element where MS and FS roughly have about the same size (the nuclear radius decreases with increasing mass number for the stable isotopes). Strontium has four stable isotopes (with A = 84, 86, 87, and 88) and therefore three independent isotope pairs; the reduced IS of line λ = 689.3 nm is plotted (x axis) versus the reduced IS of line λ = 716.7 nm (y axis) in Fig. 11. The observed shifts in MHz relative to A = 88 are, for the $5s^2\ ^1S_0 \rightarrow 5s5p\ ^3P_1$ 689.3-nm line, 351.2 ± 1.8 (A' = 84), 163.7 ± 1.0 (A' = 86), 62.3 ± 1.4 (A' = 87)[48] and, for the $5s4d\ ^1D_2 \rightarrow 5s6p\ ^1P_1$ 716.7-nm line, −463.2 ± 1.0 (A' = 84), −220.6 ± 1.0 (A' = 86), −99.5 ± 1.0 (A' = 87).[49]

The standard pair, introduced to facilitate the reading of the King-plot diagrams, is arbitrarily chosen to be 88–86, giving a constant factor of $(A_{\rm std} - A'_{\rm std})/(A_{\rm std}A'_{\rm std})$ = 0.000264 for all plotted strontium values. Therefore the choice of the standard pair is not relevant to the subsequent discussion.

Figure 11 shows five King plots for strontium, where the reference isotope only has been changed from plot to plot. The numerical values of the slopes and y intercepts of the five regression lines are given in Table A.

At first glance it seems surprising that different reference isotopes should yield somewhat different slopes and intersections. The main reason is that the measured values are multiplied by mass-number-dependent factors (see Eq. (7.2)). Therefore different reference isotopes give quite different ranges in the plot (see Fig. 11). The range is introduced as (largest plotted value minus smallest value)/(largest value). In most cases, a large range gives results with the smallest errors. A detailed discussion will be given in a forthcoming paper.[50]

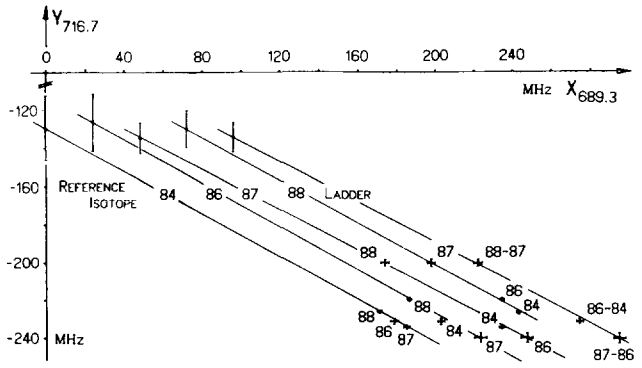

Figure 11. Two-dimensional King plots for two optical strontium lines for five different choices of the reference isotope. The x axis has been shifted from plot to plot for convenience; the respective y intercepts are indicated by the series of vertical error bars. The corresponding data are given in the text and in Table A. Plotted are the reduced IS in MHz, namely

$$X^{AA'} = \delta\nu^{AA'}_{689.3\ \mathrm{nm}} \frac{AA'}{A-A'} \frac{88-86}{88\times 86},$$

$$Y^{AA'} = \delta\nu^{AA'}_{716.7\ \mathrm{nm}} \frac{AA'}{A-A'} \frac{88-86}{88\times 86}.$$

A, A', 88, or 86 stands for the more accurate nuclear mass numbers deduced from Ref. 51.

Nevertheless, an improvement can be achieved, if for each line i the ISs of all possible isotope pairs have been measured (i.e., in strontium, six permutations) and the values for each line are equalized by a matrix. Unfortunately this thorough procedure—often executed in the prelaser days—no longer is en vogue, so most elements had to be treated individually. In this paper a line with a slope (and a corresponding intersection; Eq. (7.6)) with rather small error bars was chosen to serve as a projection line by careful inspection of King plots of all relevant optical lines. When calculating F_i and M_i factors for other optical lines by means of two-dimensional King plots (see Eqs. (7.5) and (7.6)), at least the same reference isotope (or the ladder) should be used for all lines.

It is not possible to extract M_i and F_i solely from optical measurements, no matter how many lines and how many isotope pairs have been investigated. However, the F_i and M_i factors can be found by a special King plot, in which the $\lambda^{AA'}_{\mu e}$ values deduced from muonic and electron scattering data are plotted versus the experimental $\delta\nu^{AA'}_{\mathrm{proj}}$ values for one line. If one uses the *reduced* IS (see Eqs. (6.2) and (7.3)) and the *reduced* $\lambda^{AA'}_{\mu e}$ (see Eq. (7.4)) King plot, the slope gives F_i in GHz/fm^2 and the intersection with the y axis (where the optical values are plotted) determines the mass shift for the *standard pair* in GHz. That procedure is used in this paper.

8. Appendix B: Sign Convention

We define $\delta\nu^{AA'}$ and $\lambda^{AA'}$ in a straightforward way which is in agreement with Otten:[5]

$$\delta\nu^{AA'} = \nu^{A} - \nu^{A'} \tag{8.1}$$

$$\delta E^{AA'}_{\mathrm{coul}} = E^{A}_{\mathrm{Coul}} - E^{A'}_{\mathrm{Coul}} \tag{8.2}$$

$$\lambda^{AA'} \approx \delta\langle r^2\rangle^{AA'} = \langle r^2\rangle^{A} - \langle r^2\rangle^{A'} \tag{8.3}$$

$$\delta\nu^{AA'}_{i,\mathrm{NMS}} = \frac{\nu_i}{1822.9} \frac{A-A'}{AA'}. \tag{8.4}$$

The NMS always shifts the line for the *heavier isotope* toward *larger wavenumbers;* this is called a *positive* shift.

The SMS may be positive or negative, depending on the type of transition and the element.

In many cases the rms radius of the isotopes of an element increases with increasing neutron number. Then $\lambda^{AA'}$ is positive, if $A > A'$, and the FS in an $s \rightarrow p$ transition (with s the lower and p the upper energy level) is negative:

TABLE A
Numerical Values of the Slopes and Intersections (with the y Axis) of the Five King Plots Drawn in Fig. 11

Reference isotope	Isotope pairs	Slope = $\frac{F_{716.7}}{F_{689.3}}$	Intersection = MS^{88-86} [MHz]	Range (%)
84	86–84, 87–84, 88–84	−0.562 (96)	−130 (17)	7.7
86	86–84, 87–86, 88–86	−0.583 (87)	−126 (15)	18.2
87	87–84, 87–86, 88–87	−0.533 (44)	−135 (8)	36.9
88	88–84, 88–86, 88–87	−0.559 (57)	−130 (10)	26.4
Ladder	86–84, 87–86, 88–87	−0.583 (50)	−134 (8)	36.9

the line for the *heavier isotope* is shifted toward *smaller wavenumbers*. Therefore F_i for an $s \rightarrow p$ transition (with s the lower, and p the upper energy level) is negative. For a $p \rightarrow s$ transition, F_i is positive.

Acknowledgments

This work was supported by the Bundesministerium für Forschung und Technologie, Germany, and by the Swiss National Foundation. We thank B. Fricke, Universität Kassel, for MCDF calculations of optical factors. One of us (C.B.) is indebted to the Institut de Physique de l'Université de Fribourg for its friendly hospitality.

References for the Introduction

1. P. Aufmuth, K. Heilig, and A. Steudel, ATOMIC DATA AND NUCLEAR DATA TABLES **37,** 455 (1987)
2. F. Boehm and P. L. Lee, ATOMIC DATA AND NUCLEAR DATA TABLES **14,** 605 (1974)
3. R. Engfer, H. Schneuwly, J. L. Vuilleumier, H. K. Walter, and A. Zehnder, ATOMIC DATA AND NUCLEAR DATA TABLES **14,** 509 (1974)
4. H. de Vries, C. W. de Jager, and C. de Vries, ATOMIC DATA AND NUCLEAR DATA TABLES **36,** 495 (1987)
5. E. W. Otten, in *Treatise on Heavy Ion Physics,* edited by D. A. Bromley (Plenum, New York, 1987), Vol. 8, p. 517
6. K. Heilig, Spectrochim. Acta B **32,** 1 (1977); **37,** 417 (1982); **42,** 1237 (1987); **47,** 303 (1991)
7. R. C. Barrett, Phys. Lett. B **33,** 388 (1970)
8. K. Heilig and A. Steudel, ATOMIC DATA AND NUCLEAR DATA TABLES **14,** 613 (1974)
9. W. H. King, *Isotope Shifts in Atomic Spectra,* Physics of Atoms and Molecules Series, edited by P. G. Burke and H. Kleinpoppen (Plenum, New York/London, 1984)
10. E. Lindroth, A. M. Mårtensson-Pendrill, and S. Salomonson, Phys. Rev. A **31,** 58 (1985)
11. E. C. Seltzer, Phys. Rev. **188,** 1916 (1969)
12. S. A. Blundell, P. E. G. Baird, C. W. P. Palmer, D. N. Stacey, and G. K. Woodgate, J. Phys. B **20,** 3663 (1987)
13. K. Heilig, Hyperfine Interact. **38,** 803 (1987)
14. F. A. Babushkin, Sov. Phys. JETP **15,** 1113 (1962); JETP **17,** 1118 (1963)
15. D. Zimmermann, Z. Phys. A **315,** 123 (1984); **321,** 23 (1985)
16. Z. Fang, O. Redi, and H. H. Stroke, J. Phys. II France **2,** 877 (1992)
17. G. Torbohm, B. Fricke, and A. Rosén, Phys. Rev. A **31,** 2038 (1985)
18. B. Fricke, private communication, Universität Kassel, 1993
19. C. W. P. Palmer, P. E. G. Baird, S. A. Blundell, J. R. Brandenberger, C. J. Foot, D. N. Stacey, and G. K. Woodgate, J. Phys. B **17,** 2197 (1984)
20. K. Wendt, S. A. Ahmad, F. Buchinger, A. C. Mueller, R. Neugart, and E. W. Otten, Z. Phys. A **318,** 125 (1984)
21. B. Hoffmann, G. Baur, and J. Speth, Z. Phys. A **315,** 57 (1984)
22. R. B. Chesler and F. Boehm, Phys. Rev. **166,** 1202 (1968)
23. G. L. Borchert, O. W. B. Schult, J. Speth, P. G. Hansen, B. Jonson, H. L. Raven, and J. B. McGrory, Nuovo Cimento A **73,** 273 (1983)
24. P. L. Lee and F. Boehm, Phys. Rev. **8,** 819 (1973)
25. G. Fricke, C. Bernhardt, G. Mallot, Th. Hennemann, J. Herberz, L. A. Schaller, L. Schellenberg, and E. B. Shera, *Confit,* Institute Report, Institut für Kernphysik, KPH 16/93, Universität Mainz, 1993
26. P. Mazanek, Diplomarbeit, Institut für Kernphysik, KPH 11/89, Universität Mainz, 1989
27. G. A. Rinker, private communication, LANL, Los Alamos, NM, 1976
28. C. S. Wu and L. Wilets, Annu. Rev. Nucl. Sci. **19,** 527 (1969)
29. C. Bernhardt, Ph.D. thesis, Institut für Kernphysik, KPH 6/92, Universität Mainz, 1992
30. G. Fricke, J. Herberz, Th. Hennemann, G. Mallot, L. A. Schaller, L. Schellenberg, C. Piller, and R. Jacot-Guillarmod, Phys. Rev. C **45,** 80 (1992)
31. H. J. Emrich, G. Fricke, M. V. Hoehn, K. Kaeser, G. Mallot, H. Miska, B. Robert-Tissot, D. Rychel, L. A. Schaller, L. Schellenberg, H. Schneuwly, E. B. Shera, H. G. Sieberling, R. M. Steffen, H. D. Wohlfahrt, and Y. Yamazaki, *Proceedings, 4th International Conference on Nuclei far from Stability, Helsingør, Denmark, 1981,* edited by L. O. Skolen, p. 33
32. L. A. Schaller, Z. Phys. C **56,** 48 (1992)
33. K. Merle, Ph.D. thesis, Institut für Kernphysik, KPH 20/76, Universität Mainz, 1976

34. L. R. B. Elton, *Nuclear Sizes* (Oxford Univ. Press, London, 1961)

35. B. Dreher, J. Friedrich, K. Merle, H. Rothaas, and G. Lührs, Nucl. Phys. A **235,** 219 (1974)

36. I. Sick, Nucl. Phys. A **218,** 509 (1974)

37. J. L. Friar and M. Rosén, Ann. Phys. (N.Y.) **87,** 289 (1974)

38. E. A. J. M. Offermann, L. S. Cardman, C. W. de Jager, H. Miska, C. de Vries, and H. de Vries, Phys. Rev. C **44,** 1096 (1991)

39. P. Mazanek, Ph.D. thesis, Institut für Kernphysik, KPH 5/92, Universität Mainz, 1992

40. J. Herberz, Ph.D. thesis, Institut für Kernphysik, KPH 6/89, Universität Mainz, 1989

41. M. M. Sharma, G. A. Laladisis, and P. Ring, Phys. Lett. B **317,** 9 (1993)

42. J. Friedrich and P.-G. Reinhard, Phys. Rev. C **33,** 335 (1986)

43. B. Nerlo-Pomorska, K. Pomorski, and B. Skorupska-Mach, Nucl. Phys. A **562,** 180 (1993)

44. E. B. Shera, H. D. Wohlfahrt, M. V. Hoehn, and Y. Tanaka, Phys. Lett. B **112,** 124 (1982)

45. R. Hofmann, Ph.D. thesis, Institut für Kernphysik, KPH 80, Universität Mainz, 1980

46. X. H. Phan, H. G. Andresen, L. S. Cardman, J.-M. Cavedon, J.-C. Clemens, B. Frois, M. Girod, D. Gogny, D. Goutte, B. Grammaticos, R. Hofmann, M. Huet, P. Leconte, S. K. Platchkov, I. Sick, and S. E. Williamson, Phys. Rev. C **38,** 1173 (1988)

47. H. Kopfermann, *Kernmomente,* Akad. Verlagsges, Frankfurt/Main, 1956; *Nuclear Moments* (Academic Press, New York, 1958)

48. D. Bender, H. Brand, and V. Pfeufer, Z. Phys. A **318,** 291 (1984)

49. P. Grundevik, M. Gustavsson, I. Lindgren, G. Olsson, T. Olsson, and A. Rosén, Z. Phys. A **311,** 143 (1983)

50. K. Heilig, to be published

51. A. H. Wapstra and G. Audi, Nucl. Phys. A **432,** 1 (1985)

EXPLANATION OF TABLES

TABLE I. Observed (Projected) Optical Isotope Shifts of Selected Elements

Only optical isotope shifts for those elements and isotopes for which a combined analysis has been made (see Table X) are listed.

Z element	The transition is listed below the atomic number and element designation. Wavelengths given are in air, and wavenumbers in vacuum. The frequency graph shows isotope shifts relative to the reference isotope.
A	Atomic weight, shorthand notation; for all calculations the more accurate values for the nuclear masses from Wapstra and Audi[51] were used.
$\delta\nu_{\text{proj}}$	Observed optical isotope shift (IS) relative to the indicated reference isotope, projected onto one transition per element (see Section 2 and Appendix A). Errors are given in parentheses. When used in the combined analysis, IS is taken as positive when the transition of the heavier isotope is shifted toward higher frequencies (see Appendix B).
references	Source of experimental data, keyed to the list of References for Tables.

TABLE II. Observed $K\alpha$ X-Ray Isotope Shifts δE and Charge Radius Variations λ

Isotope Pair	Element symbol and isotope pair A–A', A being the lighter isotope.
$\delta E^{AA'}_{Coul.}$	Observed energy shift of the $2p_{3/2} \rightarrow 1s_{1/2}$ $K\alpha_1$ x-ray transition, in meV, corrected for the mass shift (see Refs. 2 and 22). The errors are standard deviations.

$$\delta E^{AA'}_{\text{Coul}} = E_{\text{Coul}}(A) - E_{\text{Coul}}(A')$$

$$-\delta E^{AA'}_{\text{Coul}} = C_1\delta\langle r^2\rangle^{AA'} + C_2\delta\langle r^4\rangle^{AA'} + C_3\delta\langle r^6\rangle^{AA'} + \cdots$$

The C_i are Seltzer coefficients (Refs. 2, 11, and 12). $\delta\langle r^2\rangle^{AA'} = \langle r^2\rangle^{A} - \langle r^2\rangle^{A'}$.

$-\lambda^{AA'}$	$\lambda^{AA'} = -\delta E^{AA'}_{\text{Coul}}/C_1$ (see Eq. 2.7). In this Table and the equations above, the lighter isotope always appears first. Hence λ has an opposite sign from δE.
Ref.	Source of experimental data, keyed to the list of References for Tables.

TABLE IIIA. Muonic $2p \rightarrow 1s$ Transition Energies and Barrett Radii for $Z < 60$ and $Z > 77$

$E_{exp.}$	Experimental energy taken from a comprehensive matrix error analysis procedure [Fr93a], if not stated otherwise. If two energies are listed, the first (second) value given corresponds to the $2p_{1/2} \rightarrow 1s_{1/2}$ ($2p_{3/2} \rightarrow 1s_{1/2}$) transition. Otherwise the given value corresponds to the center of gravity of the $2p \rightarrow 1s$ transition, or, for some elements, to the ($2p_{3/2} \rightarrow 1s_{1/2}$) transition as indicated. The statistical error in the last quoted digits is listed below each energy.

EXPLANATION OF TABLES continued

$E_{theo.}$ — Energy of the transition calculated with a two-parameter Fermi distribution (Eq. (4.4)),

$$\rho(r) = \rho_0\left(1 + \exp\left[\frac{r-c}{a}\right]\right)^{-1},$$

including QED and nuclear polarization corrections. The skin thickness $t = 4a \ln 3$ is fixed at 2.30 fm, whereas the half-density radius c is fitted to reproduce the experimental transition energy.

NPol — Calculated nuclear polarization correction ([Ri76], [Ri78]). The nuclear data for these calculations are taken from Nuclear Data Sheets up to 1992.

c — Half-density parameter c of the two-parameter Fermi distribution. The error in the last digits listed below each value is the fit error only and does not include model-dependent effects.

$\langle r^2 \rangle^{1/2}_{model}$ — Rms value of the charge radius (Eq. (1.2)) calculated using the two-parameter Fermi distribution with $t = 2.30$ fm.

α, k — Parameters of the Barrett moment fitted to reproduce the differences of the muon potentials in the initial and final state.

C_z — Sensitivity factor $C_z = dR^{\alpha}_{k\alpha}/dE$ in am/eV or am/keV as indicated. 1 am = 10^{-18} m.

$R^{\alpha}_{k\alpha}$ — Model-independent Barrett equivalent radius calculated from Eq. (4.3) with the parameters k, α fitted to the corresponding transition energy. The first error corresponds to statistical errors but not to systematical errors. The second error is due to uncertainties in calculating the nuclear polarization correction. This error was conservatively estimated to be 30% of the total nuclear polarization value ([Ri76], [Ri78]).

Ref. — Source of experimental data, keyed to the list of References for Tables.

TABLE IIIB. Muonic $2p \rightarrow 1s$ Transition Energies and Relative Intensities of Deformed Nuclei with $60 \leq Z \leq 77$

Transition
Initial state
Final state — The coupled muon/nucleus states which form the major component of the wave functions of the initial and final state involved in each transition. Listed are the muon orbital followed by the spin parity of the nuclear state, I^{π}, and the hyperfine level.

$E_{exp.}$ — Experimental energy of the listed hyperfine component. The given error includes statistical errors and the fit error. Since an entire hyperfine structure complex was fitted and not just a single component, every component of such a complex has the same experimental error independent of the intensity of the component.

EXPLANATION OF TABLES continued

$E_{theo.}$	Energy of the listed hyperfine component calculated with a deformed Fermi distribution including QED and nuclear polarization corrections. The charge density distribution parameters and the nuclear polarization corrections are listed in Table IIIC.
Relative Intensity	Intensity relative to the strongest component, which is listed as 1.000.

This table includes static and dynamic hyperfine components measured in nuclei between ^{150}Nd and ^{193}Ir, which in general have not been published before. For nuclei with an even (odd) number of nucleons, the 10 (20) strongest components are listed. All values in this table are taken from the references quoted in Table IIIC.

TABLE IIIC. Barrett Radii and Related Parameters of Deformed Nuclei with $60 \leq Z \leq 77$

NPol	Calculated nuclear polarization correction ([Ri76], [Ri78]) for the center of gravity of the $2p_{1/2} \rightarrow 1s_{1/2}$ (upper value) and the $2p_{3/2} \rightarrow 1s_{1/2}$ (lower value) hyperfine components found in Table IIIB and/or in the quoted references.
R_0, a, β_2	Parameters of the deformed Fermi distribution, $$\rho(r) = \rho_{\text{Norm}}\left(1 + \exp\left[\frac{r - R_0[1 + \beta_2 Y_{20}(\theta, \phi)]}{a}\right]\right)^{-1}.$$ ρ_{Norm} is determined by normalizing the total charge to Ze.
$\langle r^2 \rangle^{1/2}_{model}$	Rms value of the charge radius calculated from R_0, a, and β_2.
α, k	Same as in Table IIIA.
C_z	Same as in Table IIIA.
$R^{\mu}_{k\alpha}$	Model-independent Barrett equivalent radius (Eq. (4.3)). Errors in the last quoted digits given in parentheses below each value are obtained with the help of the sensitivity factors C_z. The first error listed corresponds to the statistical and fit error of E_{exp} for each complex. The second error, corresponding to uncertainties in calculating the nuclear polarization corrections, was estimated as follows: A 28% error was assigned to the calculation of the contribution of the high-lying nuclear states to the total nuclear polarization correction. The error for the calculation of the contribution of the low-lying states was estimated to be 2%, resulting essentially from the errors of the transition probabilities $B(E2)$ [Ri76].
Ref.	Source of tabulated data, keyed to the list of References for Tables.

EXPLANATION OF TABLES continued

TABLE IV. *Confit* Matrices for Muonic $2p \rightarrow 1s$ Energy Differences of Isotopes, $31 \leq Z \leq 58$

In this table the energy differences (in keV) of isotopes resulting from a comprehensive matrix error analysis procedure are given [Fr93a]. The upper right half shows the energy difference for the $2p_{1/2} \rightarrow 1s_{1/2}$ transition between the lighter and the heavier nucleus, and in the lower left half is the difference for the $2p_{3/2} \rightarrow 1s_{1/2}$ transition between the heavier and the lighter nucleus. The quoted errors include statistical but no systematic errors.

TABLE V. Differences of Barrett Radii for Isotopes, $6 \leq Z \leq 82$

$\Delta R^{\mu}_{k\alpha}$ Difference of the model-independent equivalent radius (in am = 10^{-18} m) based on the energy differences given in Table IV and the parameters α and k in Table IIIA or Table IIIC.

In this table the value for the heavier minus the lighter nucleus is given. The first error is derived from the error of the experimental energy, whereas the second one results from uncertainties in calculating the nuclear polarization corrections. As an upper limit, this second error was estimated assuming a 10% error for the larger of the nuclear polarization corrections of the two isotopes (see Table IIIA). For deformed nuclei (see Table IIIC), $\frac{1}{3}$ of the larger error of the two isotopes—as assigned to the absolute values of $R^{\mu}_{k\alpha}$—is given [Ri76].

TABLE VI. *Confit* Matrices for Muonic $2p \rightarrow 1s$ Energy Differences of Isotones, $10 \leq N \leq 82$

See explanation for Table IV.

TABLE VII. Differences of Barrett Radii for Isotones, $8 \leq N \leq 126$

Same explanation as for Table V, but based on the energy differences given in Table VI and the parameters α and k in Tables IIIA or IIIC. Shifts between isotones which have not been measured simultaneously are marked by an asterisk. In these cases the given experimental error is just the quadratic sum of the errors assigned to the absolute values of the $R^{\mu}_{k\alpha}$ listed in Table IIIA or Table IIIC. Not all measured isotone shifts have been listed. Those values can be deduced in combination with Table V.

TABLE VIII. Charge Density Distribution Parameters from Elastic Electron Scattering

Data published subsequent to Ref. 4, from 1987 until 1993, are given in this Table. The normalization of the charge distribution is such that $4\pi \int \rho(r) r^2 dr = Ze$.

model

FB Model-independent analysis by means of a Fourier–Bessel expansion for the charge distribution.

SOG Model-independent analysis by means of an expansion for the charge distribution as a sum of Gaussians.

EXPLANATION OF TABLES continued

2pF — Two-parameter Fermi model:

$$\rho(r) = \rho_0/(1 + \exp((r - c)/a)).$$

3pF — Three-parameter Fermi model:

$$\rho(r) = \rho_0(1 + wr^2/c^2)/(1 + \exp((r - c)/a)).$$

2pG — Two-parameter Gaussian model:

$$\rho(r) = \rho_0/(1 + \exp((r^2 - c^2)/a^2)).$$

3pG — Three-parameter Gaussian model:

$$\rho(r) = \rho_0(1 + wr^2/c^2)/(1 + \exp((r^2 - c^2)/a^2)).$$

$\langle r^2\rangle^{1/2}$ — Rms radius of the charge distribution, Eq. (1.2).

c, a, w — Parameters of the given charge distribution.

q-range — The momentum-transfer range covered by the data used in the analysis.

Ref. — Source of the tabulated data, keyed to the list of references following the Tables.

TABLE IX. Fourier–Bessel Coefficients from Elastic Electron Scattering

Data published subsequent to Ref. 4, from 1987 until 1993, are given in this Table.

$\langle r^n\rangle^{1/n}$, $n = 2, 4, 6$ — Radial moments of the charge distribution, Eq. (1.3).

$R^e_{k\alpha}$ — Barrett equivalent radius calculated from the given charge distribution with α and k taken from Table IIIA.

a1 · · · a18 — List of the Fourier–Bessel coefficients a_ν, with $\nu = 1$ up to 18. The coefficients are defined by

$$\rho(r) = \sum_\nu a_\nu j_0(\nu\pi r/R_{\text{cut}}) \quad \text{for } r \leq R_{\text{cut}}$$

$$\rho(r) = 0 \quad \text{for } r > R_{\text{cut}}$$

The normalization is chosen such that

$$4\pi \int \rho(r) r^2 dr = Ze.$$

The momentum-transfer range (q range) covered by the data used in the analysis is given in Table VIII.

R_{cut} — Value of the cutoff radius, beyond which the charge density is assumed to be zero.

Ref. — Source of the tabulated data, keyed to the list of references following the Tables.

TABLE X. King Plots: Optical versus Combined Muonic and Elastic Electron Scattering Data

The plots in this Table refer to the same element and transition combinations as in Table I.

$R^e_{k\alpha}$ (A_{ref}) — Barrett radius of the reference isotope.

C_i/C_1 — Ratios of Seltzer coefficients (see Eq. (2.7)).

EXPLANATION OF TABLES continued

λ_{proj}	Wavelength of the selected optical line against which all other optical lines have been projected (see Section 2 and Table I).
F_i	Electronic factor for the transition i (see Eqs. (2.6) and (6.1)).
$FS^{A-A'}$	Field shift for the standard isotope pair, that is, between isotopes $A = A_{std}$ and $A' = A'_{std}$.
$MS^{A-A'}$	Total mass shift for the standard isotope pair.
$NMS^{A-A'}$	Normal mass shift for the standard isotope pair.
$SMS^{A-A'}$	Specific mass shift for the standard isotope pair.
χ^2/D.F.	Chi squared per degree of freedom for the combined analysis.
V_n, n = 2, 4, 6	V_n values (see Eq. (5.6) for definition and see Note at the end of each plot). The V_n factors are used *without error* (see Section 6). Superscript e on the mass number of the isotope indicates V_n values derived from experiment.
$\delta\langle r^2\rangle_{o\mu e}$	Differences of the mean-square radii ($=\langle r^2\rangle^A - \langle r^2\rangle^{A'}$) resulting from the combined analysis for the isotope pair A–A'.
HM	Contribution of the higher radial moments $\langle r^4\rangle$ and $\langle r^6\rangle$ to the nuclear λ parameter (see Eq. (2.7)). HM is always negative; therefore $\lambda < \delta\langle r^2\rangle$.
x axis: $X_{\mu e}$	Plotted is the reduced λ (Eq. (7.4)) $$\lambda_{\mu e}^{AA'} \frac{A_{std} - A'_{std}}{A_{std} A'_{std}} \frac{AA'}{A - A'},$$ with $\lambda_{\mu e}^{AA'}$ taken from combined muonic and electron scattering data.
y axis: Y_{optic}	Plotted is the reduced IS (Eq. (7.3)) $$\delta\nu_i^{AA'} \frac{A_{std} - A'_{std}}{A_{std} A'_{std}} \frac{AA'}{A - A'},$$ with $\delta\nu_i^{AA'}$ the measured, projected optical isotope shift between isotopes A and A'. The slope of the regression line gives the electronic factor F_i. The intersection of the line with the y axis gives the MS for the standard pair: $\delta\nu_{i,MS}^{A_{std}A'_{std}}$ (see Eq. (2.3)). Subtracting the calculated NMS from the MS determines the SMS.

TABLE XI. Electronic Factor *F* and Specific to Normal Mass Shift Ratio SMS/NMS for Projected Optical Lines

λ	Wavelength of the optical reference line (see Tables I and X) for the indicated element.
type of transition	Orbital designations for lower → upper state.
SMS/NMS	Ratio of specific to normal mass shift for the optical reference line.

EXPLANATION OF TABLES continued

F_i	Electronic factor F_i (see Eqs. (2.6) and (6.1)) for the given optical line.
calc. (MCDF)	Electronic factor based on multiconfiguration Dirac–Fock calculations. The errors, when quoted, result from an optical King plot (see Appendix) where the line used in the combined analysis is projected on the line for which MCDF calculations are made. For the above three sets of data, errors in the last quoted digits are given in parentheses following the respective values.
Ref.	Source of MCDF calculation, keyed to the list of References for Tables.

Semiempirical values for the electronic factor can be found in [Au87] and references therein.

TABLE XII. Root-Mean-Square Charge Radii from the Combined Analysis of Optical, Muonic, and Elastic Electron Scattering Data

$\langle r^2\rangle_{o\mu e}^{1/2}$	Rms radius from a combined analysis of optical (o), muonic (μ), and electron (e) scattering data. The error for the last digits, given in parentheses, does not include uncertainties from the V_n factors.
$\Delta\langle r^2\rangle^{1/2}$	Difference between the rms radius resulting from electron scattering and muonic data and the rms radius from the combined analysis: $$\Delta\langle r^2\rangle^{1/2} = \langle r^2\rangle_{\mu e}^{1/2} - \langle r^2\rangle_{o\mu e}^{1/2}.$$

The $\langle r^2\rangle_{o\mu e}^{1/2}$ are the results of a least-squares adjustment of the $\delta\langle r^2\rangle_{o\mu e}$ taken from Table X. The $\langle r^2\rangle_{\mu e}^{1/2}$ are obtained directly from the $R_{k\alpha}^{\mu}$ listed in Tables IIIA and IIIC with the help of the V_2 factors from Table X (see Eq. (5.6)). Radii for radioactive isotopes of lead are from a separate analysis for the nonprojected isotope shifts given in Table I.

TABLE I. Observed (Projected) Optical Isotope Shifts of Selected Elements

See page 194 for Explanation of Tables

Z element transition (lower→upper) wavelength wavenumber observed isot. positions	A	$\delta\nu_{proj}$ [MHz]	references
20 calcium $4s^2\ {}^1S_0 \rightarrow 4s5s\ {}^1S_0$ $2 \cdot 599.9nm \quad 33317.3cm^{-1}$ 40 42 43 44 46 48 ν 0 1 2 GHz	40 42 43 44 46 48	0 (0) 607.08 (.12) 907.13 (.12) 1170.08 (.11) 1705.28 (.30) 2194.08 (.24)	Be80, An82, Pa84, As91, Ma92b
36 krypton $4p^5\ 5s[3/2]^\circ_2 \rightarrow 5p[5/2]_2$ $810.7nm \quad 12335.7cm^{-1}$ 78 80 82 83 84 86 ν 0 100 MHz 200	78 80 82 83 84 86	-80.2 (0.6) 0 (0) 77.2 (0.6) 125.9 (2.1) 143.4 (1.1) 213.1 (1.3)	Ca90
38 strontium $5s^2\ {}^1S_0 \rightarrow 5s6p\ {}^1P^\circ_1$ $293.2nm \quad 34098.4cm^{-1}$ 84 86 87 88 ν -400 -200 MHz 0	84 86 87 88	-474.06 (0.05) -224.72 (0.05) -93.62 (0.06) 0 (0)	El83, Lo83, As84, An85, Bu85, An87
40 zirconium $4d^2\ 5s^2\ a^3F_2 \rightarrow 5s5p\ z^3F^\circ_2$ $613.46nm \quad 16296.5cm^{-1}$ 96 94 92 90 ν -400 -200 MHz 0	90 91 92 94 96	0 (0) *) -210.7 (0.6) -374.1 (1.0) -501.1 (1.0)	Ha88, Ha92, La93

*) The optical measurements for this isotope heavily disagree

TABLE I. Observed (Projected) Optical Isotope Shifts of Selected Elements

See page 194 for Explanation of Tables

42 molybdenum $4d^5\ 5s\ a^5S_2 \rightarrow 5p\ z^5P^o_3$ 550.6nm 18155.3cm^{-1} 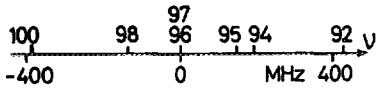	92 94 95 96 97 98 100	419.7 (6.0) 188.9 (3.0) 146.9 (3.0) 0 (0) 0.0 (3.0) -134.9 (3.0) -374.7 (6.0)	Au78, Br84, O186
62 samarium $4f^6\ 6s^2\ ^7F_1 \rightarrow 6s6p\ ^7F^o_0$ 570.68nm 17518.27cm^{-1} 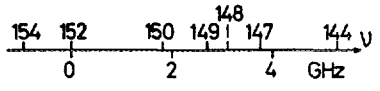	144 147 148 149 150 152 154	5322.6 (1.3) 3749.4 (0.8) 3097.2 (0.8) 2697.0 (0.8) 1801.1 (0.8) 0 (0) -990.6 (1.1)	Ha67, Br79, Br80, En90, Wa90
64 gadolinium $4f^7\ 5d6s^2\ ^9D^o_2 \rightarrow 6s6p\ ^9F_2$ 575.188nm 17380.83cm^{-1} 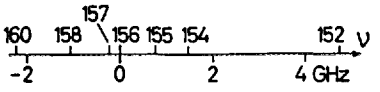	154 155 156 157 158 160	1442.8 (0.6) 737.4 (0.4) 0 (0) -205.3 (0.4) -1079.7 (0.4) -2200.0 (0.3)	Kr85, Du90, Ji90, Kr90
82 lead $6p^2\ ^3P_0 \rightarrow 6p7s\ ^3P^o_1$ 283.3nm 35287.2cm^{-1} 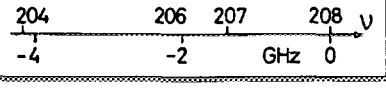	196 197 198 199 200 201 202 203 204* 205 206* 207* 208* 209 210 211 212 214	-11441 (30) -11402 (19) -9848 (3.5) -9748 (9) -8094.1 (3.5) -7727.6 (5.0) -6193.7 (3.5) -5749.0 (5.0) -4211.8 (2.5) -3712.6 (3.0) -2227.1 (2.5) -1390.9 (2.5) 0 (0) 1767 (9) 3973.7 (3.5) 5648.2 (5.6) 7815 (30) 11503 (20)	St52, Bl58, Th83, An86, Bu88

*) stable isotopes, projected values. From the investigated lighter radioactive isotopes (190 through 203) only those are given here, where the line 283.3nm was investigated. The shifts for the radioactive isotopes were not projected, but their values for the stable isotopes agree well with the projected values.

TABLE II. Observed $K\alpha$ X-Ray Isotope Shifts δE and Charge Radius Variations λ

See page 194 for Explanation of Tables

Isotope Pair	$\delta E^{AA'}_{Coul.}$ [meV]	$-\lambda^{AA'}$ [fm^2]	Ref.
$^{92-100}Mo$	35.0 ± 5.0	1.03 ± 0.15	[Se69]
$^{94-100}Mo$	31.0 ± 8.0	0.91 ± 0.23	[Se69]
$^{116-124}Sn$	35.0 ± 1.3	0.414 ± 0.016	[Ch68]
$^{121-123}Sb$	1.8 ± 1.0	0.02 ± 0.01	[Ry72]
$^{124-126}Te$	8.4 ± 2.4	0.081 ± 0.023	[Su69]
$^{126-128}Te$	5.7 ± 2.4	0.055 ± 0.023	[Su69]
$^{128-130}Te$	4.9 ± 2.4	0.047 ± 0.023	[Su69]
$^{134-135}Ba$	-6.3 ± 2.0	-0.040 ± 0.013	[Ha67]
$^{134-136}Ba$	-3.4 ± 2.0	-0.022 ± 0.013	[Ha67]
$^{136-137}Ba$	-0.2 ± 2.0	-0.001 ± 0.013	[Ha67]
$^{136-138}Ba$	9.0 ± 2.0	0.057 ± 0.013	[Ha67]
$^{140-142}Ce$	51.5 ± 1.9	0.274 ± 0.010	[Ei70a]
$^{142-143}Nd$	27.7 ± 5.1	0.116 ± 0.021	[Le73]
$^{142-144}Nd$	68.7 ± 2.6	0.289 ± 0.011	[Le73]
$^{143-144}Nd$	41.0 ± 3.6	0.172 ± 0.015	[Le73]
$^{144-145}Nd$	29.8 ± 4.2	0.126 ± 0.018	[Le73]
$^{144-146}Nd$	55.4 ± 7.7	0.233 ± 0.033	[Bh69],[Le73]
	64.0 ± 11.0	0.269 ± 0.046	[Su67]
$^{145-146}Nd$	25.5 ± 8.8	0.107 ± 0.037	[Bh69],[Le73]
$^{146-148}Nd$	65.4 ± 8.0	0.275 ± 0.034	[Bh69],[Le73]
	66.0 ± 10.0	0.277 ± 0.042	[Su67]
$^{148-150}Nd$	95.8 ± 5.0	0.403 ± 0.021	[Bh69],[Le73]
	110.0 ± 13.0	0.466 ± 0.055	[Su67]
$^{144-148}Sm$	139.0 ± 24.0	0.478 ± 0.083	[Su67]
$^{147-148}Sm$	49.8 ± 2.9	0.171 ± 0.010	[Le73]
$^{148-149}Sm$	23.2 ± 2.3	0.080 ± 0.008	[Le73]
$^{148-150}Sm$	88.3 ± 3.0	0.303 ± 0.010	[Le73]
	102.0 ± 15.0	0.350 ± 0.051	[Su67]
$^{149-150}Sm$	65.1 ± 3.0	0.224 ± 0.010	[Le73]
$^{150-152}Sm$	119.5 ± 3.5	0.411 ± 0.012	[Le73]
	110.0 ± 16.0	0.378 ± 0.055	[Su67]
$^{152-154}Sm$	64.3 ± 3.8	0.221 ± 0.013	[Le73]
$^{151-153}Eu$	186.0 ± 10.0	0.581 ± 0.031	[Ry72]
$^{154-155}Gd$	39.2 ± 8.1	0.112 ± 0.024	[Bh69]
$^{154-156}Gd$	71.4 ± 8.1	0.203 ± 0.023	[Bh69]
$^{155-156}Gd$	32.2 ± 3.6	0.092 ± 0.013	[Bh69]
$^{156-157}Gd$	10.4 ± 4.4	0.030 ± 0.013	[Bh69]

TABLE II. Observed $K\alpha$ X-Ray Isotope Shifts δE and Charge Radius Variations λ

See page 194 for Explanation of Tables

Isotope Pair	$\delta E^{AA'}_{Coul.}$ [meV]	$-\lambda^{AA'}$ [fm^2]	Ref.
$^{156-158}Gd$	50.6 ± 3.6	0.144 ± 0.010	[Bh69]
$^{157-158}Gd$	40.6 ± 3.7	0.116 ± 0.011	[Bh69]
$^{158-160}Gd$	54.0 ± 3.4	0.154 ± 0.010	[Bh69]
$^{161-162}Dy$	39.4 ± 5.1	0.092 ± 0.012	[Le73]
$^{162-163}Dy$	4.2 ± 3.3	0.010 ± 0.008	[Le73]
$^{162-164}Dy$	55.6 ± 3.7	0.130 ± 0.009	[Le73]
	58.1 ± 3.3	0.136 ± 0.008	[Ei70b]
$^{163-164}Dy$	51.4 ± 4.7	0.120 ± 0.011	[Le73]
$^{166-168}Er$	69.5 ± 4.5	0.135 ± 0.009	[Bh69]
$^{168-170}Er$	80.0 ± 6.1	0.155 ± 0.012	[Bh69]
$^{170-171}Yb$	48.0 ± 20.2	0.077 ± 0.032	[Le73]
$^{170-172}Yb$	101.4 ± 11.6	0.163 ± 0.019	[Le73]
$^{171-172}Yb$	53.4 ± 8.6	0.086 ± 0.014	[Le73]
$^{172-173}Yb$	31.2 ± 16.9	0.050 ± 0.027	[Le73]
$^{172-174}Yb$	88.0 ± 8.4	0.141 ± 0.013	[Le73]
$^{173-174}Yb$	56.8 ± 20.6	0.091 ± 0.033	[Le73]
$^{174-176}Yb$	65.5 ± 7.4	0.103 ± 0.012	[Le73]
$^{178-180}Hf$	77.4 ± 5.3	0.103 ± 0.007	[Bh69]
$^{182-184}W$	92.3 ± 10.5	0.102 ± 0.012	[Ch68]
$^{184-186}W$	60.0 ± 8.0	0.066 ± 0.009	[Ch68]
$^{200-204}Hg$	254.0 ± 37.0	0.162 ± 0.024	[Ch68]
$^{204-206}Pb$	200.0 ± 38.0	0.106 ± 0.020	[Le73]
	186.0 ± 20.0	0.099 ± 0.011	[Bo83]
$^{204-208}Pb$	386.0 ± 42.0	0.205 ± 0.022	[Le73]
	414.0 ± 17.0	0.220 ± 0.009	[Bo83]
		0.2175 ± 0.0085 *	[Bo83]
$^{206-207}Pb$	50.0 ± 20.0	0.027 ± 0.011	[Le73]
	78.0 ± 14.0	0.041 ± 0.010	[Bo83]
$^{206-208}Pb$	186.0 ± 18.0	0.099 ± 0.010	[Ch68],[Le73]
	228.0 ± 14.0	0.121 ± 0.007	[Bo83]
		0.113 ± 0.008 *	[Bo83]
$^{207-208}Pb$	136.0 ± 25.0	0.072 ± 0.013	[Le73]
	150.0 ± 14.0	0.080 ± 0.007	[Bo83]
		0.0780 ± 0.0065 *	[Bo83]
$^{235-238}U$	1800 ± 200	0.383 ± 0.044	[Br65]

* Weighted average of the data-sets from [Le73] and [Bo83]

TABLE IIIA. Muonic $2p \rightarrow 1s$ Transition Energies and Barrett Radii for $Z < 60$ and $Z > 77$

See page 194 for Explanation of Tables

Isotope	$E_{exp.}$ [keV]	$E_{theo.}$ [keV]	NPol [keV]	c [fm]	$\langle r^2 \rangle^{1/2}_{model}$ [fm]	α [1/fm]	k	C_z [am/eV]	$R^{\mu}_{k\alpha}$ [fm]	Ref.
$^{9}Be^{\dagger}$	33.402 10	33.402	0.001	1.7890 3700	2.390	0.0420	2.1160	-20.80	3.0725 (2080;60)	[Sc80a]
$^{nat}B^{\dagger}$	52.257 7	52.262	0.001	1.9280 900	2.452	0.0440	2.1190	-8.600	3.1549 (602;30)	[Sc80a]
^{12}C	75.2582 5	75.2582	0.0025	2.0005 23	2.468	0.0208	2.0231	-4.141	3.1996 (21;33)	[Ru84a] [Sc82]
$^{13}C^{\ddagger}$	75.3127 40	75.3127	0.0025	1.9958 187	2.466	0.0208	2.0231	-4.135	3.1967 (165;31)	[Sc82] [Ru84a]
$^{14}C^{\ddagger}$	75.3514 30	75.3514	0.0025	2.0445 137	2.492	0.0208	2.0234	-4.095	3.2273 (123;29)	[Sc82] [Ru84a]
$^{nat}N^{\dagger}$	102.403 5	102.404	0.003	2.1510 230	2.560	0.0470	2.1120	-2.200	3.2921 (110;20)	[Sc80a]
^{16}O	133.535 2	133.534	0.005	2.4130 26	2.693	0.0272	2.0330	-1.287	3.4694 (26;22)	[Fr92]
^{18}O	133.572 9	133.572	0.005	2.5540 130	3.586	0.0258	2.0287	-1.258	3.5680 (113;21)	[Fr92]
^{19}F	168.515 2	168.515	0.009	2.7759 15	2.898	0.0300	2.0392	-0.782	3.7291 (16;24)	[Fr92]
^{20}Ne	207.282 5	207.282	0.019	2.9589 24	3.006	0.0329	2.0445	-0.516	3.8656 (26;33)	[Fr92]
^{21}Ne	207.429 4	207.430	0.018	2.8941 20	2.967	0.0330	2.0441	-0.521	3.8163 (21;31)	[Fr92]
^{22}Ne	207.512 4	207.512	0.018	2.8706 11	2.954	0.0330	2.0439	-0.522	3.7986 (21;31)	[Fr92]

† Here, all data are taken from the quoted reference
‡ Given energy based on E(^{12}C) [Ru84a] and [Sc82]

TABLE IIIA. Muonic $2p \rightarrow 1s$ Transition Energies and Barrett Radii for $Z < 60$ and $Z > 77$

See page 194 for Explanation of Tables

Isotope	$E_{exp.}$ [keV]	$E_{theo.}$ [keV]	NPol [keV]	c [fm]	$\langle r^2 \rangle^{1/2}_{model}$ [fm]	α [1/fm]	k	C_z [am/eV]	$R^{\mu}_{k\alpha}$ [fm]	Ref.
^{23}Na	250.229 2	250.229	0.025	2.9393 7	2.994	0.0360	2.0484	-0.364	3.8492 (7;30)	[Fr92]
^{24}Mg	296.534 2	296.533	0.038	3.0453 5	3.057	0.0389	2.0533	-0.262	3.9291 (5;30)	[Fr92]
^{25}Mg	296.721 3	296.721	0.031	2.9978 7	3.029	0.0390	2.0529	-0.264	3.8924 (8;25)	[Fr92]
^{26}Mg	296.745 3	296.745	0.033	3.0066 7	3.034	0.0390	2.0530	-0.263	3.8992 (8;26)	[Fr92]
^{27}Al	346.828 2	346.827	0.040	3.0554 4	3.063	0.0419	2.0573	-0.196	3.9354 (4;24)	[Fr92]
^{28}Si	400.173 5	400.173	0.055	3.1544 7	3.123	0.0446	2.0621	-0.149	4.0112 (7;25)	[Fr92]
^{29}Si†	400.375 45	400.375	0.053	3.1482 86	3.120	0.0446	2.0620	-0.149	4.0060 (67;26)	[Fr92]
^{30}Si†	400.295 44	400.295	0.051	3.1720 84	3.134	0.0446	2.0622	-0.149	4.0250 (66;26)	[Fr92]
^{31}P	456.800 11	456.803	0.061	3.2646 11	3.190	0.0473	2.0671	-0.116	4.0969 (13;21)	[Sc85]
^{32}S	516.330 12	516.329	0.083	3.3816 6	3.263	0.0498	2.0722	-0.092	4.1892 (11;23)	[Sc85]
^{34}S	516.106 14	516.109	0.079	3.4175 7	3.285	0.0497	2.0726	-0.091	4.2181 (13;22)	[Sc85]
^{36}S	515.981 13	515.981	0.055	3.4411 10	3.300	0.0497	2.0728	-0.091	4.2371 (12;15)	[Sc85]

† Here, all data are taken from the quoted reference

TABLE IIIA. Muonic $2p \rightarrow 1s$ Transition Energies and Barrett Radii for $Z < 60$ and $Z > 77$

See page 194 for Explanation of Tables

Isotope	$E_{exp.}$ [keV]	$E_{theo.}$ [keV]	NPol [keV]	c [fm]	$\langle r^2 \rangle^{1/2}_{model}$ [fm]	α [1/fm]	k	C_z [am/eV]	$R^{\mu}_{k\alpha}$ [fm]	Ref.
^{36}Ar	644.597 24	644.597	0.118	3.5845 18	3.390	0.0548	2.0821	-0.060	4.3515 (14;21)	[Fr82]
^{38}Ar	644.434 24	644.432	0.107	3.6025 17	3.402	0.0547	2.0822	-0.060	4.3664 (14;19)	[Fr82]
^{40}Ar	644.004 25	644.000	0.126	3.6416 18	3.427	0.0546	2.0827	-0.060	4.3986 (15;23)	[Fr82]
$^{39}K^{*}$	713.118 32	713.118	0.119	3.6542 19	3.435	0.0572	2.0866	-0.050	4.4077 (16;18)	[Wo81]
$^{41}K^{*}$	712.769 28	712.769	0.132	3.6815 17	3.452	0.0571	2.0869	-0.050	4.4303 (14;20)	[Wo81]
$^{40}Ca^{*}$	784.180 25	784.180	0.142	3.7221 13	3.478	0.0596	2.0911	-0.042	4.4628 (11;18)	[Wo81]
$^{42}Ca^{*}$	783.369 29	783.369	0.166	3.7690 15	3.508	0.0595	2.0917	-0.042	4.5018 (12;21)	[Wo81]
$^{43}Ca^{*}$	783.811 27	783.811	0.145	3.7477 14	3.495	0.0595	2.0914	-0.042	4.4840 (11;18)	[Wo81]
$^{44}Ca^{*}$	783.156 26	783.156	0.175	3.7843 13	3.518	0.0594	2.0919	-0.042	4.5146 (11;22)	[Wo81]
$^{46}Ca^{*}$	783.817 107	783.817	0.156	3.7537 54	3.498	0.0595	2.0915	-0.042	4.4891 (45;20)	[Wo81]
$^{48}Ca^{*}$	784.487 26	784.487	0.153	3.7231 13	3.479	0.0596	2.0912	-0.042	4.4636 (11;19)	[Wo81]
$^{45}Sc^{**}$	855.185 41	855.184	0.182	3.8279	3.546	0.0619	2.0962	-0.036	4.5499 (15;20)	[He86]
	857.005 41	857.005	0.203	12		0.0618	2.0961	-0.036	4.5499 (15;22)	

* The energy corresponds to the $2p_{3/2} \rightarrow 1s_{1/2}$ transition

** The first (second) energy value corresponds to the $2p_{1/2} \rightarrow 1s_{1/2}$ ($2p_{3/2} \rightarrow 1s_{1/2}$) transition

TABLE IIIA. Muonic $2p \rightarrow 1s$ Transition Energies and Barrett Radii for $Z < 60$ and $Z > 77$

See page 194 for Explanation of Tables

Isotope	$E_{exp.}$ [keV]	$E_{theo.}$ [keV]	NPol [keV]	c [fm]	$\langle r^2 \rangle^{1/2}_{model}$ [fm]	α [1/fm]	k	C_z [am/eV]	$R^{\mu}_{k\alpha}$ [fm]	Ref.
$^{46}Ti^*$	931.944 26	931.994	0.257	3.9201 9	3.606	0.0640	2.1009	-0.031	4.6263 (8;24)	[Wo81]
$^{47}Ti^*$	932.474 25	932.474	0.252	3.9039 9	3.596	0.0641	2.1007	-0.031	4.6126 (8;23)	[Wo81]
$^{48}Ti^*$	932.652 26	932.652	0.241	3.8984 9	3.592	0.0641	2.1007	-0.031	4.6079 (8;22)	[Wo81]
$^{49}Ti^*$	933.426 33	933.426	0.215	3.8705 12	3.574	0.0642	2.1003	-0.031	4.5845 (10;20)	[Wo81]
$^{50}Ti^*$	933.588 26	933.588	0.216	3.8659 10	3.571	0.0642	2.1003	-0.031	4.5806 (8;20)	[Wo81]
$^{51}V^*$	1012.201 26	1012.201	0.245	3.9101 8	3.600	0.0665	2.1044	-0.027	4.6166 (7;20)	[Wo81]
$^{50}Cr^*$	1091.178 27	1091.178	0.333	4.0035 7	3.661	0.0686	2.1092	-0.023	4.6946 (6;23)	[Wo81]
$^{52}Cr^*$	1092.286 21	1092.286	0.299	3.9742 6	3.645	0.0687	2.1088	-0.023	4.6697 (5;21)	[Wo81]
$^{53}Cr^*$	1091.381 25	1091.381	0.302	4.0001 7	3.659	0.0686	2.1092	-0.023	4.6917 (6;21)	[Wo81]
$^{54}Cr^*$	1089.888 31	1089.888	0.318	4.0424 9	3.686	0.0684	2.1097	-0.023	4.7277 (7;22)	[Wo81]
$^{55}Mn^*$	1172.854 34	1172.854	0.364	4.0728 8	3.706	0.0707	2.1136	-0.021	4.7525 (7;23)	[Wo81]

* The energy corresponds to the $2p_{3/2} \rightarrow 1s_{1/2}$ transition.

TABLE IIIA. Muonic $2p \rightarrow 1s$ Transition Energies and Barrett Radii for $Z < 60$ and $Z > 77$

See page 194 for Explanation of Tables

Isotope	$E_{exp.}$ [keV]	$E_{theo.}$ [keV]	NPol [keV]	c [fm]	$\langle r^2 \rangle^{1/2}_{model}$ [fm]	α [1/fm]	k	C_s [am/keV]	$R^{\mu}_{k\alpha}$ [fm]	Ref.
^{54}Fe	1255.849 63	1255.849	0.362	4.0546	3.694	0.0732	2.1170	-18.180	4.7357 (11;20)	[Sh76]
	1260.011 48	1260.011	0.362	8		0.0731	2.1168	-18.150	4.7358 (9;20)	
^{56}Fe	1252.919 58	1252.901	0.403	4.1198	3.738	0.0729	2.1179	-18.170	4.7915 (11;22)	[Sh76]
	1257.047 44	1257.057	0.403	3		0.0728	2.1177	-18.140	4.7915 (8;22)	
^{57}Fe	1251.823 73	1251.771	0.390	4.1442	3.754	0.0728	2.1183	-18.170	4.8124 (13;21)	[Sh76]
	1255.896 56	1255.926	0.391	1		0.0727	2.1181	-18.140	4.8125 (10;21)	
^{58}Fe	1250.381 67	1250.336	0.400	4.1755	3.774	0.0727	2.1187	-18.170	4.8393 (12;22)	[Sh76]
	1254.460 54	1254.489	0.401	9		0.0726	2.1185	-18.140	4.8393 (10;22)	
^{59}Co	1336.553 65	1336.565	0.320	4.1958	3.788	0.0749	2.1224	-16.210	4.8556 (11;16)	[Sh76]
	1341.500 50	1341.493	0.438	8		0.0748	2.1222	-16.170	4.8557 (8;21)	
^{58}Ni	1427.112 60	1427.033	0.436	4.1772	3.776	0.0772	2.1256	-14.520	4.8386 (9;19)	[Sh76]
	1432.534 46	1432.580	0.437	6		0.0771	2.1253	-14.490	4.8386 (7;19)	
^{60}Ni	1423.860 58	1423.835	0.461	4.2328	3.813	0.0770	2.1264	-14.530	4.8865 (8;20)	[Sh76]
	1429.360 45	1429.375	0.461	6		0.0769	2.1261	-14.500	4.8865 (7;20)	
^{61}Ni	1422.849 69	1422.832	0.387	4.2490	3.823	0.0769	2.1266	-14.530	4.9005 (10;17)	[Sh76]
	1428.397 54	1428.408	0.426	7		0.0768	2.1264	-14.500	4.9005 (8;19)	

TABLE IIIA. Muonic $2p \rightarrow 1s$ Transition Energies and Barrett Radii for $Z < 60$ and $Z > 77$

See page 194 for Explanation of Tables

Isotope	$E_{exp.}$ [keV]	$E_{theo.}$ [keV]	NPol [keV]	c [fm]	$\langle r^2 \rangle^{1/2}_{model}$ [fm]	α [1/fm]	k	C_z [am/keV]	$R^{\mu}_{k\alpha}$ [fm]	Ref.
^{62}Ni	1421.342 59	1421.303	0.457	4.2765 6	3.842	0.0768	2.1270	-14.540	4.9242 (9;20)	[Sh76]
	1426.814 45	1426.837	0.458			0.0767	2.1268	-14.510	4.9242 (7;20)	
^{64}Ni	1419.708 63	1419.699	0.436	4.3041 7	3.860	0.0767	2.1274	-14.540	4.9481 (9;19)	[Sh76]
	1425.226 49	1425.231	0.438			0.0766	2.1271	-14.510	4.9481 (7;19)	
^{63}Cu	1508.052 60	1508.049	0.467	4.3376 6	3.883	0.0788	2.1312	-13.120	4.9761 (8;18)	[Sh76]
	1514.452 47	1514.454	0.538			0.0786	2.1310	-13.080	4.9762 (6;21)	
^{65}Cu	1506.147 62	1506.146	0.428	4.3667 6	3.902	0.0786	2.1317	-13.120	5.0014 (8;17)	[Sh76]
	1512.534 49	1512.535	0.489			0.0785	2.1314	-13.090	5.0015 (6;19)	
^{64}Zn	1595.528 59	1595.510	0.608	4.4046 5	3.928	0.0806	2.1355	-11.890	5.0333 (7;22)	[Sh76]
	1602.709 47	1602.721	0.609			0.0805	2.1352	-11.860	5.0334 (6;22)	
^{66}Zn	1593.313 61	1593.336	0.594	4.4349 5	3.948	0.0805	2.1360	-11.900	5.0598 (7;21)	[Sh76]
	1600.553 45	1600.541	0.595			0.0803	2.1357	-11.860	5.0599 (5;21)	
^{68}Zn	1591.521 38	1591.568	0.580	4.4597 3	3.965	0.0804	2.1364	-11.910	5.0814 (5;21)	[Sh76]
	1598.800 32	1598.767	0.581			0.0802	2.1361	-11.870	5.0815 (4;21)	
^{70}Zn	1589.863 180	1589.706	0.614	4.4862 14	3.983	0.0803	2.1368	-11.920	5.1046 (21;22)	[Sh76]
	1596.817 131	1596.900	0.615			0.0801	2.1364	-11.880	5.1047 (15;22)	

TABLE IIIA. Muonic $2p \rightarrow 1s$ Transition Energies and Barrett Radii for $Z < 60$ and $Z > 77$

See page 194 for Explanation of Tables

Isotope	$E_{exp.}$ [keV]	$E_{theo.}$ [keV]	NPol [keV]	c [fm]	$\langle r^2 \rangle^{1/2}_{model}$ [fm]	α [1/fm]	k	C_z [am/keV]	$R^{\mu}_{k\alpha}$ [fm]	Ref.
^{69}Ga	1680.775 14	1680.802	0.512	4.5066 1	3.996	0.0823	2.1404	-10.840	5.1214 (2;17)	[Ma83]
	1689.036 12	1689.016	0.567			0.0821	2.1400	-10.810	5.1215 (1;18)	
^{71}Ga	1679.141 14	1679.147	0.526	4.5279 1	4.011	0.0822	2.1407	-10.850	5.1401 (2;17)	[Ma83]
	1687.331 12	1687.327	0.551			0.0820	2.1403	-10.820	5.1402 (1;18)	
^{70}Ge	1769.859 23	1769.865	0.704	4.5687 2	4.039	0.0841	2.1446	-9.925	5.1749 (2;21)	[Si82a]
	1779.070 16	1779.073	0.706			0.0839	2.1442	-9.891	5.1750 (2;21)	
^{72}Ge	1767.835 17	1767.841	0.735	4.5926 2	4.055	0.0840	2.1449	-9.936	5.1959 (2;22)	[Si82a]
	1777.043 12	1777.040	0.738			0.0838	2.1445	-9.902	5.1960 (1;22)	
^{73}Ge	1766.998 34	1767.022	0.682	4.6015 2	4.061	0.0840	2.1451	-9.940	5.2038 (3;20)	[Si82a]
	1776.244 24	1776.232	0.700			0.0837	2.1447	-9.899	5.2039 (2;21)	
^{74}Ge	1765.729 26	1765.702	0.836	4.6185 2	4.072	0.0839	2.1453	-9.947	5.2187 (3;25)	[Si82a]
	1774.881 17	1774.892	0.839			0.0837	2.1449	-9.912	5.2188 (2;25)	
^{76}Ge	1764.778 23	1764.765	0.817	4.6294 1	4.080	0.0838	2.1455	-9.946	5.2283 (2;24)	[Si82a]
	1773.946 15	1773.951	0.819			0.0836	2.1451	-9.912	5.2284 (2;24)	
^{75}As	1857.124 12	1857.130	0.557	4.6527 1	4.096	0.0858	2.1491	-9.132	5.2479 (1;15)	[Ma83]
	1867.664 10	1867.660	0.761			0.0855	2.1486	-9.094	5.2480 (1;21)	

TABLE IIIA. Muonic $2p \rightarrow 1s$ Transition Energies and Barrett Radii for $Z < 60$ and $Z > 77$

See page 194 for Explanation of Tables

Isotope	$E_{exp.}$ [keV]	$E_{theo.}$ [keV]	NPol [keV]	c [fm]	$\langle r^2 \rangle^{1/2}_{model}$ [fm]	α [1/fm]	k	C_z [am/keV]	$R^{\mu}_{k\alpha}$ [fm]	Ref.
^{76}Se	1947.121 21	1947.086	1.028	4.7162 1	4.139	0.0875	2.1532	-8.428	5.3031 (2;26)	[Si82b]
	1958.620 16	1958.641	1.036			0.0872	2.1528	-8.388	5.3032 (1;26)	
^{77}Se	1946.854 20	1946.860	0.784	4.7163 1	4.139	0.0875	2.1532	-8.428	5.3031 (2;20)	[Si82b]
	1958.417 16	1958.413	0.790			0.0872	2.1528	-8.388	5.3033 (1;20)	
^{78}Se	1946.852 17	1946.826	0.941	4.7184 1	4.140	0.0875	2.1533	-8.428	5.3049 (1;24)	[Si82b]
	1958.366 13	1958.381	0.949			0.0872	2.1528	-8.390	5.3051 (1;24)	
^{80}Se	1946.859 14	1946.854	0.866	4.7178 1	4.140	0.0875	2.1533	-8.427	5.3045 (1;22)	[Si82b]
	1958.404 12	1958.407	0.872			0.0872	2.1528	-8.389	5.3046 (1;22)	
^{82}Se	1946.854 23	1946.829	0.808	4.7179 1	4.140	0.0875	2.1533	-8.426	5.3045 (2;21)	[Si82b]
	1958.366 19	1958.383	0.814			0.0872	2.1528	-8.388	5.3047 (2;21)	
^{79}Br	2039.746 20	2039.729	0.728	4.7519 1	4.163	0.0893	2.1570	-7.792	5.3337 (2;17)	[Ma83]
	2052.798 17	2052.810	0.933			0.0890	2.1564	-7.756	5.3338 (1;22)	
^{81}Br	2040.214 24	2040.209	0.651	4.7474 1	4.160	0.0893	2.1569	-7.789	5.3297 (2;15)	[Ma83]
	2053.261 20	2053.265	0.827			0.0890	2.1563	-7.753	5.3299 (2;19)	
^{78}Kr	2130.917 43	2130.896	1.174	4.8099 2	4.203	0.0910	2.1610	-7.242	5.3842 (3;26)	[Ma85]
	2145.180 40	2145.198	1.183			0.0906	2.1604	-7.201	5.3844 (3;26)	

TABLE IIIA. Muonic $2p \rightarrow 1s$ Transition Energies and Barrett Radii for $Z < 60$ and $Z > 77$

See page 194 for Explanation of Tables

Isotope	$E_{exp.}$ [keV]	$E_{theo.}$ [keV]	NPol [keV]	c [fm]	$\langle r^2 \rangle^{1/2}_{model}$ [fm]	α [1/fm]	k	C_s [am/keV]	$R^{\mu}_{k\alpha}$ [fm]	Ref.
^{80}Kr	2131.839 44	2131.810	1.064	4.8019 3	4.198	0.0910	2.1609	-7.235	5.3771 (3;23)	[Ma85]
	2146.091 40	2146.115	1.071			0.0907	2.1603	-7.199	5.3773 (3;23)	
^{82}Kr	2132.696 43	3132.679	0.931	4.7941 2	4.192	0.0911	2.1607	-7.235	5.3701 (3;20)	[Ma85]
	2146.976 40	2146.990	0.938			0.0907	2.1601	-7.195	5.3703 (3;20)	
^{83}Kr	2133.601 52	2133.570	0.683	4.7850 3	4.186	0.0911	2.1606	-7.228	5.3621 (4;15)	[Ma85]
	2148.108 47	2148.133	0.936			0.0908	2.1600	-7.193	5.3622 (3;20)	
^{84}Kr	2133.406 41	2133.330	0.833	4.7883 2	4.188	0.0911	2.1607	-7.230	5.3651 (3;18)	[Ma85]
	2147.574 39	2147.643	0.838			0.0908	2.1601	-7.194	5.3652 (3;18)	
^{86}Kr	2134.191 35	2134.186	0.861	4.7819 2	4.184	0.0911	2.1606	-7.225	5.3594 (3;19)	[Ma85]
	2148.498 34	2148.503	0.866			0.0908	2.1600	-7.189	5.3595 (2;19)	
^{85}Rb	2229.014 12	2229.022	0.770	4.8107 1	4.204	0.0929	2.1641	-6.722	5.3840 (1;16)	[He86] [Ma83]
	2244.964 10	2244.959	0.853			0.0926	2.1634	-6.688	5.3841 (1;17)	
^{87}Rb	2230.030 20	2230.007	0.758	4.8035 1	4.199	0.0930	2.1640	-6.721	5.3775 (1;15)	[He86] [Ma83]
	2245.904 14	2245.915	0.807			0.0926	2.1633	-6.682	5.3777 (1;16)	
^{84}Sr	2321.161 33	2321.176	1.125	4.8654 2	4.241	0.0946	2.1680	-6.285	5.4317 (2;21)	[He86] [Ma83]
	2338.677 24	2338.669	1.136			0.0942	2.1673	-6.247	5.4319 (2;21)	

TABLE IIIA. Muonic $2p \rightarrow 1s$ Transition Energies and Barrett Radii for $Z < 60$ and $Z > 77$

See page 194 for Explanation of Tables

Isotope	$E_{exp.}$ [keV]	$E_{theo.}$ [keV]	NPol [keV]	c [fm]	$\langle r^2 \rangle^{1/2}_{model}$ [fm]	α [1/fm]	k	C_s [am/keV]	$R^{\mu}_{k\alpha}$ [fm]	Ref.
^{86}Sr	2323.151 14	2323.154	0.920	4.8503 1	4.231	0.0946	2.1678	-6.274	5.4183 (1;17)	[He86] [Ma83]
	2340.660 11	2340.658	0.929	1		0.0943	2.1671	-6.240	5.4184 (1;17)	
^{87}Sr	2324.412 62	2324.396	0.724	4.8403 3	4.224	0.0947	2.1676	-6.272	5.4093 (4;14)	[He86] [Ma83]
	2342.009 49	2342.019	0.843	3		0.0943	2.1669	-6.234	5.4095 (3;16)	
^{88}Sr	2324.673 10	2324.677	0.929	4.8399 1	4.224	0.0947	2.1676	-6.272	5.4090 (1;17)	[He86] [Ma83]
	2342.192 08	2342.190	0.937	1		0.0943	2.1669	-6.233	5.4092 (1;18)	
^{89}Y	2420.793 10	2420.789	0.861	4.8672 1	4.243	0.0965	2.1711	-5.867	5.4324 (1;15)	[He86] [Ma83]
	2440.062 9	2440.065	0.867	1		0.0960	2.1703	-5.826	5.4326 (1;15)	
^{90}Zr	2515.368 11	2515.362	0.968	4.9075 1	4.270	0.0981	2.1747	-5.504	5.4675 (1;16)	[He86] [Ma83]
	2536.500 10	2536.505	0.975	1		0.0977	2.1738	-5.469	5.4676 (1;16)	
^{90}Zr†	2515.122 23	2515.118	1.083	4.9011 2	4.272	0.1029	2.1950	-5.510	5.4684 (1;16)	[Ph85]
	2536.237 22	2536.239	0.964	2		0.1029	2.1970	-5.470	5.4683 (1;16)	
^{91}Zr	2511.861 43	2511.860	0.880	4.9288 2	4.285	0.0980	2.1751	-5.513	5.4864 (2;15)	[He86] [Ma83]
	2533.047 33	2533.048	0.957	2		0.0975	2.1742	-5.474	5.4867 (2;16)	
^{92}Zr	2507.227 18	2507.198	0.976	4.9583 1	4.305	0.0978	2.1755	-5.525	5.5129 (1;16)	[He86] [Ma83]
	2528.268 13	2528.283	0.984	1		0.0974	2.1747	-5.488	5.5131 (1;16)	

† Here, all data are taken from the quoted reference

TABLE IIIA. Muonic $2p \rightarrow 1s$ Transition Energies and Barrett Radii for $Z < 60$ and $Z > 77$

See page 194 for Explanation of Tables

Isotope	$E_{exp.}$ [keV]	$E_{theo.}$ [keV]	NPol [keV]	c [fm]	$\langle r^2 \rangle^{1/2}_{model}$ [fm]	α [1/fm]	k	C_z [am/keV]	$R^{\mu}_{k\alpha}$ [fm]	Ref.
^{94}Zr	2501.373 21	2501.363	0.953	4.9945	4.330	0.0976	2.1761	-5.541	5.5453 (1;16)	[He86] [Ma83]
	2522.386 15	2522.391	0.946	1		0.0972	2.1753	-5.503	5.5455 (1;16)	
^{96}Zr	2497.167 49	2497.104	0.959	5.0212	4.349	0.0975	2.1766	-5.553	5.5692 (3;16)	[He86] [Ma83]
	2518.081 36	2518.115	0.966	2		0.0970	2.1757	-5.512	5.5694 (2;16)	
^{93}Nb	2603.418 20	2603.461	0.991	4.9853	4.324	0.0995	2.1789	-5.194	5.5361 (1;15)	[He86] [Ma83]
	2626.680 16	2626.653	1.060	1		0.0990	2.1780	-5.154	5.5363 (1;16)	
^{92}Mo	2706.804 33	2706.806	1.116	4.9754	4.317	0.1014	2.1817	-4.878	5.5264 (2;16)	[Sc80b]
	2732.050 23	2732.049	1.127	1		0.1009	2.1807	-4.840	5.5266 (1;16)	
^{94}Mo	2697.664 23	2697.605	1.191	5.0264	4.353	0.1011	2.1825	-4.899	5.5720 (1;18)	[Sc80b]
	2722.739 17	2722.771	1.203	1		0.1006	2.1815	-4.861	5.5723 (1;18)	
^{95}Mo	2694.931 17	2694.929	1.105	5.0407	4.362	0.1011	2.1828	-4.908	5.5848 (1;16)	[Sc80b]
	2720.072 14	2720.073	1.116	1		0.1005	2.1818	-4.865	5.5851 (1;16)	
^{96}Mo	2689.546 11	2689.542	1.258	5.0711	4.384	0.1009	2.1833	-4.919	5.6122 (1;19)	[Sc80b]
	2714.638 11	2714.642	1.272	1		0.1003	2.1823	-4.877	5.6125 (1;19)	
^{97}Mo	2688.468 20	2688.456	0.995	5.0757	4.387	0.1009	2.1834	-4.922	5.6163 (1;15)	[Sc80b]
	2713.671 16	2713.679	1.139	1		0.1003	2.1824	-4.879	5.6166 (1;17)	

TABLE IIIA. Muonic $2p \rightarrow 1s$ Transition Energies and Barrett Radii for $Z < 60$ and $Z > 77$

See page 194 for Explanation of Tables

Isotope	$E_{exp.}$ [keV]	$E_{theo.}$ [keV]	NPol [keV]	c [fm]	$\langle r^2 \rangle^{1/2}_{model}$ [fm]	α [1/fm]	k	C_z [am/keV]	$R^{\mu}_{k\alpha}$ [fm]	Ref.
^{98}Mo	2683.347 26	2683.335	1.259	5.1054 1	4.407	0.1007	2.1839	-4.933	5.6430 (1;19)	[Sc80b]
	2708.373 19	2708.379	1.272			0.1001	2.1829	-4.890	5.6433 (1;19)	
^{100}Mo	2674.022 26	2673.999	1.398	5.1564 1	4.444	0.1004	2.1848	-4.954	5.6901 (1;21)	[Sc80b]
	2698.955 18	2698.966	1.411			0.0998	2.1838	-4.911	5.6904 (1;21)	
^{96}Ru	2889.893 228	2889.925	1.316	5.0845 1	4.393	0.1044	2.1893	-4.379	5.6224 (10;17)	[Ha89]
	2919.669 29	2919.668	1.332			0.1038	2.1881	-4.339	5.6226 (1;17)	
^{98}Ru	2880.842 530	2881.096	1.389	5.1281 10	4.423	0.1042	2.1900	-4.399	5.6616 (23;18)	[Ha89]
	2910.801 230	2910.754	1.405			0.1035	2.1889	-4.354	5.6620 (10;18)	
^{99}Ru	2877.569 78	2877.585	1.271	5.1448 2	4.435	0.1041	2.1903	-4.405	5.6767 (3;17)	[Ha89]
	2907.233 50	2907.227	1.238			0.1034	2.1892	-4.360	5.6770 (2;16)	
^{100}Ru	2872.289 79	2872.362	1.458	5.1714 2	4.453	0.1039	2.1908	-4.414	5.7007 (4;19)	[Ha89]
	2901.977 62	2901.932	1.472			0.1033	2.1896	-4.373	5.7010 (3;19)	
^{101}Ru	2869.600 63	2869.606	1.034	5.1829 3	4.461	0.1038	2.1910	-4.418	5.7111 (3;14)	[Ha89]
	2899.563 102	2899.548	1.443			0.1032	2.1898	-4.377	5.7114 (5;19)	
^{102}Ru	2864.404 35	2864.412	1.547	5.2110 1	4.481	0.1037	2.1915	-4.431	5.7365 (2;21)	[Ha89]
	2893.906 29	2893.900	1.557			0.1030	2.1903	-4.386	5.7368 (1;20)	

TABLE IIIA. Muonic $2p \rightarrow 1s$ Transition Energies and Barrett Radii for $Z < 60$ and $Z > 77$

See page 194 for Explanation of Tables

Isotope	$E_{exp.}$ [keV]	$E_{theo.}$ [keV]	NPol [keV]	c [fm]	$\langle r^2 \rangle^{1/2}_{model}$ [fm]	α [1/fm]	k	C_z [am/keV]	$R^{\mu}_{k\alpha}$ [fm]	Ref.
^{104}Ru	2856.267 45	2856.265	1.618	5.2516 2	4.509	0.1034	2.1922	-4.445	5.7732 (2;22)	[Ha89]
	2885.657 37	2885.659	1.614			0.1028	2.1910	-4.404	5.7735 (2;22)	
^{103}Rh	2961.294 30	2961.240	1.439	5.2293 1	4.494	0.1053	2.1946	-4.198	5.7521 (1;18)	[Ha89]
	2993.146 22	2993.175	1.431			0.1046	2.1934	-4.153	5.7525 (1;18)	
^{102}Pd	3065.579 109	3065.568	1.517	5.2156 3	4.484	0.1072	2.1972	-3.974	5.7388 (4;19)	[Ha89]
	3100.193 80	3100.199	1.532			0.1064	2.1959	-3.928	5.7392 (3;19)	
^{104}Pd	3057.604 139	3057.606	1.537	5.2509 4	4.509	0.1069	2.1978	-3.985	5.7708 (6;18)	[Ha89]
	3092.152 120	3092.150	1.553			0.1062	2.1965	-3.942	5.7712 (5;18)	
^{105}Pd	3054.538 104	3054.551	0.821	5.2613 4	4.516	0.1069	2.1980	-3.991	5.7802 (4;10)	[Ha89]
	3090.021 149	3089.995	1.764			0.1062	2.1967	-3.948	5.7806 (6;21)	
^{106}Pd	3050.087 76	3050.088	1.619	5.2847 2	4.532	0.1067	2.1984	-3.999	5.8014 (3;19)	[Ha89]
	3084.545 53	3084.544	1.632			0.1060	2.1971	-3.955	5.8017 (2;19)	
^{108}Pd	3042.551 72	3042.504	1.632	5.3184 2	4.556	0.1065	2.1990	-4.012	5.8320 (3;20)	[Ha89]
	3076.847 47	3076.867	1.637			0.1058	2.1976	-3.969	5.8324 (2;20)	
^{110}Pd	3035.646 138	3035.663	1.654	5.3490 3	4.577	0.1064	2.1995	-4.027	5.8597 (6;20)	[Ha89]
	3069.941 88	3069.934	1.643			0.1056	2.1982	-3.980	5.8601 (4;20)	

TABLE IIIA. Muonic $2p \rightarrow 1s$ Transition Energies and Barrett Radii for $Z < 60$ and $Z > 77$

See page 194 for Explanation of Tables

Isotope	$E_{exp.}$ [keV]	$E_{theo.}$ [keV]	NPol [keV]	c [fm]	$\langle r^2 \rangle^{1/2}_{model}$ [fm]	α [1/fm]	k	C_s [am/keV]	$R^{\mu}_{k\alpha}$ [fm]	Ref.
^{107}Ag	3147.135 28	3147.140	1.487	5.3006 1	4.544	0.1084	2.2015	-3.804	5.8149 (1;17)	[Ha89]
	3184.302 21	3184.299	1.485			0.1076	2.2000	-3.759	5.8153 (1;17)	
^{109}Ag	3140.061 31	3140.048	1.483	5.3306 1	4.565	0.1082	2.2020	-3.815	5.8421 (1;17)	[Ha89]
	3177.124 23	3177.131	1.478			0.1074	2.2006	-3.769	5.8425 (1;17)	
^{106}Cd	3251.740 109	3251.659	1.546	5.2875 2	4.534	0.1102	2.2040	-3.611	5.8022 (4;17)	[Fr87]
	3291.755 66	3291.784	1.567			0.1094	2.2025	-3.567	5.8026 (2;17)	
^{108}Cd	3244.736 74	3244.699	1.529	5.3154 2	4.554	0.1101	2.2046	-3.622	5.8275 (3;17)	[Fr87]
	3284.706 61	3284.731	1.547			0.1093	2.2031	-3.577	5.8279 (2;17)	
^{110}Cd	3237.749 47	3237.741	1.556	5.3435 1	4.574	0.1099	2.2051	-3.632	5.8530 (2;17)	[Fr87]
	3277.678 40	3277.684	1.573			0.1091	2.2036	-3.587	5.8534 (1;17)	
^{111}Cd	3235.848 59	3235.873	1.434	5.3506 1	4.579	0.1098	2.2051	-3.636	5.8594 (2;16)	[Fr87]
	3275.805 43	3275.792	1.444			0.1089	2.2035	-3.589	5.8598 (2;16)	
^{112}Cd	3230.988 39	3231.015	1.578	5.3707 1	4.593	0.1096	2.2054	-3.643	5.8777 (1;17)	[Fr87]
	3270.895 30	3270.879	1.596			0.1088	2.2039	-3.598	5.8781 (1;17)	
^{113}Cd	3229.189 53	3229.151	1.393	5.3775 1	4.597	0.1096	2.2056	-3.644	5.8839 (2;15)	[Fr87]
	3268.959 40	3268.980	1.400			0.1088	2.2041	-3.599	5.8843 (1;15)	

TABLE IIIA. Muonic $2p \rightarrow 1s$ Transition Energies and Barrett Radii for $Z < 60$ and $Z > 77$

See page 194 for Explanation of Tables

Isotope	$E_{exp.}$ [keV]	$E_{theo.}$ [keV]	NPol [keV]	c [fm]	$\langle r^2 \rangle^{1/2}_{model}$ [fm]	α [1/fm]	k	C_s [am/keV]	$R^{\mu}_{k\alpha}$ [fm]	Ref.
^{114}Cd	3224.852 31	3224.887	1.576	5.3954 1	4.610	0.1093	2.2056	-3.653	5.9002 (1;17)	[Fr87]
	3264.699 25	3264.677	1.593			0.1085	2.2041	-3.607	5.9006 (1;17)	
^{116}Cd	3219.689 37	3219.718	1.593	5.4164 1	4.625	0.1093	2.2061	-3.661	5.9193 (1;17)	[Fr87]
	3259.454 31	3259.434	1.606			0.1085	2.2046	-3.616	5.9197 (1;17)	
^{113}In	3329.129 397	3328.947	0.928	5.3789 10	4.598	0.1113	2.2084	-3.471	5.8843 (14;10)	[Ja89]
	3372.659 338	3372.789	1.935			0.1105	2.2067	-3.428	5.8846 (12;20)	
^{115}In	3322.991 32	3322.987	0.915	5.4018 1	4.614	0.1112	2.2088	-3.481	5.9051 (1;10)	[Ja89]
	3366.759 21	3366.761	1.933			0.1103	2.2072	-3.434	5.9055 (1;20)	
^{112}Sn	3432.564 60	3432.516	1.537	5.3714 2	4.593	0.1131	2.2109	-3.310	5.8765 (2;15)	[Pi90]
	3478.531 56	3478.572	1.565			0.1121	2.2092	-3.261	5.8770 (2;15)	
^{114}Sn	3426.613 71	3426.266	1.539	5.3943 2	4.609	0.1129	2.2113	-3.317	5.8974 (2;15)	[Pi90]
	3471.921 68	3472.235	1.568			0.1120	2.2096	-3.271	5.8979 (2;15)	
^{116}Sn	3420.091 62	3419.977	1.510	5.4173 2	4.625	0.1128	2.2118	-3.326	5.9183 (2;15)	[Pi90]
	3465.757 58	3465.856	1.539			0.1119	2.2101	-3.280	5.9188 (2;15)	
^{117}Sn	3418.140 63	3418.024	1.407	5.4241 2	4.630	0.1127	2.2119	-3.327	5.9246 (2;14)	[Pi90]
	3463.810 60	3463.914	1.473			0.1118	2.2102	-3.281	5.9250 (2;14)	

TABLE IIIA. Muonic $2p \rightarrow 1s$ Transition Energies and Barrett Radii for $Z < 60$ and $Z > 77$

See page 194 for Explanation of Tables

Isotope	$E_{exp.}$ [keV]	$E_{theo.}$ [keV]	NPol [keV]	c [fm]	$\langle r^2 \rangle^{1/2}_{model}$ [fm]	α [1/fm]	k	C_z [am/keV]	$R^{\mu}_{k\alpha}$ [fm]	Ref.
^{118}Sn	3414.352 112	3414.118	1.554	5.4391 3	4.641	0.1126	2.2121	-3.333	5.9381 (4;15)	[Be93]
	3459.748 95	3459.914	1.584			0.1117	2.2104	-3.286	5.9386 (3;15)	
^{119}Sn	3412.848 61	3412.928	1.452	5.4431 2	4.643	0.1126	2.2122	-3.335	5.9418 (2;14)	[Pi90]
	3458.780 60	3458.703	1.477			0.1117	2.2105	-3.288	5.9423 (2;14)	
^{120}Sn	3408.975 52	3408.849	1.637	5.4588 1	4.655	0.1125	2.2125	-3.340	5.9561 (2;16)	[Pi90]
	3454.453 50	3454.568	1.667			0.1116	2.2108	-3.294	5.9566 (2;16)	
^{122}Sn	3404.231 124	3404.091	1.548	5.4761 3	4.667	0.1124	2.2128	-3.347	5.9718 (4;15)	[Be93]
	3449.638 107	3449.741	1.576			0.1115	2.2111	-3.300	5.9723 (4;15)	
^{124}Sn	3400.182 61	3400.025	1.454	5.4907 2	4.677	0.1123	2.2131	-3.352	5.9853 (2;15)	[Pi90]
	3445.482 57	3445.617	1.481			0.1114	2.2114	-3.305	5.9857 (2;15)	
^{121}Sb	3497.991 58	3498.091	1.354	5.4963 2	4.681	0.1139	2.2159	-3.203	5.9895 (2;13)	[Kl88]
	3547.434 56	3547.342	1.800			0.1130	2.2141	-3.157	5.9899 (2;17)	
^{123}Sb	3494.562 78	3494.553	1.063	5.5078 2	4.689	0.1139	2.2161	-3.209	5.9999 (3;10)	[Kl88]
	3544.247 56	3544.252	2.006			0.1129	2.2143	-3.161	6.0004 (2;19)	
^{122}Te	3586.480 355	3586.453	1.814	5.5368 11	4.710	0.1153	2.2193	-3.078	6.0257 (9;17)	[Sh89]
	3638.459 355	3638.486	1.827			0.1143	2.2174	-3.030	6.0262 (11;17)	

TABLE IIIA. Muonic $2p \rightarrow 1s$ Transition Energies and Barrett Radii for $Z < 60$ and $Z > 77$

See page 194 for Explanation of Tables

Isotope	$E_{exp.}$ [keV]	$E_{theo.}$ [keV]	NPol [keV]	c [fm]	$\langle r^2 \rangle^{1/2}_{model}$ [fm]	α [1/fm]	k	C_z [am/keV]	$R^{\mu}_{k\alpha}$ [fm]	Ref.
^{123}Te	3585.238 38	3585.195	1.635	5.5405	4.712	0.1153	2.2193	-3.081	6.0290 (1;15)	[Sh89]
	3637.191 30	3637.218	1.614	1		0.1143	2.2174	-3.033	6.0295 (1;15)	
^{124}Te	3582.489 27	3582.481	1.791	5.5503	4.719	0.1152	2.2195	-3.083	6.0379 (1;16)	[Sh89]
	3634.444 24	3634.451	1.777	1		0.1142	2.2176	-3.035	6.0384 (1;16)	
^{125}Te	3581.583 34	3581.581	1.580	5.5526	4.721	0.1152	2.2196	-3.084	6.0401 (1;15)	[Sh89]
	3633.531 27	3633.532	1.586	1		0.1142	2.2177	-3.036	6.0406 (1;15)	
^{126}Te	3578.997 26	3578.967	1.642	5.5617	4.727	0.1152	2.2197	-3.089	6.0484 (1;15)	[Sh89]
	3630.878 23	3630.901	1.664	1		0.1142	2.2178	-3.041	6.0489 (1;15)	
^{128}Te	3575.702 30	3575.702	1.617	5.5728	4.735	0.1151	2.2199	-3.092	6.0585 (1;15)	[Sh89]
	3627.576 25	3627.575	1.644	1		0.1141	2.2180	-3.044	6.0590 (1;15)	
^{130}Te	3572.642 21	3572.644	1.601	5.5832	4.742	0.1150	2.2201	-3.095	6.0680 (1;15)	[Sh89]
	3624.472 18	3624.471	1.628	1		0.1140	2.2182	-3.047	6.0685 (1;15)	
^{127}J	3667.361 35	3667.466	0.532	5.5931	4.749	0.1166	2.2229	-2.969	6.0762 (1;5)	[Kl88]
	3723.742 33	3723.650	1.454	1		0.1155	2.2209	-2.919	6.0768 (1;13)	
^{124}Xe	3761.655 36	3761.572	1.554	5.6114	4.762	0.1181	2.2259	-2.853	6.0921 (1;13)	[He85] [He84]
	3820.200 27	3820.251	1.423	1		0.1170	2.2238	-2.804	6.0927 (1;12)	

TABLE IIIA. Muonic $2p \rightarrow 1s$ Transition Energies and Barrett Radii for $Z < 60$ and $Z > 77$

See page 194 for Explanation of Tables

Isotope	$E_{exp.}$ [keV]	$E_{theo.}$ [keV]	NPol [keV]	c [fm]	$\langle r^2 \rangle^{1/2}_{model}$ [fm]	α [1/fm]	k	C_z [am/keV]	$R^{\mu}_{k\alpha}$ [fm]	Ref.
^{126}Xe	3757.900 100	3757.961	1.592	5.6229	4.770	0.1180	2.2261	-2.857	6.1026 (3;14)	[He85] [He84]
	3816.690 100	3816.630	1.517	2		0.1169	2.2240	-2.807	6.1032 (3;13)	
^{128}Xe	3755.586 103	3755.626	1.636	5.6304	4.776	0.1180	2.2262	-2.860	6.1095 (3;14)	[He85] [He84]
	3814.334 103	3814.295	1.603	2		0.1169	2.2241	-2.811	6.1100 (3;14)	
^{129}Xe	3755.135 30	3755.165	1.507	5.6315	4.776	0.1180	2.2263	-2.860	6.1105 (1;13)	[He85] [He84]
	3813.976 27	3813.952	1.598	1		0.1169	2.2242	-2.811	6.1110 (1;13)	
^{130}Xe	3752.245 197	3752.272	1.720	5.6412	4.783	0.1179	2.2264	-2.864	6.1194 (6;15)	[He85] [He84]
	3810.929 197	3810.903	1.711	4		0.1168	2.2243	-2.814	6.1200 (6;15)	
^{131}Xe	3753.060 27	3753.078	1.610	5.6384	4.781	0.1179	2.2264	-2.862	6.1168 (1;14)	[He85] [He84]
	3811.768 24	3811.754	1.629	1		0.1168	2.2243	-2.812	6.1174 (1;14)	
^{132}Xe	3750.737 62	3750.677	1.696	5.6460	4.787	0.1179	2.2265	-2.866	6.1238 (2;15)	[He85] [He84]
	3809.286 42	3809.313	1.719	1		0.1168	2.2244	-2.816	6.1244 (1;15)	
^{134}Xe	3748.217 36	3748.238	1.690	5.6539	4.792	0.1178	2.2267	-2.867	6.1311 (1;15)	[He85] [He84]
	3806.850 27	3806.838	1.722	1		0.1167	2.2246	-2.817	6.1316 (1;15)	
^{136}Xe	3744.956 20	3744.960	1.646	5.6641	4.799	0.1178	2.2269	-2.872	6.1404 (1;14)	[He85] [He84]
	3803.508 18	3803.505	1.681	1		0.1166	2.2248	-2.820	6.1410 (1;14)	

TABLE IIIA. Muonic $2p \rightarrow 1s$ Transition Energies and Barrett Radii for $Z < 60$ and $Z > 77$

See page 194 for Explanation of Tables

Isotope	$E_{exp.}$ [keV]	$E_{theo.}$ [keV]	NPol [keV]	c [fm]	$\langle r^2 \rangle^{1/2}_{model}$ [fm]	α [1/fm]	k	C_z [am/keV]	$R^{\mu}_{k\alpha}$ [fm]	Ref.
^{133}Cs	3840.702 39	3840.670	1.531	5.6710 1	4.804	0.1193	2.2296	-2.759	6.1459 (1;13)	[Kl88]
	3902.636 31	3902.656	1.289			0.1182	2.2274	-2.710	6.1464 (1;11)	
^{134}Ba	3926.785 31	3926.792	1.757	5.7065 1	4.829	0.1207	2.2328	-2.665	6.1776 (1;14)	[Ku83] [Sh82]
	3992.683 24	3992.679	1.755			0.1195	2.2305	-2.614	6.1782 (1;14)	
^{135}Ba	3927.721 75	3927.687	1.548	5.7033 1	4.827	0.1207	2.2327	-2.663	6.1747 (2;12)	[Sh82]
	3993.742 47	3993.755	1.705			0.1195	2.2305	-2.612	6.1753 (1;13)	
^{136}Ba	3925.232 25	3925.214	1.756	5.7111 1	4.833	0.1207	2.2329	-2.667	6.1819 (1;14)	[Ku83] [Sh82]
	3991.093 19	3991.103	1.788			0.1194	2.2306	-2.614	6.1825 (1;14)	
$^{137}Ba^{*}$	3991.390 60	3991.390	1.522 1	5.7103	4.832	0.1194	2.2306	-2.613	6.1818 (2;12)	[Sh82]
^{138}Ba	3922.189 15	3922.166	1.737	5.7200 1	4.839	0.1206	2.2331	-2.669	6.1900 (1;14)	[Fr88a] [Ku83]
	3987.988 14	3988.007	1.781			0.1194	2.2308	-2.618	6.1906 (1;14)	[Sh82]
^{139}La	4011.557 40	4011.595	1.626	5.7423 1	4.855	0.1220	2.2360	-2.575	6.2097 (1;13)	[Re87]
	4081.408 35	4081.379	1.759			0.1208	2.2336	-2.524	6.2103 (1;13)	
^{140}Ce	4097.389 36	4097.361	1.834	5.7739 1	4.877	0.1234	2.2391	-2.492	6.2379 (1;14)	[Re87]
	4170.934 34	4170.959	1.885			0.1221	2.2366	-2.439	6.2385 (1;14)	

* The quoted experimental energy corresponds to the $2p_{3/2} \rightarrow 1s_{1/2}$ transition

TABLE IIIA. Muonic $2p \rightarrow 1s$ Transition Energies and Barrett Radii for $Z < 60$ and $Z > 77$

See page 194 for Explanation of Tables

Isotope	$E_{exp.}$ [keV]	$E_{theo.}$ [keV]	NPol [keV]	c [fm]	$\langle r^2 \rangle^{1/2}_{model}$ [fm]	α [1/fm]	k	C_z [am/keV]	$R^{\mu}_{k\alpha}$ [fm]	Ref.
^{142}Ce	4082.091 127	4082.045	1.739	5.8153	4.907	0.1231	2.2399	-2.505	6.2760 (3;13)	[Re87]
	4155.245 89	4155.267	1.749	2		0.1218	2.2374	-2.452	6.2767 (2;13)	
^{141}Pr	4185.908 27	4185.905	1.726	5.7950	4.892	0.1248	2.2420	-2.409	6.2565 (1;12)	[Re87]
	4263.595 27	4263.598	1.784	1		0.1234	2.2394	-2.355	6.2572 (1;13)	
$^{142}Nd^{\dagger}$	4352.354 51		1.957	5.8249	4.914	0.1244	2.2433	-2.280	6.2842 (1;13)	[Re87]
$^{143}Nd^{\dagger}$	4346.261 148		1.962	5.8400	4.924	0.1244	2.2433	-2.280	6.2981 (3;13)	[Re87]
$^{144}Nd^{\dagger}$	4336.628 58		1.799	5.8636	4.941	0.1244	2.2433	-2.290	6.3197 (1;12)	[Re87]
$^{145}Nd^{\dagger}$	4330.555 152		2.459	5.8805	4.953	0.1244	2.2433	-2.300	6.3351 (3;17)	[Re87]
$^{146}Nd^{\dagger}$	4321.108 61		1.492	5.9017	4.968	0.1244	2.2433	-2.310	6.3546 (1;10)	[Re87]
$^{148}Nd^{\dagger}$	4303.519 73		0.566	5.9436	4.998	0.1244	2.2433	-2.320	6.3930 (2;4)	[Re87]

The data for deformed nuclei (from ^{150}Nd to ^{193}Ir) can be found in TABLE III-C

† The quoted energy corresponds to the $2p_{3/2} \rightarrow 1s_{1/2}$ transition. All data are taken from the quoted reference.

TABLE IIIA. Muonic $2p \rightarrow 1s$ Transition Energies and Barrett Radii for $Z < 60$ and $Z > 77$

See page 194 for Explanation of Tables

Isotope	$E_{exp.}$ [keV]	$E_{theo.}$ [keV]	NPol [keV]	c [fm]	$\langle r^2 \rangle^{1/2}_{model}$ [fm]	α [1/fm]	k	C_z [am/keV]	$R^{\mu}_{k\alpha}$ [fm]	Ref.
^{194}Pt	5520.321 153	5520.342	-0.700	6.5370	5.425	0.1465	2.2981	-1.576	6.9305 (2;23)	[Be90]
	5680.145 163	5680.123	-5.151	2		0.1443	2.2943	-1.506	6.9317 (2;23)	
^{195}Pt	5517.956 214	5518.092	-0.778	6.5407	5.427	0.1465	2.2982	-1.577	6.9339 (3;23)	[Be90]
	5677.304 222	5677.164	-5.839	2		0.1443	2.2944	-1.508	6.9352 (3;23)	
^{196}Pt	5514.916 198	5514.918	-0.125	6.5472	5.432	0.1464	2.2983	-1.578	6.9400 (3;18)	[Be90]
	5675.898 206	5675.896	-3.105	1		0.1443	2.2945	-1.510	6.9412 (3;18)	
^{198}Pt	5507.857 246	5508.135	0.506	6.5597	5.441	0.1463	2.2986	-1.581	6.9518 (4;5)	[Be90]
	5670.357 252	5670.078	-1.170	1		0.1442	2.2947	-1.513	6.9530 (4;5)	
^{197}Au	5591.710 146	5591.790	-0.538	6.5541	5.437	0.1477	2.3004	-1.546	6.9457 (2;6)	[Be90]
	5760.792 153	5760.708	-1.305	1		0.1455	2.2965	-1.477	6.9469 (2;6)	
$^{198}Hg^{*}$	5664.540 255	5664.667	0.593	6.5691	5.448	0.1488	2.3025	-1.516	6.9590 (4;6)	[Bu89] [Ha79]
	5838.270 256	5838.148	-1.174	1		0.1466	2.2986	-1.447	6.9603 (4;6)	
$^{199}Hg^{*}$	5663.150 540	5662.815	-1.254	6.5708	5.449	0.1488	2.3026	-1.517	6.9598 (8;9)	[Gu83] [Ha79]
	5839.480 460	5840.405	2.137	4		0.1466	2.2986	-1.448	6.9612 (7;9)	
$^{200}Hg^{*}$	5656.360 272	5656.618	0.694	6.5824	5.457	0.1487	2.3028	-1.520	6.9714 (4;6)	[Bu89] [Gu83]
	5829.690 255	5829.474	-1.305	3		0.1465	2.2989	-1.450	6.9727 (4;6)	[Ha79]

* Energies are taken from the first quoted reference

TABLE IIIA. Muonic $2p \rightarrow 1s$ Transition Energies and Barrett Radii for $Z < 60$ and $Z > 77$

See page 194 for Explanation of Tables

Isotope	$E_{exp.}$ [keV]	$E_{theo.}$ [keV]	NPol [keV]	c [fm]	$\langle r^2 \rangle^{1/2}_{model}$ [fm]	α [1/fm]	k	C_z [am/keV]	$R^{\mu}_{k\alpha}$ [fm]	Ref.
^{202}Hg*	5649.350	5649.103	1.240			0.1486	2.3030	-1.523	6.9838	[Bu89]
	327			6.5955	5.467				(5;6)	[Ha79]
	5822.550	5822.693	0.364	3		0.1464	2.2991	-1.454	6.9850	
	255								(4;6)	
^{204}Hg*	5641.600	5640.627	2.069			0.1485	2.3033	-1.528	6.9980	[Bu89]
	825			6.6107	5.478				(13;10)	[Ha79]
	5814.420	5814.617	2.040	6		0.1463	2.2994	-1.458	6.9993	
	380								(6;9)	
^{203}Tl†	5726.140	5727.210	3.737			0.1520	2.3170	-1.496	6.9903	[En74]
	670			6.6023	5.472				(10;19)	[Ba72]
	5906.380	5907.500	3.737	6		0.1520	2.3270	-1.426	6.9911	
	670								(10;19)	
^{205}Tl†	5717.210	5717.870	3.737			0.1520	2.3180	-1.500	7.0037	[En74]
	650			6.6173	5.483				(10;19)	[Ba72]
	5897.290	5897.690	3.737	6		0.1520	2.3280	-1.429	7.0042	
	670								(10;19)	
^{204}Pb‡	5796.318	5796.205	2.086			0.1510	2.3071	-1.467	7.0022	[Ke75]
	180			6.6169	5.482				(3;9)	[Be88]
	5982.124	5982.207	2.136	2		0.1487	2.3031	-1.396	7.0036	
	158								(3;9)	
^{206}Pb‡	5787.208	5787.219	2.129			0.1509	2.3073	-1.471	7.0155	[Ke75]
	172			6.6311	5.493				(3;9)	[Be88]
	5972.794	5972.785	2.201	2		0.1486	2.3034	-1.400	7.0169	
	158								(2;9)	
^{207}Pb‡	5783.988	5783.709	2.209			0.1508	2.3074	-1.472	7.0209	[Ke75]
	215			6.6367	5.497				(3;10)	[Be88]
	5968.864	5969.117	2.304	2		0.1486	2.3035	-1.402	7.0222	
	210								(3;10)	
^{208}Pb	5778.058	5778.076	2.945			0.1507	2.3076	-1.474	7.0303	[Be88]
	100			6.6468	5.504				(2;13)	
	5962.854	5962.840	2.718	1		0.1485	2.3037	-1.404	7.0316	
	90								(1;11)	

* Energies are taken from the first quoted reference

† Here, all data are taken from the quoted reference

‡ Energies are based on $E(^{208}Pb)$ [Be88] and ΔE [Ke75]

TABLE IIIA. Muonic $2p \rightarrow 1s$ Transition Energies and Barrett Radii for $Z < 60$ and $Z > 77$

See page 194 for Explanation of Tables

Isotope	$E_{exp.}$ [keV]	$E_{theo.}$ [keV]	NPol [keV]	c [fm]	$\langle r^2 \rangle^{1/2}_{model}$ [fm]	α [1/fm]	k	C_z [am/keV]	$R^{\mu}_{k\alpha}$ [fm]	Ref.
^{209}Bi†	5843.200		3.844			0.1540	2.329	-1.458	7.0501	[En74]
	2.500			6.6869	5.533				(36;18)	[Po68]
	6034.000		3.844	11		0.1540	2.339	-1.386	7.0504	[Ru84b]
	2.200								(30;18)	
^{232}Th										[Zu86]
$^{233,234,235,238}U$										[Zu84]
$^{239,240,242}Pu$										[Zu86]

† Here, all data are taken from the quoted reference

TABLE IIIB. Muonic $2p \rightarrow 1s$ Transition Energies and Relative Intensities of Deformed Nuclei with $60 \leqslant Z \leqslant 77$

See page 194 for Explanation of Tables

Isotope	Transition *Initial state*	*Final state*	Energy [keV] $E_{exp.}$	$E_{theo.}$	Relative Intensity
$^{150}_{60}$Nd	$\|2p_{1/2} \otimes 0^+; \frac{1}{2}^-\rangle$	$\|1s_{1/2} \otimes 0^+; \frac{1}{2}^+\rangle$	4198.118 (55)	4198.086	0.951
	$\|2p_{1/2} \otimes 2^+; \frac{3}{2}^-\rangle$	$\|1s_{1/2} \otimes 2^+; \frac{5}{2}^+\rangle$	4212.492 (55)	4212.460	0.218
	$\|2p_{1/2} \otimes 2^+; \frac{3}{2}^-\rangle$	$\|1s_{1/2} \otimes 0^+; \frac{1}{2}^+\rangle$	4343.963 (55)	4343.926	0.068
	$\|2p_{1/2} \otimes 0^+; \frac{1}{2}^-\rangle$	$\|1s_{1/2} \otimes 2^+; \frac{3}{2}^+\rangle$	4067.077 (55)	4067.046	0.033
	$\|2p_{1/2} \otimes 2^+; \frac{3}{2}^-\rangle$	$\|1s_{1/2} \otimes 2^+; \frac{3}{2}^+\rangle$	4212.918 (55)	4212.886	0.018
	$\|2p_{3/2} \otimes 0^+; \frac{3}{2}^-\rangle$	$\|1s_{1/2} \otimes 0^+; \frac{1}{2}^+\rangle$	4266.573 (52)	4266.593	1.000
	$\|2p_{3/2} \otimes 0^+; \frac{3}{2}^-\rangle$	$\|1s_{1/2} \otimes 2^+; \frac{5}{2}^+\rangle$	4135.104 (52)	4135.127	0.259
	$\|2p_{3/2} \otimes 2^+; \frac{1}{2}^-\rangle$	$\|1s_{1/2} \otimes 2^+; \frac{3}{2}^+\rangle$	4265.684 (52)	4265.704	0.048
	$\|2p_{3/2} \otimes 2^+; \frac{3}{2}^-\rangle$	$\|1s_{1/2} \otimes 2^+; \frac{3}{2}^+\rangle$	4294.264 (52)	4294.284	0.038
$^{155}_{64}$Gd	$\|2p_{1/2} \otimes \frac{3}{2}^-; 2^+\rangle$	$\|1s_{1/2} \otimes \frac{3}{2}^-; 2^-\rangle$	4510.809 (116)	4510.787	1.000
	$\|2p_{1/2} \otimes \frac{3}{2}^-; 1^+\rangle$	$\|1s_{1/2} \otimes \frac{3}{2}^-; 2^-\rangle$	4505.706 (116)	4505.684	0.449
	$\|2p_{1/2} \otimes \frac{3}{2}^-; 1^+\rangle$	$\|1s_{1/2} \otimes \frac{3}{2}^-; 1^-\rangle$	4505.469 (116)	4505.448	0.389
	$\|2p_{1/2} \otimes \frac{3}{2}^-; 2^+\rangle$	$\|1s_{1/2} \otimes \frac{3}{2}^-; 1^-\rangle$	4510.572 (116)	4510.551	0.359
	$\|2p_{1/2} \otimes \frac{5}{2}^-; 2^+\rangle$	$\|1s_{1/2} \otimes \frac{5}{2}^-; 3^-\rangle$	4487.347 (116)	4487.318	0.329
	$\|2p_{1/2} \otimes \frac{5}{2}^-; 2^+\rangle$	$\|1s_{1/2} \otimes \frac{3}{2}^-; 1^-\rangle$	4547.267 (116)	4547.245	0.246
	$\|2p_{1/2} \otimes \frac{5}{2}^-; 3^+\rangle$	$\|1s_{1/2} \otimes \frac{5}{2}^-; 3^-\rangle$	4510.635 (116)	4510.606	0.151
	$\|2p_{3/2} \otimes \frac{3}{2}^-; 1^+\rangle$	$\|1s_{1/2} \otimes \frac{3}{2}^-; 2^-\rangle$	4633.141 (108)	4633.150	0.403
	$\|2p_{3/2} \otimes \frac{3}{2}^-; 3^+\rangle$	$\|1s_{1/2} \otimes \frac{3}{2}^-; 2^-\rangle$	4599.782 (108)	4599.791	0.399
	$\|2p_{3/2} \otimes \frac{3}{2}^-; 3^+\rangle$	$\|1s_{1/2} \otimes \frac{3}{2}^-; 2^-\rangle$	4679.117 (108)	4679.124	0.380
	$\|2p_{3/2} \otimes \frac{3}{2}^-; 1^+\rangle$	$\|1s_{1/2} \otimes \frac{3}{2}^-; 1^-\rangle$	4632.904 (108)	4632.914	0.333
	$\|2p_{3/2} \otimes \frac{3}{2}^-; 2^+\rangle$	$\|1s_{1/2} \otimes \frac{3}{2}^-; 1^-\rangle$	4639.526 (108)	4639.534	0.331
	$\|2p_{3/2} \otimes \frac{3}{2}^-; 0^+\rangle$	$\|1s_{1/2} \otimes \frac{3}{2}^-; 2^-\rangle$	4660.116 (108)	4660.125	0.302
	$\|2p_{3/2} \otimes \frac{3}{2}^-; 3^+\rangle$	$\|1s_{1/2} \otimes \frac{5}{2}^-; 2^-\rangle$	4539.616 (108)	4539.627	0.300
	$\|2p_{3/2} \otimes \frac{3}{2}^-; 3^+\rangle$	$\|1s_{1/2} \otimes \frac{7}{2}^-; 4^-\rangle$	4532.977 (108)	4532.990	0.225
	$\|2p_{3/2} \otimes \frac{3}{2}^-; 3^+\rangle$	$\|1s_{1/2} \otimes \frac{7}{2}^-; 4^-\rangle$	4453.640 (108)	4453.656	0.187
	$\|2p_{3/2} \otimes \frac{5}{2}^-; 2^+\rangle$	$\|1s_{1/2} \otimes \frac{5}{2}^-; 3^-\rangle$	4579.605 (108)	4579.608	0.178
	$\|2p_{3/2} \otimes \frac{3}{2}^-; 2^+\rangle$	$\|1s_{1/2} \otimes \frac{5}{2}^-; 2^-\rangle$	4579.597 (108)	4579.615	0.154
	$\|2p_{3/2} \otimes \frac{3}{2}^-; 3^+\rangle$	$\|1s_{1/2} \otimes \frac{5}{2}^-; 3^-\rangle$	4618.958 (108)	4618.961	0.148
	$\|2p_{3/2} \otimes \frac{3}{2}^-; 2^+\rangle$	$\|1s_{1/2} \otimes \frac{3}{2}^-; 2^-\rangle$	4639.762 (108)	4639.762	0.146

TABLE IIIB. Muonic $2p \rightarrow 1s$ Transition Energies and Relative Intensities of Deformed Nuclei with $60 \leqslant Z \leqslant 77$

See page 194 for Explanation of Tables

Isotope	Transition *Initial state (major component)*	*Final state*	Energy [keV] $E_{exp.}$	$E_{theo.}$	Relative Intensity
$^{157}_{64}$Gd	$\|2p_{1/2} \otimes \frac{3}{2}^-; 2^+\rangle$	$\|1s_{1/2} \otimes \frac{3}{2}^-; 2^-\rangle$	4499.699 (131)	4499.674	1.000
	$\|2p_{1/2} \otimes \frac{3}{2}^-; 1^+\rangle$	$\|1s_{1/2} \otimes \frac{3}{2}^-; 2^-\rangle$	4494.491 (131)	4494.465	0.434
	$\|2p_{1/2} \otimes \frac{3}{2}^-; 1^+\rangle$	$\|1s_{1/2} \otimes \frac{3}{2}^-; 1^-\rangle$	4494.182 (131)	4494.156	0.414
	$\|2p_{1/2} \otimes \frac{3}{2}^-; 2^+\rangle$	$\|1s_{1/2} \otimes \frac{3}{2}^-; 1^-\rangle$	4499.390 (131)	4499.365	0.320
	$\|2p_{1/2} \otimes \frac{5}{2}^-; 2^+\rangle$	$\|1s_{1/2} \otimes \frac{5}{2}^-; 3^-\rangle$	4477.674 (131)	4477.646	0.311
	$\|2p_{1/2} \otimes \frac{5}{2}^-; 2^+\rangle$	$\|1s_{1/2} \otimes \frac{3}{2}^-; 1^-\rangle$	4531.881 (131)	4531.854	0.232
	$\|2p_{1/2} \otimes \frac{5}{2}^-; 3^+\rangle$	$\|1s_{1/2} \otimes \frac{5}{2}^-; 3^-\rangle$	4500.156 (131)	4500.131	0.140
	$\|2p_{1/2} \otimes \frac{5}{2}^-; 3^+\rangle$	$\|1s_{1/2} \otimes \frac{5}{2}^-; 2^-\rangle$	4500.152 (131)	4500.126	0.112
	$\|2p_{3/2} \otimes \frac{3}{2}^-; 3^+\rangle$	$\|1s_{1/2} \otimes \frac{3}{2}^-; 2^-\rangle$	4666.160 (138)	4666.179	0.346
	$\|2p_{3/2} \otimes \frac{3}{2}^-; 1^+\rangle$	$\|1s_{1/2} \otimes \frac{3}{2}^-; 2^-\rangle$	4625.363 (138)	4625.382	0.284
	$\|2p_{3/2} \otimes \frac{3}{2}^-; 2^+\rangle$	$\|1s_{1/2} \otimes \frac{3}{2}^-; 1^-\rangle$	4630.580 (138)	4630.600	0.248
	$\|2p_{3/2} \otimes \frac{3}{2}^-; 3^+\rangle$	$\|1s_{1/2} \otimes \frac{3}{2}^-; 2^-\rangle$	4582.190 (138)	4582.212	0.212
	$\|2p_{3/2} \otimes \frac{3}{2}^-; 3^+\rangle$	$\|1s_{1/2} \otimes \frac{5}{2}^-; 2^-\rangle$	4527.666 (138)	4527.690	0.207
	$\|2p_{3/2} \otimes \frac{3}{2}^-; 1^+\rangle$	$\|1s_{1/2} \otimes \frac{3}{2}^-; 1^-\rangle$	4625.053 (138)	4625.073	0.204
	$\|2p_{3/2} \otimes \frac{3}{2}^-; 0^+\rangle$	$\|1s_{1/2} \otimes \frac{3}{2}^-; 1^-\rangle$	4654.042 (138)	4654.057	0.195
	$\|2p_{3/2} \otimes \frac{3}{2}^-; 3^+\rangle$	$\|1s_{1/2} \otimes \frac{7}{2}^-; 4^-\rangle$	4534.672 (138)	4534.693	0.166
	$\|2p_{3/2} \otimes \frac{3}{2}^-; 3^+\rangle$	$\|1s_{1/2} \otimes \frac{7}{2}^-; 4^-\rangle$	4450.704 (138)	4450.726	0.151
	$\|2p_{3/2} \otimes \frac{3}{2}^-; 2^+\rangle$	$\|1s_{1/2} \otimes \frac{5}{2}^-; 2^-\rangle$	4576.365 (138)	4576.388	0.117
	$\|2p_{3/2} \otimes \frac{3}{2}^-; 2^+\rangle$	$\|1s_{1/2} \otimes \frac{5}{2}^-; 3^-\rangle$	4576.370 (138)	4576.393	0.115
	$\|2p_{3/2} \otimes \frac{3}{2}^-; 2^+\rangle$	$\|1s_{1/2} \otimes \frac{3}{2}^-; 2^-\rangle$	4630.889 (138)	4630.889	0.099

TABLE IIIB. Muonic $2p \rightarrow 1s$ Transition Energies and Relative Intensities of Deformed Nuclei with $60 \leqslant Z \leqslant 77$

See page 194 for Explanation of Tables

Isotope	Transition *Initial state* *Final state* *(major component)*		Energy [keV] $E_{exp.}$	$E_{theo.}$	Relative Intensity
$^{161}_{66}$Dy	$\|2p_{1/2} \otimes \frac{5}{2}^+; 3^-\rangle$	$\|1s_{1/2} \otimes \frac{5}{2}^+; 3^+\rangle$	4645.365 (231)	4645.213	1.000
	$\|2p_{1/2} \otimes \frac{5}{2}^+; 2^-\rangle$	$\|1s_{1/2} \otimes \frac{5}{2}^+; 2^+\rangle$	4641.223 (231)	4641.073	0.621
	$\|2p_{1/2} \otimes \frac{5}{2}^+; 2^-\rangle$	$\|1s_{1/2} \otimes \frac{5}{2}^+; 3^+\rangle$	4641.627 (231)	4641.476	0.372
	$\|2p_{1/2} \otimes \frac{5}{2}^+; 3^-\rangle$	$\|1s_{1/2} \otimes \frac{5}{2}^+; 2^+\rangle$	4644.963 (231)	4644.810	0.244
	$\|2p_{1/2} \otimes \frac{7}{2}^+; 3^-\rangle$	$\|1s_{1/2} \otimes \frac{7}{2}^+; 4^+\rangle$	4632.112 (231)	4631.965	0.215
	$\|2p_{1/2} \otimes \frac{7}{2}^+; 3^-\rangle$	$\|1s_{1/2} \otimes \frac{5}{2}^+; 2^+\rangle$	4675.324 (231)	4675.163	0.160
	$\|2p_{1/2} \otimes \frac{7}{2}^+; 3^-\rangle$	$\|1s_{1/2} \otimes \frac{7}{2}^+; 3^+\rangle$	4632.022 (231)	4631.876	0.135
	$\|2p_{1/2} \otimes \frac{7}{2}^+; 4^-\rangle$	$\|1s_{1/2} \otimes \frac{7}{2}^+; 4^+\rangle$	4647.050 (231)	4646.987	0.121
	$\|2p_{1/2} \otimes \frac{5}{2}^+; 3^-\rangle$	$\|1s_{1/2} \otimes \frac{7}{2}^+; 4^+\rangle$	4601.750 (231)	4601.613	0.108
	$\|2p_{1/2} \otimes \frac{9}{2}^+; 4^-\rangle$	$\|1s_{1/2} \otimes \frac{9}{2}^+; 5^+\rangle$	4618.561 (231)	4618.422	0.095
	$\|2p_{3/2} \otimes \frac{5}{2}^+; 4^-\rangle$	$\|1s_{1/2} \otimes \frac{5}{2}^+; 3^+\rangle$	4813.290 (245)	4813.458	0.434
	$\|2p_{3/2} \otimes \frac{5}{2}^+; 2^-\rangle$	$\|1s_{1/2} \otimes \frac{5}{2}^+; 3^+\rangle$	4780.806 (245)	4780.989	0.387
	$\|2p_{3/2} \otimes \frac{5}{2}^+; 1^-\rangle$	$\|1s_{1/2} \otimes \frac{5}{2}^+; 2^+\rangle$	4819.535 (245)	4819.711	0.378
	$\|2p_{3/2} \otimes \frac{5}{2}^+; 3^-\rangle$	$\|1s_{1/2} \otimes \frac{5}{2}^+; 2^+\rangle$	4785.269 (245)	4785.448	0.325
	$\|2p_{3/2} \otimes \frac{5}{2}^+; 2^-\rangle$	$\|1s_{1/2} \otimes \frac{5}{2}^+; 2^+\rangle$	4780.403 (245)	4780.586	0.164
	$\|2p_{3/2} \otimes \frac{5}{2}^+; 3^-\rangle$	$\|1s_{1/2} \otimes \frac{7}{2}^+; 3^+\rangle$	4741.967 (245)	4742.161	0.125
	$\|2p_{3/2} \otimes \frac{5}{2}^+; 4^-\rangle$	$\|1s_{1/2} \otimes \frac{9}{2}^+; 4^+\rangle$	4710.953 (245)	4711.157	0.111
	$\|2p_{3/2} \otimes \frac{5}{2}^+; 3^-\rangle$	$\|1s_{1/2} \otimes \frac{5}{2}^+; 3^+\rangle$	4785.671 (245)	4785.851	0.099
	$\|2p_{3/2} \otimes \frac{7}{2}^+; 2^-\rangle$	$\|1s_{1/2} \otimes \frac{7}{2}^+; 3^+\rangle$	4808.584 (245)	4808.765	0.097
	$\|2p_{3/2} \otimes \frac{5}{2}^+; 4^-\rangle$	$\|1s_{1/2} \otimes \frac{9}{2}^+; 5^+\rangle$	4711.106 (245)	4711.308	0.096
$^{162}_{66}$Dy	$\|2p_{1/2} \otimes 0^+; \frac{1}{2}^-\rangle$	$\|1s_{1/2} \otimes 0^+; \frac{1}{2}^+\rangle$	4643.252 (57)	4643.264	1.000
	$\|2p_{1/2} \otimes 2^+; \frac{3}{2}^-\rangle$	$\|1s_{1/2} \otimes 2^+; \frac{5}{2}^+\rangle$	4610.120 (57)	4610.113	0.590
	$\|2p_{1/2} \otimes 2^+; \frac{3}{2}^-\rangle$	$\|1s_{1/2} \otimes 0^+; \frac{1}{2}^+\rangle$	4690.973 (57)	4690.973	0.328
	$\|2p_{1/2} \otimes 0^+; \frac{1}{2}^-\rangle$	$\|1s_{1/2} \otimes 2^+; \frac{3}{2}^+\rangle$	4563.041 (57)	4563.048	0.138
	$\|2p_{3/2} \otimes 0^+; \frac{3}{2}^-\rangle$	$\|1s_{1/2} \otimes 0^+; \frac{1}{2}^+\rangle$	4803.151 (60)	4803.165	0.525
	$\|2p_{3/2} \otimes 0^+; \frac{3}{2}^-\rangle$	$\|1s_{1/2} \otimes 2^+; \frac{5}{2}^+\rangle$	4722.294 (60)	4722.305	0.240
	$\|2p_{3/2} \otimes 0^+; \frac{3}{2}^-\rangle$	$\|1s_{1/2} \otimes 2^+; \frac{3}{2}^+\rangle$	4722.937 (60)	4722.948	0.115
	$\|2p_{3/2} \otimes 2^+; \frac{3}{2}^-\rangle$	$\|1s_{1/2} \otimes 2^+; \frac{3}{2}^+\rangle$	4795.185 (60)	4795.185	0.112
	$\|2p_{3/2} \otimes 2^+; \frac{1}{2}^-\rangle$	$\|1s_{1/2} \otimes 2^+; \frac{3}{2}^+\rangle$	4751.244 (60)	4751.229	0.089
	$\|2p_{3/2} \otimes 2^+; \frac{5}{2}^-\rangle$	$\|1s_{1/2} \otimes 2^+; \frac{5}{2}^+\rangle$	4803.426 (60)	4803.408	0.016

TABLE IIIB. Muonic $2p \rightarrow 1s$ Transition Energies and Relative Intensities of Deformed Nuclei with $60 \leq Z \leq 77$

See page 194 for Explanation of Tables

Isotope	Transition *Initial state* (*major component*)	*Final state* (*major component*)	Energy [keV] $E_{exp.}$	$E_{theo.}$	Relative Intensity
$^{163}_{66}$Dy	$\|2p_{1/2} \otimes \frac{5}{2}^-; 3^+\rangle$	$\|1s_{1/2} \otimes \frac{5}{2}^-; 3^-\rangle$	4636.172 (88)	4636.194	1.000
	$\|2p_{1/2} \otimes \frac{5}{2}^-; 2^+\rangle$	$\|1s_{1/2} \otimes \frac{5}{2}^-; 2^-\rangle$	4631.395 (88)	4631.418	0.613
	$\|2p_{1/2} \otimes \frac{5}{2}^-; 2^+\rangle$	$\|1s_{1/2} \otimes \frac{5}{2}^-; 3^-\rangle$	4630.823 (88)	4630.846	0.357
	$\|2p_{1/2} \otimes \frac{7}{2}^-; 3^+\rangle$	$\|1s_{1/2} \otimes \frac{5}{2}^-; 2^-\rangle$	4682.759 (88)	4682.780	0.246
	$\|2p_{1/2} \otimes \frac{5}{2}^-; 3^+\rangle$	$\|1s_{1/2} \otimes \frac{5}{2}^-; 2^-\rangle$	4636.744 (88)	4636.766	0.241
	$\|2p_{1/2} \otimes \frac{7}{2}^-; 3^+\rangle$	$\|1s_{1/2} \otimes \frac{7}{2}^-; 4^-\rangle$	4608.927 (88)	4608.950	0.200
	$\|2p_{1/2} \otimes \frac{7}{2}^-; 4^+\rangle$	$\|1s_{1/2} \otimes \frac{7}{2}^-; 4^-\rangle$	4634.606 (88)	4634.629	0.173
	$\|2p_{1/2} \otimes \frac{7}{2}^-; 4^+\rangle$	$\|1s_{1/2} \otimes \frac{7}{2}^-; 3^-\rangle$	4673.021 (88)	4673.043	0.163
	$\|2p_{1/2} \otimes \frac{7}{2}^-; 3^+\rangle$	$\|1s_{1/2} \otimes \frac{7}{2}^-; 3^-\rangle$	4608.892 (88)	4608.915	0.117
	$\|2p_{1/2} \otimes \frac{7}{2}^-; 4^+\rangle$	$\|1s_{1/2} \otimes \frac{5}{2}^-; 3^-\rangle$	4746.316 (88)	4746.336	0.095
	$\|2p_{3/2} \otimes \frac{5}{2}^-; 2^+\rangle$	$\|1s_{1/2} \otimes \frac{5}{2}^-; 3^-\rangle$	4773.997 (86)	4773.980	0.391
	$\|2p_{3/2} \otimes \frac{5}{2}^-; 1^+\rangle$	$\|1s_{1/2} \otimes \frac{5}{2}^-; 2^-\rangle$	4811.920 (86)	4811.902	0.357
	$\|2p_{3/2} \otimes \frac{5}{2}^-; 4^+\rangle$	$\|1s_{1/2} \otimes \frac{5}{2}^-; 3^-\rangle$	4828.164 (86)	4828.147	0.283
	$\|2p_{3/2} \otimes \frac{5}{2}^-; 3^+\rangle$	$\|1s_{1/2} \otimes \frac{5}{2}^-; 2^-\rangle$	4789.052 (86)	4789.033	0.203
	$\|2p_{3/2} \otimes \frac{5}{2}^-; 2^+\rangle$	$\|1s_{1/2} \otimes \frac{5}{2}^-; 2^-\rangle$	4774.570 (86)	4774.542	0.186
	$\|2p_{3/2} \otimes \frac{5}{2}^-; 3^+\rangle$	$\|1s_{1/2} \otimes \frac{7}{2}^-; 3^-\rangle$	4715.184 (86)	4715.169	0.107
	$\|2p_{3/2} \otimes \frac{5}{2}^-; 4^+\rangle$	$\|1s_{1/2} \otimes \frac{7}{2}^-; 4^-\rangle$	4754.906 (86)	4754.889	0.101
	$\|2p_{3/2} \otimes \frac{5}{2}^-; 3^+\rangle$	$\|1s_{1/2} \otimes \frac{7}{2}^-; 4^-\rangle$	4715.220 (86)	4715.203	0.093
	$\|2p_{3/2} \otimes \frac{5}{2}^-; 4^+\rangle$	$\|1s_{1/2} \otimes \frac{9}{2}^-; 5^-\rangle$	4659.867 (86)	4659.850	0.083
	$\|2p_{3/2} \otimes \frac{5}{2}^-; 3^+\rangle$	$\|1s_{1/2} \otimes \frac{5}{2}^-; 3^-\rangle$	4788.479 (86)	4788.479	0.066
$^{164}_{66}$Dy	$\|2p_{1/2} \otimes 0^+; \frac{1}{2}^-\rangle$	$\|1s_{1/2} \otimes 0^+; \frac{1}{2}^+\rangle$	4632.431 (180)	4632.372	1.000
	$\|2p_{1/2} \otimes 2^+; \frac{3}{2}^-\rangle$	$\|1s_{1/2} \otimes 2^+; \frac{5}{2}^+\rangle$	4601.669 (180)	4601.616	0.612
	$\|2p_{1/2} \otimes 2^+; \frac{3}{2}^-\rangle$	$\|1s_{1/2} \otimes 0^+; \frac{1}{2}^+\rangle$	4675.456 (180)	4675.378	0.302
	$\|2p_{1/2} \otimes 0^+; \frac{1}{2}^-\rangle$	$\|1s_{1/2} \otimes 2^+; \frac{3}{2}^+\rangle$	4559.233 (180)	4559.199	0.155
	$\|2p_{3/2} \otimes 0^+; \frac{3}{2}^-\rangle$	$\|1s_{1/2} \otimes 0^+; \frac{1}{2}^+\rangle$	4791.566 (160)	4791.592	0.560
	$\|2p_{3/2} \otimes 0^+; \frac{3}{2}^-\rangle$	$\|1s_{1/2} \otimes 2^+; \frac{5}{2}^+\rangle$	4717.779 (160)	4717.830	0.229
	$\|2p_{3/2} \otimes 0^+; \frac{3}{2}^-\rangle$	$\|1s_{1/2} \otimes 2^+; \frac{3}{2}^+\rangle$	4718.368 (160)	4718.419	0.133
	$\|2p_{3/2} \otimes 2^+; \frac{3}{2}^-\rangle$	$\|1s_{1/2} \otimes 2^+; \frac{3}{2}^+\rangle$	4786.975 (160)	4786.997	0.128
	$\|2p_{3/2} \otimes 2^+; \frac{1}{2}^-\rangle$	$\|1s_{1/2} \otimes 2^+; \frac{3}{2}^+\rangle$	4742.312 (160)	4742.352	0.097
	$\|2p_{3/2} \otimes 2^+; \frac{5}{2}^-\rangle$	$\|1s_{1/2} \otimes 2^+; \frac{5}{2}^+\rangle$	4794.664 (160)	4794.684	0.022

TABLE IIIB. Muonic $2p \rightarrow 1s$ Transition Energies and Relative Intensities of Deformed Nuclei with $60 \leq Z \leq 77$

See page 194 for Explanation of Tables

Isotope	Transition *Initial state (major component)*	*Final state*	Energy [keV] $E_{exp.}$	$E_{theo.}$	Relative Intensity
$^{166}_{68}$Er	$\|2p_{1/2} \otimes 0^+; \frac{1}{2}^-\rangle$	$\|1s_{1/2} \otimes 0^+; \frac{1}{2}^+\rangle$	4790.858 (123)	4790.869	1.000
	$\|2p_{1/2} \otimes 2^+; \frac{3}{2}^-\rangle$	$\|1s_{1/2} \otimes 2^+; \frac{5}{2}^+\rangle$	4757.059 (123)	4757.072	0.607
	$\|2p_{1/2} \otimes 2^+; \frac{3}{2}^-\rangle$	$\|1s_{1/2} \otimes 0^+; \frac{1}{2}^+\rangle$	4838.748 (123)	4838.757	0.307
	$\|2p_{1/2} \otimes 0^+; \frac{1}{2}^-\rangle$	$\|1s_{1/2} \otimes 2^+; \frac{3}{2}^+\rangle$	4709.645 (123)	4709.658	0.151
	$\|2p_{3/2} \otimes 0^+; \frac{3}{2}^-\rangle$	$\|1s_{1/2} \otimes 0^+; \frac{1}{2}^+\rangle$	4963.709 (157)	4963.689	0.537
	$\|2p_{3/2} \otimes 0^+; \frac{3}{2}^-\rangle$	$\|1s_{1/2} \otimes 2^+; \frac{5}{2}^+\rangle$	4882.020 (157)	4882.003	0.221
	$\|2p_{3/2} \otimes 0^+; \frac{3}{2}^-\rangle$	$\|1s_{1/2} \otimes 2^+; \frac{3}{2}^+\rangle$	4882.496 (157)	4882.478	0.133
	$\|2p_{3/2} \otimes 2^+; \frac{3}{2}^-\rangle$	$\|1s_{1/2} \otimes 2^+; \frac{3}{2}^+\rangle$	4957.499 (157)	4957.479	0.125
	$\|2p_{3/2} \otimes 2^+; \frac{1}{2}^-\rangle$	$\|1s_{1/2} \otimes 2^+; \frac{3}{2}^+\rangle$	4909.981 (157)	4909.964	0.096
	$\|2p_{3/2} \otimes 2^+; \frac{5}{2}^-\rangle$	$\|1s_{1/2} \otimes 2^+; \frac{5}{2}^+\rangle$	4965.379 (157)	4965.365	0.022
$^{167}_{68}$Er	$\|2p_{1/2} \otimes \frac{7}{2}^+; 4^-\rangle$	$\|1s_{1/2} \otimes \frac{7}{2}^+; 4^+\rangle$	4781.145 (120)	4781.031	1.000
	$\|2p_{1/2} \otimes \frac{7}{2}^+; 3^-\rangle$	$\|1s_{1/2} \otimes \frac{7}{2}^+; 3^+\rangle$	4775.911 (120)	4775.798	0.710
	$\|2p_{1/2} \otimes \frac{7}{2}^+; 3^-\rangle$	$\|1s_{1/2} \otimes \frac{7}{2}^+; 4^+\rangle$	4776.377 (120)	4776.262	0.305
	$\|2p_{1/2} \otimes \frac{7}{2}^+; 4^-\rangle$	$\|1s_{1/2} \otimes \frac{7}{2}^+; 3^+\rangle$	4780.680 (120)	4780.567	0.205
	$\|2p_{1/2} \otimes \frac{9}{2}^+; 4^-\rangle$	$\|1s_{1/2} \otimes \frac{7}{2}^+; 3^+\rangle$	4837.005 (120)	4836.887	0.195
	$\|2p_{1/2} \otimes \frac{9}{2}^+; 4^-\rangle$	$\|1s_{1/2} \otimes \frac{9}{2}^+; 5^+\rangle$	4757.831 (120)	4757.716	0.145
	$\|2p_{1/2} \otimes \frac{9}{2}^+; 5^-\rangle$	$\|1s_{1/2} \otimes \frac{7}{2}^+; 4^+\rangle$	4781.279 (120)	4781.164	0.135
	$\|2p_{1/2} \otimes \frac{9}{2}^+; 4^-\rangle$	$\|1s_{1/2} \otimes \frac{9}{2}^+; 4^+\rangle$	4757.814 (120)	4757.698	0.135
	$\|2p_{1/2} \otimes \frac{11}{2}^+; 5^-\rangle$	$\|1s_{1/2} \otimes \frac{9}{2}^+; 4^+\rangle$	4829.394 (120)	4829.275	0.120
	$\|2p_{1/2} \otimes \frac{7}{2}^+; 4^-\rangle$	$\|1s_{1/2} \otimes \frac{9}{2}^+; 4^+\rangle$	4701.508 (120)	4701.396	0.070
	$\|2p_{3/2} \otimes \frac{7}{2}^+; 3^-\rangle$	$\|1s_{1/2} \otimes \frac{7}{2}^+; 4^+\rangle$	4931.087 (99)	4931.115	0.428
	$\|2p_{3/2} \otimes \frac{7}{2}^+; 2^-\rangle$	$\|1s_{1/2} \otimes \frac{7}{2}^+; 3^+\rangle$	4974.696 (99)	4974.720	0.414
	$\|2p_{3/2} \otimes \frac{7}{2}^+; 5^-\rangle$	$\|1s_{1/2} \otimes \frac{7}{2}^+; 4^+\rangle$	4987.093 (99)	4987.120	0.312
	$\|2p_{3/2} \otimes \frac{7}{2}^+; 4^-\rangle$	$\|1s_{1/2} \otimes \frac{7}{2}^+; 3^+\rangle$	4944.811 (99)	4944.840	0.215
	$\|2p_{3/2} \otimes \frac{7}{2}^+; 3^-\rangle$	$\|1s_{1/2} \otimes \frac{7}{2}^+; 3^+\rangle$	4930.624 (99)	4930.651	0.161
	$\|2p_{3/2} \otimes \frac{7}{2}^+; 4^-\rangle$	$\|1s_{1/2} \otimes \frac{9}{2}^+; 5^+\rangle$	4865.619 (99)	4865.651	0.101
	$\|2p_{3/2} \otimes \frac{7}{2}^+; 5^-\rangle$	$\|1s_{1/2} \otimes \frac{9}{2}^+; 5^+\rangle$	4907.456 (99)	4907.485	0.076
	$\|2p_{3/2} \otimes \frac{7}{2}^+; 4^-\rangle$	$\|1s_{1/2} \otimes \frac{7}{2}^+; 5^+\rangle$	4865.638 (99)	4865.669	0.075
	$\|2p_{3/2} \otimes \frac{7}{2}^+; 5^+\rangle$	$\|1s_{1/2} \otimes \frac{11}{2}^+; 6^+\rangle$	4807.786 (99)	4807.815	0.075
	$\|2p_{3/2} \otimes \frac{7}{2}^+; 4^-\rangle$	$\|1s_{1/2} \otimes \frac{7}{2}^+; 4^+\rangle$	4945.274 (99)	4945.304	0.062

TABLE IIIB. Muonic $2p \rightarrow 1s$ Transition Energies and Relative Intensities of Deformed Nuclei with $60 \leq Z \leq 77$

See page 194 for Explanation of Tables

Isotope	Transition *Initial state* (*major component*)	*Final state* (*major component*)	Energy [keV] $E_{exp.}$	$E_{theo.}$	Relative Intensity
$^{168}_{68}$Er	$\|2p_{1/2} \otimes 0^+; \frac{1}{2}^-\rangle$	$\|1s_{1/2} \otimes 0^+; \frac{1}{2}^+\rangle$	4780.221 (89)	4780.270	1.000
	$\|2p_{1/2} \otimes 2^+; \frac{3}{2}^-\rangle$	$\|1s_{1/2} \otimes 2^+; \frac{5}{2}^+\rangle$	4746.844 (89)	4746.843	0.621
	$\|2p_{1/2} \otimes 2^+; \frac{3}{2}^-\rangle$	$\|1s_{1/2} \otimes 0^+; \frac{1}{2}^+\rangle$	4827.057 (89)	4827.052	0.325
	$\|2p_{1/2} \otimes 0^+; \frac{1}{2}^-\rangle$	$\|1s_{1/2} \otimes 2^+; \frac{3}{2}^+\rangle$	4700.586 (89)	4700.637	0.153
	$\|2p_{3/2} \otimes 0^+; \frac{3}{2}^-\rangle$	$\|1s_{1/2} \otimes 0^+; \frac{1}{2}^+\rangle$	4954.628 (101)	4954.656	0.138
	$\|2p_{3/2} \otimes 0^+; \frac{3}{2}^-\rangle$	$\|1s_{1/2} \otimes 2^+; \frac{5}{2}^+\rangle$	4874.415 (101)	4874.447	0.057
	$\|2p_{3/2} \otimes 0^+; \frac{3}{2}^-\rangle$	$\|1s_{1/2} \otimes 2^+; \frac{3}{2}^+\rangle$	4874.993 (101)	4875.023	0.035
	$\|2p_{3/2} \otimes 2^+; \frac{3}{2}^-\rangle$	$\|1s_{1/2} \otimes 2^+; \frac{3}{2}^+\rangle$	4949.263 (101)	4949.231	0.033
	$\|2p_{3/2} \otimes 2^+; \frac{1}{2}^-\rangle$	$\|1s_{1/2} \otimes 2^+; \frac{3}{2}^+\rangle$	4901.723 (101)	4901.790	0.024
	$\|2p_{3/2} \otimes 2^+; \frac{5}{2}^-\rangle$	$\|1s_{1/2} \otimes 2^+; \frac{5}{2}^+\rangle$	4956.622 (101)	4956.565	0.006
$^{170}_{68}$Er	$\|2p_{1/2} \otimes 0^+; \frac{1}{2}^-\rangle$	$\|1s_{1/2} \otimes 0^+; \frac{1}{2}^+\rangle$	4770.262 (98)	4770.201	1.000
	$\|2p_{1/2} \otimes 2^+; \frac{3}{2}^-\rangle$	$\|1s_{1/2} \otimes 2^+; \frac{5}{2}^+\rangle$	4737.271 (98)	4737.182	0.617
	$\|2p_{1/2} \otimes 2^+; \frac{3}{2}^-\rangle$	$\|1s_{1/2} \otimes 0^+; \frac{1}{2}^+\rangle$	4816.399 (98)	4816.308	0.307
	$\|2p_{1/2} \otimes 0^+; \frac{1}{2}^-\rangle$	$\|1s_{1/2} \otimes 2^+; \frac{3}{2}^+\rangle$	4691.756 (98)	4691.699	0.158
	$\|2p_{3/2} \otimes 0^+; \frac{3}{2}^-\rangle$	$\|1s_{1/2} \otimes 0^+; \frac{1}{2}^+\rangle$	4943.467 (108)	4943.552	0.493
	$\|2p_{3/2} \otimes 0^+; \frac{3}{2}^-\rangle$	$\|1s_{1/2} \otimes 2^+; \frac{5}{2}^+\rangle$	4864.337 (108)	4864.426	0.124
	$\|2p_{3/2} \otimes 0^+; \frac{3}{2}^-\rangle$	$\|1s_{1/2} \otimes 2^+; \frac{3}{2}^+\rangle$	4864.960 (108)	4865.051	0.116
	$\|2p_{3/2} \otimes 2^+; \frac{3}{2}^-\rangle$	$\|1s_{1/2} \otimes 2^+; \frac{3}{2}^+\rangle$	4938.771 (108)	4938.830	0.084
	$\|2p_{3/2} \otimes 2^+; \frac{1}{2}^-\rangle$	$\|1s_{1/2} \otimes 2^+; \frac{3}{2}^+\rangle$	4890.855 (108)	4890.934	0.021
	$\|2p_{3/2} \otimes 2^+; \frac{5}{2}^-\rangle$	$\|1s_{1/2} \otimes 2^+; \frac{5}{2}^+\rangle$	4945.814 (108)	4945.805	0.015

TABLE IIIB. Muonic $2p \rightarrow 1s$ Transition Energies and Relative Intensities of Deformed Nuclei with $60 \leq Z \leq 77$

See page 194 for Explanation of Tables

Isotope	Transition *Initial state* *Final state* *(major component)*		Energy [keV] $E_{exp.}$	$E_{theo.}$	Relative Intensity
$^{174}_{70}$Yb	$\|2p_{1/2} \otimes 0^+; \frac{1}{2}^-\rangle$	$\|1s_{1/2} \otimes 0^+; \frac{1}{2}^+\rangle$	4918.175 (74)	4918.169	1.000
	$\|2p_{1/2} \otimes 2^+; \frac{3}{2}^-\rangle$	$\|1s_{1/2} \otimes 2^+; \frac{5}{2}^+\rangle$	4887.344 (74)	4887.349	0.621
	$\|2p_{1/2} \otimes 2^+; \frac{3}{2}^-\rangle$	$\|1s_{1/2} \otimes 0^+; \frac{1}{2}^+\rangle$	4963.997 (74)	4963.971	0.271
	$\|2p_{1/2} \otimes 0^+; \frac{1}{2}^-\rangle$	$\|1s_{1/2} \otimes 2^+; \frac{3}{2}^+\rangle$	4841.498 (74)	4841.529	0.166
	$\|2p_{3/2} \otimes 0^+; \frac{3}{2}^-\rangle$	$\|1s_{1/2} \otimes 0^+; \frac{1}{2}^+\rangle$	5100.914 (79)	5100.898	0.575
	$\|2p_{3/2} \otimes 0^+; \frac{3}{2}^-\rangle$	$\|1s_{1/2} \otimes 2^+; \frac{5}{2}^+\rangle$	5024.261 (79)	5024.276	0.201
	$\|2p_{3/2} \otimes 0^+; \frac{3}{2}^-\rangle$	$\|1s_{1/2} \otimes 2^+; \frac{3}{2}^+\rangle$	5024.238 (79)	5024.258	0.159
	$\|2p_{3/2} \otimes 2^+; \frac{3}{2}^-\rangle$	$\|1s_{1/2} \otimes 2^+; \frac{3}{2}^+\rangle$	5100.184 (79)	5100.205	0.139
	$\|2p_{3/2} \otimes 2^+; \frac{1}{2}^-\rangle$	$\|1s_{1/2} \otimes 2^+; \frac{3}{2}^+\rangle$	5049.073 (79)	5049.091	0.092
	$\|2p_{3/2} \otimes 2^+; \frac{5}{2}^-\rangle$	$\|1s_{1/2} \otimes 2^+; \frac{5}{2}^+\rangle$	5106.883 (79)	5106.881	0.030
$^{180}_{72}$Hf	$\|2p_{1/2} \otimes 0^+; \frac{1}{2}^-\rangle$	$\|1s_{1/2} \otimes 0^+; \frac{1}{2}^+\rangle$	5068.614 (103)	5068.619	1.000
	$\|2p_{1/2} \otimes 2^+; \frac{3}{2}^-\rangle$	$\|1s_{1/2} \otimes 2^+; \frac{5}{2}^+\rangle$	5036.020 (103)	5036.020	0.536
	$\|2p_{1/2} \otimes 2^+; \frac{3}{2}^-\rangle$	$\|1s_{1/2} \otimes 0^+; \frac{1}{2}^+\rangle$	5128.832 (103)	5128.836	0.253
	$\|2p_{1/2} \otimes 0^+; \frac{1}{2}^-\rangle$	$\|1s_{1/2} \otimes 2^+; \frac{3}{2}^+\rangle$	4976.243 (103)	4976.254	0.115
	$\|2p_{3/2} \otimes 0^+; \frac{3}{2}^-\rangle$	$\|1s_{1/2} \otimes 0^+; \frac{1}{2}^+\rangle$	5254.559 (114)	5254.553	0.582
	$\|2p_{3/2} \otimes 0^+; \frac{3}{2}^-\rangle$	$\|1s_{1/2} \otimes 2^+; \frac{5}{2}^+\rangle$	5161.741 (114)	5161.737	0.208
	$\|2p_{3/2} \otimes 0^+; \frac{3}{2}^-\rangle$	$\|1s_{1/2} \otimes 2^+; \frac{3}{2}^+\rangle$	5162.190 (114)	5162.187	0.124
	$\|2p_{3/2} \otimes 2^+; \frac{3}{2}^-\rangle$	$\|1s_{1/2} \otimes 2^+; \frac{3}{2}^+\rangle$	5250.319 (114)	5250.313	0.095
	$\|2p_{3/2} \otimes 2^+; \frac{1}{2}^-\rangle$	$\|1s_{1/2} \otimes 2^+; \frac{3}{2}^+\rangle$	5199.335 (114)	5199.330	0.064
	$\|2p_{3/2} \otimes 2^+; \frac{5}{2}^-\rangle$	$\|1s_{1/2} \otimes 2^+; \frac{5}{2}^+\rangle$	5259.301 (114)	5259.294	0.017

TABLE IIIB. Muonic $2p \rightarrow 1s$ Transition Energies and Relative Intensities of Deformed Nuclei with $60 \leqslant Z \leqslant 77$

See page 194 for Explanation of Tables

Isotope	Transition *Initial state* *Final state* *(major component)*		Energy [keV] $E_{exp.}$	$E_{theo.}$	Relative Intensity
$^{181}_{73}$Ta	$\|2p_{1/2} \otimes \frac{7}{2}^+; 4^-\rangle$	$\|1s_{1/2} \otimes \frac{7}{2}^+; 4^+\rangle$	5142.882 (132)	5142.985	1.000
	$\|2p_{1/2} \otimes \frac{7}{2}^+; 3^-\rangle$	$\|1s_{1/2} \otimes \frac{7}{2}^+; 3^+\rangle$	5138.396 (132)	5138.502	0.693
	$\|2p_{1/2} \otimes \frac{7}{2}^+; 3^-\rangle$	$\|1s_{1/2} \otimes \frac{7}{2}^+; 4^+\rangle$	5136.456 (132)	5136.562	0.380
	$\|2p_{1/2} \otimes \frac{7}{2}^+; 4^-\rangle$	$\|1s_{1/2} \otimes \frac{7}{2}^+; 3^+\rangle$	5144.820 (132)	5144.925	0.302
	$\|2p_{1/2} \otimes \frac{9}{2}^+; 5^-\rangle$	$\|1s_{1/2} \otimes \frac{9}{2}^+; 5^+\rangle$	5133.685 (132)	5133.788	0.189
	$\|2p_{1/2} \otimes \frac{9}{2}^+; 5^-\rangle$	$\|1s_{1/2} \otimes \frac{7}{2}^+; 4^+\rangle$	5269.005 (132)	5269.106	0.151
	$\|2p_{1/2} \otimes \frac{9}{2}^+; 4^-\rangle$	$\|1s_{1/2} \otimes \frac{7}{2}^+; 3^+\rangle$	5341.927 (132)	5342.034	0.111
	$\|2p_{1/2} \otimes \frac{9}{2}^+; 4^-\rangle$	$\|1s_{1/2} \otimes \frac{9}{2}^+; 4^+\rangle$	5204.665 (132)	5204.778	0.097
	$\|2p_{3/2} \otimes \frac{7}{2}^+; 2^-\rangle$	$\|1s_{1/2} \otimes \frac{7}{2}^+; 3^+\rangle$	5356.403 (132)	5356.333	0.448
	$\|2p_{3/2} \otimes \frac{7}{2}^+; 3^-\rangle$	$\|1s_{1/2} \otimes \frac{7}{2}^+; 4^+\rangle$	5307.393 (132)	5307.325	0.438
	$\|2p_{3/2} \otimes \frac{7}{2}^+; 4^-\rangle$	$\|1s_{1/2} \otimes \frac{7}{2}^+; 3^+\rangle$	5232.945 (132)	5232.866	0.326
	$\|2p_{3/2} \otimes \frac{7}{2}^+; 3^-\rangle$	$\|1s_{1/2} \otimes \frac{7}{2}^+; 3^+\rangle$	5309.331 (132)	5309.265	0.234
	$\|2p_{3/2} \otimes \frac{7}{2}^+; 5^-\rangle$	$\|1s_{1/2} \otimes \frac{7}{2}^+; 4^+\rangle$	5325.140 (132)	5325.074	0.210
	$\|2p_{3/2} \otimes \frac{7}{2}^+; 5^-\rangle$	$\|1s_{1/2} \otimes \frac{9}{2}^+; 4^+\rangle$	5189.821 (132)	5189.758	0.204
	$\|2p_{3/2} \otimes \frac{7}{2}^+; 4^-\rangle$	$\|1s_{1/2} \otimes \frac{9}{2}^+; 5^+\rangle$	5095.685 (132)	5095.629	0.153
	$\|2p_{3/2} \otimes \frac{7}{2}^+; 4^-\rangle$	$\|1s_{1/2} \otimes \frac{9}{2}^+; 4^+\rangle$	5095.685 (132)	5095.631	0.113
	$\|2p_{3/2} \otimes \frac{7}{2}^+; 4^-\rangle$	$\|1s_{1/2} \otimes \frac{7}{2}^+; 4^+\rangle$	5231.006 (132)	5230.946	0.091
	$\|2p_{3/2} \otimes \frac{9}{2}^+; 5^-\rangle$	$\|1s_{1/2} \otimes \frac{9}{2}^+; 5^+\rangle$	5276.511 (132)	5276.465	0.073
	$\|2p_{3/2} \otimes \frac{9}{2}^+; 5^-\rangle$	$\|1s_{1/2} \otimes \frac{7}{2}^+; 4^+\rangle$	5411.833 (132)	5411.783	0.055
	$\|2p_{3/2} \otimes \frac{9}{2}^+; 5^-\rangle$	$\|1s_{1/2} \otimes \frac{9}{2}^+; 4^+\rangle$	5276.514 (132)	5276.467	0.037

TABLE IIIB. Muonic $2p \rightarrow 1s$ Transition Energies and Relative Intensities of Deformed Nuclei with $60 \leq Z \leq 77$

See page 194 for Explanation of Tables

Isotope	Transition *Initial state (major component)*	*Final state*	Energy [keV] $E_{exp.}$	$E_{theo.}$	Relative Intensity
$^{182}_{74}$W	$\|2p_{1/2} \otimes 0^+; \frac{1}{2}^-\rangle$	$\|1s_{1/2} \otimes 0^+; \frac{1}{2}^+\rangle$	5227.401 (156)	5227.421	1.000
	$\|2p_{1/2} \otimes 2^+; \frac{3}{2}^-\rangle$	$\|1s_{1/2} \otimes 2^+; \frac{5}{2}^+\rangle$	5196.613 (156)	5196.646	0.486
	$\|2p_{1/2} \otimes 2^+; \frac{3}{2}^-\rangle$	$\|1s_{1/2} \otimes 0^+; \frac{1}{2}^+\rangle$	5296.680 (156)	5296.709	0.227
	$\|2p_{1/2} \otimes 0^+; \frac{1}{2}^-\rangle$	$\|1s_{1/2} \otimes 2^+; \frac{3}{2}^+\rangle$	5127.350 (156)	5127.371	0.092
	$\|2p_{3/2} \otimes 0^+; \frac{3}{2}^-\rangle$	$\|1s_{1/2} \otimes 0^+; \frac{1}{2}^+\rangle$	5419.888 (178)	5419.864	0.580
	$\|2p_{3/2} \otimes 0^+; \frac{3}{2}^-\rangle$	$\|1s_{1/2} \otimes 2^+; \frac{5}{2}^+\rangle$	5319.823 (178)	5319.801	0.192
	$\|2p_{3/2} \otimes 0^+; \frac{3}{2}^-\rangle$	$\|1s_{1/2} \otimes 2^+; \frac{3}{2}^+\rangle$	5319.834 (178)	5319.814	0.132
	$\|2p_{3/2} \otimes 2^+; \frac{3}{2}^-\rangle$	$\|1s_{1/2} \otimes 2^+; \frac{3}{2}^+\rangle$	5414.544 (178)	5414.520	0.090
	$\|2p_{3/2} \otimes 2^+; \frac{1}{2}^-\rangle$	$\|1s_{1/2} \otimes 2^+; \frac{3}{2}^+\rangle$	5367.270 (178)	5367.266	0.052
	$\|2p_{3/2} \otimes 2^+; \frac{5}{2}^-\rangle$	$\|1s_{1/2} \otimes 2^+; \frac{5}{2}^+\rangle$	5423.889 (178)	5423.864	0.013
$^{184}_{74}$W	$\|2p_{1/2} \otimes 0^+; \frac{1}{2}^-\rangle$	$\|1s_{1/2} \otimes 0^+; \frac{1}{2}^+\rangle$	5222.414 (137)	5222.386	1.000
	$\|2p_{1/2} \otimes 2^+; \frac{3}{2}^-\rangle$	$\|1s_{1/2} \otimes 2^+; \frac{5}{2}^+\rangle$	5187.721 (137)	5187.704	0.496
	$\|2p_{1/2} \otimes 2^+; \frac{3}{2}^-\rangle$	$\|1s_{1/2} \otimes 0^+; \frac{1}{2}^+\rangle$	5300.924 (137)	5300.901	0.276
	$\|2p_{1/2} \otimes 0^+; \frac{1}{2}^-\rangle$	$\|1s_{1/2} \otimes 2^+; \frac{3}{2}^+\rangle$	5109.550 (137)	5109.525	0.078
	$\|2p_{3/2} \otimes 0^+; \frac{3}{2}^-\rangle$	$\|1s_{1/2} \otimes 0^+; \frac{1}{2}^+\rangle$	5413.612 (158)	5413.636	0.590
	$\|2p_{3/2} \otimes 0^+; \frac{3}{2}^-\rangle$	$\|1s_{1/2} \otimes 2^+; \frac{5}{2}^+\rangle$	5300.412 (158)	5300.439	0.231
	$\|2p_{3/2} \otimes 0^+; \frac{3}{2}^-\rangle$	$\|1s_{1/2} \otimes 2^+; \frac{3}{2}^+\rangle$	5300.746 (158)	5300.775	0.120
	$\|2p_{3/2} \otimes 2^+; \frac{3}{2}^-\rangle$	$\|1s_{1/2} \otimes 2^+; \frac{3}{2}^+\rangle$	5401.973 (158)	5401.996	0.077
	$\|2p_{3/2} \otimes 2^+; \frac{1}{2}^-\rangle$	$\|1s_{1/2} \otimes 2^+; \frac{3}{2}^+\rangle$	5357.019 (158)	5357.059	0.047
	$\|2p_{3/2} \otimes 2^+; \frac{5}{2}^-\rangle$	$\|1s_{1/2} \otimes 2^+; \frac{5}{2}^+\rangle$	5414.810 (158)	5414.829	0.008
$^{186}_{74}$W	$\|2p_{1/2} \otimes 0^+; \frac{1}{2}^-\rangle$	$\|1s_{1/2} \otimes 0^+; \frac{1}{2}^+\rangle$	5217.662 (163)	5217.690	1.000
	$\|2p_{1/2} \otimes 2^+; \frac{3}{2}^-\rangle$	$\|1s_{1/2} \otimes 2^+; \frac{5}{2}^+\rangle$	5181.047 (163)	5181.076	0.493
	$\|2p_{1/2} \otimes 2^+; \frac{3}{2}^-\rangle$	$\|1s_{1/2} \otimes 0^+; \frac{1}{2}^+\rangle$	5304.214 (163)	5304.239	0.322
	$\|2p_{1/2} \otimes 0^+; \frac{1}{2}^-\rangle$	$\|1s_{1/2} \otimes 2^+; \frac{3}{2}^+\rangle$	5095.109 (163)	5095.146	0.064
	$\|2p_{3/2} \otimes 0^+; \frac{3}{2}^-\rangle$	$\|1s_{1/2} \otimes 0^+; \frac{1}{2}^+\rangle$	5408.225 (188)	5408.201	0.595
	$\|2p_{3/2} \otimes 0^+; \frac{3}{2}^-\rangle$	$\|1s_{1/2} \otimes 2^+; \frac{5}{2}^+\rangle$	5285.059 (188)	5285.038	0.277
	$\|2p_{3/2} \otimes 0^+; \frac{3}{2}^-\rangle$	$\|1s_{1/2} \otimes 2^+; \frac{3}{2}^+\rangle$	5285.676 (188)	5285.657	0.106
	$\|2p_{3/2} \otimes 2^+; \frac{3}{2}^-\rangle$	$\|1s_{1/2} \otimes 2^+; \frac{3}{2}^+\rangle$	5393.672 (188)	5393.642	0.065
	$\|2p_{3/2} \otimes 2^+; \frac{1}{2}^-\rangle$	$\|1s_{1/2} \otimes 2^+; \frac{3}{2}^+\rangle$	5349.116 (188)	5349.096	0.042
	$\|2p_{3/2} \otimes 2^+; \frac{5}{2}^-\rangle$	$\|1s_{1/2} \otimes 2^+; \frac{5}{2}^+\rangle$	5405.740 (188)	5405.709	0.007

TABLE IIIC. Barrett Radii and Related Parameters of Deformed Nuclei with $60 \leq Z \leq 77$

See page 194 for Explanation of Tables

Isotope	NPol [keV]	R_0 [fm]	a [fm]	β_2	$\langle r^2\rangle^{1/2}_{model}$ [fm]	α [1/fm]	k	C_s [am/keV]	$R^{\mu}_{k\alpha}$ [fm]	Ref.
$^{150}Nd^{\dagger}$	-0.531	5.8821	0.523	0.278	5.047	0.1381	2.3456	-2.387	6.4422 (1;13)	[Be92]
	-13.961					0.1359	2.3369	-2.331	6.4431 (1;18)	
^{144}Sm	1.941	5.8624	0.523	0.090	4.949	0.1383	2.3186	-2.198	6.3254 (2;13)	[Ja89] [Po79]
	2.003					0.1359	2.3093	-2.141	6.3262 (1;13)	[Ma92a]
^{147}Sm	1.565	5.9445	0.501	0.118	4.983	0.1378	2.3191	-2.215	6.3741 (1;14)	[Ja89] [Ba81]
	1.056					0.1378	2.2862	-2.158	6.3748 (1;13)	[Ma92a]
^{148}Sm	1.653	6.0079	0.473	0.127	4.994	0.1345	2.2947	-2.224	6.3942 (1;13)	[Ja89] [Po79]
	1.565					0.1357	2.3123	-2.166	6.3947 (1;12)	[Ma92a]
^{149}Sm	0.753	5.9814	0.492	0.151	5.008	0.1357	2.3042	-2.227	6.4069 (1;13)	[Ja89] [Ba81]
	1.530					0.1371	2.3246	-2.169	6.4076 (1;12)	[Ma92a]
^{150}Sm	1.270	5.8560	0.557	0.231	5.047	0.1250	2.2206	-2.245	6.4364 (9;12)	[Ya78] [Ma92a]
	0.207					0.1250	2.2297	-2.185	6.4374 (9;12)	
^{152}Sm	1.403	5.8688	0.554	0.297	5.092	0.1332	2.2884	-2.248	6.4891 (1;14)	[Ja89] [Po79]
	-24.220					0.1322	2.2893	-2.188	6.4902 (1;23)	[Ma92a]
^{154}Sm		5.3601	0.4984	0.328	5.113				6.5215 (29)*	[Po79] [Ja89]

† The other Nd-isotopes can be found in TABLE III A.

* The given value is the total error including experimental and theoretical uncertainties

TABLE IIIC. Barrett Radii and Related Parameters of Deformed Nuclei with $60 \leq Z \leq 77$

See page 194 for Explanation of Tables

Isotope	NPol [keV]	R_0 [fm]	a [fm]	β_2	$\langle r^2 \rangle^{1/2}_{model}$ [fm]	α [1/fm]	k	C_z [am/keV]	R^{μ}_{ka} [fm]	Ref.
^{151}Eu	0.216					0.1358	2.3005	-2.171	6.4531 (1;13)	[Ja89] [Ta84b]
		6.0374	0.496	0.120	5.044					
	1.185					0.1373	2.3219	-2.112	6.4539 (1;12)	
^{153}Eu	-11.754					0.1362	2.3071	-2.190	6.5258 (1;18)	[Ja89] [Ta84b]
		5.9350	0.527	0.320	5.118					
	3.636					0.1333	2.9235	-2.130	6.5268 (1;13)	
^{154}Gd	-17.039					0.1357	2.2946	-2.125	6.5322 (7;20)	[Ja89] [La83]
		5.9625	0.531	0.290	5.122					
	-20.926					0.1337	2.2873	-2.066	6.5332 (7;21)	[Ma92a]
^{155}Gd	-17.604					0.1400	2.3319	-2.130	6.5475 (3;20)	[Be92] [Ja89]
		6.0196	0.493	0.305	5.130					
	18.839					0.1399	2.3417	-2.071	6.5485 (2;19)	[La83] [Ma92a]
^{156}Gd	-26.810					0.1374	2.3111	-2.134	6.5607 (1;24)	[Ja89] [La83]
		6.0094	0.510	0.310	5.142					
	32.342					0.1340	2.2928	-2.074	6.5617 (1;24)	[Ma92a]
^{157}Gd	-20.113					0.1350	2.2917	-2.136	6.5653 (3;21)	[Be92] [Ja89]
		6.0100	0.501	0.323	5.146					
	20.681					0.1362	2.3118	-2.077	6.5664 (3;20)	[La83] [Ma92a]
^{158}Gd	-27.629					0.1365	2.3096	-2.141	6.5807 (1;25)	[Ja89] [La83]
		6.0229	0.509	0.320	5.159					
	30.249					0.1323	2.2798	-2.081	6.5817 (1;23)	[Ma92a]
^{160}Gd	-28.926					0.1319	2.2678	-2.149	6.6018 (1;25)	[Ja89] [La83]
		6.0606	0.493	0.330	5.174					
	29.932					0.1329	2.2868	-2.088	6.6029 (1;23)	[Ma92a]
^{159}Tb										[Ta84a]

TABLE IIIC. Barrett Radii and Related Parameters of Deformed Nuclei with $60 \leq Z \leq 77$

See page 194 for Explanation of Tables

Isotope	NPol [keV]	R_0 [fm]	a [fm]	β_2	$\langle r^2 \rangle^{1/2}_{model}$ [fm]	α [1/fm]	k	C_z [am/keV]	R^{μ}_{ha} [fm]	Ref.
^{161}Dy	-26.834	6.0375	0.523	0.321	5.196	0.1385	2.3059	-2.027	6.6224 (5;22)	[Be92]
	24.533					0.1390	2.3218	-1.966	6.6237 (5;21)	
^{162}Dy	-29.695	6.0415	0.523	0.334	5.209	0.1385	2.3069	-2.032	6.6368 (1;24)	[Be92]
	29.713					0.1378	2.3123	-1.971	6.6380 (1;23)	
^{163}Dy	-24.686	6.0438	0.523	0.334	5.211	0.1387	2.3095	-2.033	6.6426 (2;22)	[Be92]
	31.232					0.1382	2.3171	-1.972	6.6439 (2;23)	
^{164}Dy	-30.578	6.0584	0.523	0.338	5.224	0.1383	2.3075	-2.037	6.6562 (4;25)	[Be92]
	28.477					0.1385	2.3206	-1.976	6.6574 (3;22)	
^{165}Ho										[Po76]
^{166}Er	-22.036	6.0978	0.523	0.340	5.250	0.1429	2.3309	-1.934	6.6902 (4;20)	[Ma92a]
	22.183					0.1395	2.3135	-1.873	6.6914 (4;18)	
^{167}Er	-23.505	6.1075	0.523	0.341	5.258	0.1415	2.3191	-1.937	6.6977 (7;21)	[Ma92a]
	17.273					0.1390	2.3094	-1.875	6.6989 (5;16)	
^{168}Er	-22.404	6.1208	0.523	0.346	5.272	0.1410	2.3158	-1.941	6.7086 (5;20)	[Ma92a]
	22.345					0.1400	2.3190	-1.878	6.7098 (5;18)	
^{170}Er	-21.957	6.1435	0.523	0.342	5.286	0.1413	2.3202	-1.947	6.7285 (6;20)	[Ma92a]
	21.801					0.1380	2.3044	-1.885	6.7297 (4;18)	

TABLE IIIC. Barrett Radii and Related Parameters of Deformed Nuclei with $60 \leq Z \leq 77$

See page 194 for Explanation of Tables

Isotope	NPol [keV]	R_0 [fm]	a [fm]	β_2	$\langle r^2 \rangle^{1/2}_{model}$ [fm]	α [1/fm]	k	C_z [am/keV]	R^{μ}_{ka} [fm]	Ref.
^{170}Yb		6.212	0.496	0.324	5.286					[Ze75]
^{171}Yb		6.214	0.496	0.330	5.293					[Ze75]
^{172}Yb		6.227	0.496	0.328	5.301					[Ze75]
^{173}Yb		6.234	0.496	0.328	5.306					[Ze75]
^{174}Yb	-35.397					0.1444	2.3327	-1.858	6.7733 (1;25)	[Be92] [Ze75]
		6.1999	0.523	0.321	5.317					
	30.171					0.1405	2.3115	-1.794	6.7746 (1;21)	
^{176}Yb		6.271	0.496	0.313	5.321					[Ze75]
^{176}Hf						0.1388	2.2740	-1.775	6.7990 (9;11)	[Ta84c]
		6.2880	0.519	0.270	5.331					
						0.1388	2.2847	-1.710	6.8001 (9;10)	
^{177}Hf						0.1388	2.2745	-1.777	6.8030 (9;11)	[Ta84c]
		6.2970	0.517	0.263	5.334					
						0.1388	2.2852	-1.711	6.8040 (9;10)	
^{178}Hf						0.1388	2.2753	-1.779	6.8107 (9;11)	[Ta84c]
		6.3170	0.514	0.259	5.338					
						0.1388	2.2859	-1.714	6.8117 (9;10)	
^{179}Hf						0.1388	2.2762	-1.782	6.8162 (9;11)	[Ta84c]
		6.3480	0.498	0.257	5.339					
						0.1388	2.2868	-1.716	6.8172 (9;10)	
^{180}Hf	-29.536					0.1457	2.3305	-1.781	6.8218 (2;22)	[Be92] [Ta84c]
		6.3177	0.510	0.276	5.349					
	29.851					0.1440	2.3286	-1.715	6.8231 (2;20)	

TABLE IIIC. Barrett Radii and Related Parameters of Deformed Nuclei with $60 \leq Z \leq 77$

See page 194 for Explanation of Tables

Isotope	NPol [keV]	R_0 [fm]	a [fm]	β_2	$\langle r^2 \rangle^{1/2}_{model}$ [fm]	α [1/fm]	k	C_s [am/keV]	$R^{\mu}_{k\alpha}$ [fm]	Ref.
^{181}Ta	-20.175					0.1462	2.3274	-1.742	6.8343 (2;18)	[Be92] [Po77]
		6.3669	0.494	0.273	5.354					
	0.707					0.1468	2.3447	-1.676	6.8354 (2;18)	
^{182}W	-25.356					0.1464	2.3198	-1.700	6.8427 (4;19)	[Ma92a]
		6.3338	0.523	0.260	5.364					
	27.426					0.1441	2.3143	-1.635	6.8440 (4;18)	
^{184}W	-23.402					0.1483	2.3577	-1.704	6.8562 (4;18)	[Ma92a]
		6.3599	0.523	0.244	5.373					
	28.962					0.1451	2.3235	-1.638	6.8575 (4;18)	
^{186}W	-22.398					0.1465	2.3236	-1.708	6.8683 (3;18)	[Ma92a]
		6.3839	0.523	0.229	5.381					
	31.192					0.1456	2.3296	-1.642	6.8696 (4;19)	
^{185}Re										[Ko81]
^{187}Re										[Ko81]
^{186}Os	3.924					0.1445	2.2894	-1.633	6.8766 (11;19)	[Ho81]
		6.4142	0.522	0.200	5.387					
	4.102					0.1445	2.3030	-1.566	6.8779 (10;19)	
^{188}Os	3.733					0.1445	2.2892	-1.636	6.8888 (11;18)	[Ho81]
		6.4268	0.528	0.185	5.395					
	4.072					0.1445	2.3040	-1.569	6.8902 (9;19)	

TABLE IIIC. Barrett Radii and Related Parameters of Deformed Nuclei with $60 \leq Z \leq 77$

See page 194 for Explanation of Tables

Isotope	NPol [keV]	R_0 [fm]	a [fm]	β_2	$\langle r^2 \rangle^{1/2}_{model}$ [fm]	α [1/fm]	k	C_z [am/keV]	$R^{\mu}_{k\alpha}$ [fm]	Ref.
^{190}Os	3.519					0.1445	2.2917	-1.640	6.8995 (9;17)	[Ho81]
		6.4555	0.522	0.170	5.401					
	3.744					0.1445	2.3052	-1.572	6.9008 (8;18)	
^{192}Os	3.376					0.1445	2.2930	-1.644	6.9097 (9;17)	[Ho81]
		6.4829	0.511	0.170	5.406					
	3.564					0.1445	2.3065	-1.576	6.9108 (8;17)	
^{191}Ir										[Ta84a]
^{193}Ir										[Ta84a]

TABLE IV. *Confit* Matrices for Muonic $2p \rightarrow 1s$ Energy Differences of Isotopes, $31 \leq Z \leq 58$

See page 194 for Explanation of Tables

[keV]	^{69}Ga	^{71}Ga
^{69}Ga		1.634 16
^{71}Ga	-1.705 11	

[keV]	^{70}Ge	^{72}Ge	^{73}Ge	^{74}Ge	^{76}Ge
^{70}Ge		2.024 25	2.861 38	4.130 33	5.080 31
^{72}Ge	-2.031 15		0.837 35	2.106 28	3.056 26
^{73}Ge	-2.829 25	-0.798 23		1.269 41	2.219 40
^{74}Ge	-4.192 21	-2.161 16	-1.368 28		0.950 31
^{76}Ge	-5.128 20	-3.097 14	-2.299 26	-0.936 18	

[keV]	^{76}Se	^{77}Se	^{78}Se	^{80}Se	^{82}Se
^{76}Se		0.268 26	0.269 25	0.262 23	0.267 28
^{77}Se	-0.203 18		0.001 25	-0.006 22	0.001 29
^{78}Se	-0.254 18	-0.050 19		-0.007 21	-0.002 25
^{80}Se	-0.216 16	-0.013 16	0.038 16		0.005 26
^{82}Se	-0.254 20	-0.050 23	-0.000 19	-0.038 20	

TABLE IV. *Confit* Matrices for Muonic $2p \rightarrow 1s$ Energy Differences of Isotopes, $31 \leq Z \leq 58$

See page 194 for Explanation of Tables

[keV]	^{79}Br	^{81}Br
^{79}Br		-0.468 30
^{81}Br	0.462 25	

[keV]	^{78}Kr	^{80}Kr	^{82}Kr	^{83}Kr	^{84}Kr	^{86}Kr
^{78}Kr		-0.922 47	-1.779 46	-2.684 55	-2.489 44	-3.274 39
^{80}Kr	0.911 39		-0.857 47	-1.762 55	-1.567 45	-2.352 39
^{82}Kr	1.796 39	0.885 39		-0.905 55	-0.710 44	-1.495 39
^{83}Kr	2.928 47	2.017 47	1.132 47		0.195 53	-0.590 48
^{84}Kr	2.394 38	1.483 38	0.598 38	-0.534 46		-0.785 36
^{86}Kr	3.318 33	2.407 33	1.522 33	0.390 42	0.924 32	

[keV]	^{85}Rb	^{87}Rb
^{85}Rb		-1.015 23
^{87}Rb	0.940 15	

TABLE IV. *Confit* Matrices for Muonic $2p \rightarrow 1s$ Energy Differences of Isotopes, $31 \leq Z \leq 58$

See page 194 for Explanation of Tables

[keV]	^{84}Sr	^{86}Sr	^{87}Sr	^{88}Sr
^{84}Sr		-1.990	-3.251	-3.513
		35	70	34
^{86}Sr	1.983		-1.260	-1.522
	24		64	15
^{87}Sr	3.332	1.349		-0.262
	54	50		63
^{88}Sr	3.515	1.532	0.183	
	24	10	49	

[keV]	^{90}Zr	^{91}Zr	^{92}Zr	^{94}Zr	^{96}Zr
^{90}Zr		3.507	8.141	13.994	18.201
		44	20	23	50
^{91}Zr	-3.453		4.634	10.487	14.693
	33		46	47	65
^{92}Zr	-8.232	-4.779		5.853	10.060
	14	34		26	51
^{94}Zr	-14.114	-10.661	-5.882		4.206
	16	35	17		52
^{96}Zr	-18.419	-14.966	-10.187	-4.305	
	36	48	36	37	

TABLE IV. *Confit* Matrices for Muonic $2p \rightarrow 1s$ Energy Differences of Isotopes, $31 \leq Z \leq 58$

See page 194 for Explanation of Tables

[keV]	^{92}Mo	^{94}Mo	^{95}Mo	^{96}Mo	^{97}Mo	^{98}Mo	^{100}Mo
^{92}Mo		9.140	11.873	17.258	18.336	23.457	32.782
		38	35	33	37	40	40
^{94}Mo	-9.310		2.733	8.119	9.197	14.318	23.642
	26		27	24	29	33	33
^{95}Mo	-11.978	-2.668		5.385	6.463	11.584	20.909
	25	19		18	23	29	29
^{96}Mo	-17.412	-8.102	-5.434		1.078	6.199	15.523
	23	17	14		20	27	26
^{97}Mo	-18.379	-9.069	-6.401	-0.967		5.121	14.446
	26	21	17	16		31	30
^{98}Mo	-23.676	-14.366	-11.698	-6.264	-5.298		9.325
	28	22	20	19	22		35
^{100}Mo	-33.095	-23.784	-21.117	-15.683	-14.716	-9.418	
	27	22	20	18	22	23	

[keV]	^{96}Ru	^{98}Ru	^{99}Ru	^{100}Ru	^{101}Ru	^{102}Ru	^{104}Ru
^{96}Ru		9.051	12.324	17.604	20.293	25.489	33.626
		577	240	241	236	230	232
^{98}Ru	-8.868		3.273	8.553	11.242	16.438	24.575
	232		536	536	534	531	532
^{99}Ru	-12.436	-3.568		5.280	7.969	13.165	21.303
	58	235		110	100	84	89
^{100}Ru	-17.692	-8.825	-5.256		2.689	7.885	16.023
	68	238	78		101	86	90
^{101}Ru	-20.106	-11.238	-7.670	-2.414		5.196	13.333
	106	252	113	119		71	77
^{102}Ru	-25.763	-16.895	-13.326	-8.070	-5.656		8.137
	40	232	56	67	106		55
^{104}Ru	-34.012	-25.144	-21.576	-16.319	-13.906	-8.249	
	47	233	61	71	108	45	

TABLE IV. *Confit* Matrices for Muonic $2p \rightarrow 1s$ Energy Differences of Isotopes, $31 \leq Z \leq 58$

See page 194 for Explanation of Tables

[keV]	^{102}Pd	^{104}Pd	^{105}Pd	^{106}Pd	^{108}Pd	^{110}Pd
^{102}Pd		7.975	11.040	15.492	23.027	29.933
		176	150	132	130	176
^{104}Pd	-8.041		3.066	7.517	15.052	21.958
	143		173	158	156	196
^{105}Pd	-10.172	-2.131		4.451	11.987	18.893
	168	191		127	125	172
^{106}Pd	-15.648	-7.606	-5.476		7.535	14.441
	95	131	157		103	157
^{108}Pd	-23.346	-15.305	-13.175	-7.699		6.906
	91	128	155	70		155
^{110}Pd	-30.252	-22.211	-20.080	-14.605	-6.906	
	118	148	172	102	99	

[keV]	^{107}Ag	^{109}Ag
^{107}Ag		7.074
		39
^{109}Ag	-7.178	
	27	

TABLE IV. *Confit* Matrices for Muonic $2p \rightarrow 1s$ Energy Differences of Isotopes, $31 \leqslant Z \leqslant 58$

See page 194 for Explanation of Tables

[keV]	^{106}Cd	^{108}Cd	^{110}Cd	^{111}Cd	^{112}Cd	^{113}Cd	^{114}Cd	^{116}Cd
^{106}Cd		7.004	13.991	15.893	20.752	22.551	26.888	32.051
		129	118	124	114	120	113	114
^{108}Cd	-7.050		6.987	8.889	13.748	15.547	19.884	25.047
	86		84	91	82	90	79	82
^{110}Cd	-14.077	-7.027		1.901	6.761	8.560	12.897	18.060
	76	68		69	58	68	55	58
^{111}Cd	-15.951	-8.901	-1.874		4.860	6.658	10.995	16.159
	77	69	49		69	78	66	69
^{112}Cd	-20.860	-13.811	-6.784	-4.910		1.799	6.136	11.299
	70	66	46	48		59	47	49
^{113}Cd	-22.796	-15.747	-8.720	-6.846	-1.936		4.337	9.500
	75	72	54	56	39		59	59
^{114}Cd	-27.056	-20.006	-12.979	-11.105	-6.195	-4.260		5.163
	70	66	46	48	36	44		43
^{116}Cd	-32.301	-25.251	-18.224	-16.350	-11.441	-9.505	-5.245	
	71	68	49	51	37	43	34	

[keV]	^{121}Sb	^{123}Sb
^{121}Sb		3.429
		96
^{123}Sb	-3.187	
	77	

TABLE IV. *Confit* Matrices for Muonic $2p \rightarrow 1s$ Energy Differences of Isotopes, $31 \leq Z \leq 58$

See page 194 for Explanation of Tables

[keV]	^{122}Te	^{123}Te	^{124}Te	^{125}Te	^{126}Te	^{128}Te	^{130}Te
^{122}Te		1.242	3.992	4.898	7.484	10.778	13.839
		357	355	356	355	356	355
^{123}Te	-1.268		2.749	3.655	6.241	9.536	12.596
	356		38	43	38	41	38
^{124}Te	-4.015	-2.747		0.906	3.492	6.787	9.847
	355	26		35	27	31	27
^{125}Te	-4.928	-3.660	-0.913		2.586	5.881	8.941
	355	29	24		34	36	33
^{126}Te	-7.580	-6.312	-3.565	-2.652		3.294	6.355
	355	27	19	24		31	26
^{128}Te	-10.883	-9.615	-6.868	-5.955	-3.303		3.061
	355	29	22	25	22		29
^{130}Te	-13.986	-12.718	-9.971	-9.058	-6.406	-3.103	
	355	29	21	25	20	22	

[keV]	^{124}Xe	^{126}Xe	^{128}Xe	^{129}Xe	^{130}Xe	^{131}Xe	^{132}Xe	^{134}Xe	^{136}Xe
^{124}Xe		3.765	6.079	6.530	9.421	8.605	10.928	13.448	16.709
		104	107	41	199	39	68	45	35
^{126}Xe	-3.510		2.314	2.765	5.656	4.840	7.163	9.683	12.944
	101		142	102	220	101	116	104	100
^{128}Xe	-5.866	-2.356		0.451	3.341	2.526	4.849	7.369	10.630
	104	142		105	221	104	118	106	102
^{129}Xe	-6.224	-2.714	-0.358		2.890	2.075	4.398	6.918	10.179
	30	101	104		198	33	65	41	28
^{130}Xe	-9.271	-5.761	-3.405	-3.047		-0.815	1.508	4.028	7.288
	198	220	221	198		198	206	199	197
^{131}Xe	-8.432	-4.922	-2.566	-2.208	0.839		2.323	4.843	8.104
	28	100	103	27	197		64	38	24
^{132}Xe	-10.914	-7.404	-5.048	-4.690	-1.643	-2.482		2.520	5.781
	45	106	109	44	201	43		68	61
^{134}Xe	-13.351	-9.840	-7.484	-7.126	-4.079	-4.918	-2.436		3.261
	30	101	104	30	198	27	44		34
^{136}Xe	-16.693	-13.182	-10.827	-10.469	-7.421	-8.260	-5.778	-3.342	
	23	99	102	23	197	19	40	23	

TABLE IV. *Confit* Matrices for Muonic $2p \rightarrow 1s$ Energy Differences of Isotopes, $31 \leq Z \leq 58$

See page 194 for Explanation of Tables

[keV]	^{134}Ba	^{135}Ba	^{136}Ba	^{137}Ba	^{138}Ba
^{134}Ba		-0.936	1.553		4.596
		81	39		34
^{135}Ba	1.059		2.489		5.532
	51		78		76
^{136}Ba	-1.590	-2.649			3.043
	28	45			28
^{137}Ba	-1.293	-2.352	0.297		
	64	70	60		
^{138}Ba	-4.696	-5.754	-3.105	-3.402	
	25	47	21	60	

[keV]	^{140}Ce	^{142}Ce
^{140}Ce		15.298
		127
^{142}Ce	-15.689	
	86	

TABLE V. Differences of Barrett Radii for Isotopes, $6 \leq Z \leq 82$

See page 194 for Explanation of Tables

Isotope Pair	$\Delta R^{\mu}_{k\alpha}[am]$
$^{13}C \leftrightarrow {}^{12}C$	-2.9 ± 16.6 ± 1.1
$^{14}C \leftrightarrow {}^{12}C$	27.7 ± 12.4 ± 1.1
$^{18}O \leftrightarrow {}^{16}O$	98.6 ± 7.8 ± 0.7
$^{21}Ne \leftrightarrow {}^{20}Ne$	-49.3 ± 3.1 ± 1.0
$^{22}Ne \leftrightarrow {}^{20}Ne$	-67.0 ± 3.1 ± 1.0
$^{25}Mg \leftrightarrow {}^{24}Mg$	-36.7 ± 0.8 ± 1.0
$^{26}Mg \leftrightarrow {}^{24}Mg$	-29.9 ± 0.8 ± 1.0
$^{29}Si \leftrightarrow {}^{28}Si$	-5.2 ± 6.0 ± 0.8
$^{30}Si \leftrightarrow {}^{28}Si$	13.8 ± 6.0 ± 0.8
$^{34}S \leftrightarrow {}^{32}S$	28.9 ± 1.5 ± 0.8
$^{36}S \leftrightarrow {}^{34}S$	19.0 ± 1.4 ± 0.7
$^{38}Ar \leftrightarrow {}^{36}Ar$	14.9 ± 1.0 ± 0.7
$^{40}Ar \leftrightarrow {}^{38}Ar$	32.2 ± 1.0 ± 0.7
$^{42}Ca \leftrightarrow {}^{40}Ca$	39.0 ± 0.7 ± 0.7
$^{43}Ca \leftrightarrow {}^{42}Ca$	-17.8 ± 0.7 ± 0.7
$^{44}Ca \leftrightarrow {}^{42}Ca$	12.8 ± 0.7 ± 0.7
$^{46}Ca \leftrightarrow {}^{44}Ca$	-25.5 ± 4.5 ± 0.7
$^{48}Ca \leftrightarrow {}^{46}Ca$	-25.5 ± 4.5 ± 0.7

Isotope Pair	$\Delta R^{\mu}_{k\alpha}[am]$
$^{47}Ti \leftrightarrow {}^{46}Ti$	-13.7 ± 0.6 ± 0.8
$^{48}Ti \leftrightarrow {}^{46}Ti$	-18.4 ± 0.7 ± 0.8
$^{49}Ti \leftrightarrow {}^{48}Ti$	-23.4 ± 0.8 ± 0.8
$^{50}Ti \leftrightarrow {}^{48}Ti$	-27.3 ± 0.7 ± 0.8
$^{52}Cr \leftrightarrow {}^{50}Cr$	-24.9 ± 0.5 ± 0.8
$^{53}Cr \leftrightarrow {}^{52}Cr$	22.0 ± 0.4 ± 0.7
$^{54}Cr \leftrightarrow {}^{52}Cr$	58.0 ± 0.5 ± 0.7
$^{56}Fe \leftrightarrow {}^{54}Fe$	55.7 ± 0.6 ± 0.7
$^{57}Fe \leftrightarrow {}^{56}Fe$	21.0 ± 0.7 ± 0.7
$^{58}Fe \leftrightarrow {}^{56}Fe$	47.8 ± 0.6 ± 0.7
$^{60}Ni \leftrightarrow {}^{58}Ni$	47.9 ± 0.4 ± 0.7
$^{61}Ni \leftrightarrow {}^{60}Ni$	14.0 ± 0.5 ± 0.7
$^{62}Ni \leftrightarrow {}^{60}Ni$	37.7 ± 0.4 ± 0.7
$^{64}Ni \leftrightarrow {}^{62}Ni$	23.9 ± 0.4 ± 0.7
$^{65}Cu \leftrightarrow {}^{63}Cu$	25.3 ± 0.4 ± 0.7
$^{66}Zn \leftrightarrow {}^{64}Zn$	26.5 ± 0.3 ± 0.7
$^{68}Zn \leftrightarrow {}^{66}Zn$	21.6 ± 0.3 ± 0.7
$^{70}Zn \leftrightarrow {}^{68}Zn$	23.2 ± 1.3 ± 0.7

TABLE V. Differences of Barrett Radii for Isotopes, $6 \leq Z \leq 82$

See page 194 for Explanation of Tables

Isotope Pair	$\Delta R^{\mu}_{k\alpha}[am]$
$^{71}Ga \leftrightarrow {}^{69}Ga$	$18.7 \pm 0.2 \pm 0.6$
$^{72}Ge \leftrightarrow {}^{70}Ge$	$21.0 \pm 0.1 \pm 0.7$
$^{73}Ge \leftrightarrow {}^{72}Ge$	$7.9 \pm 0.2 \pm 0.7$
$^{74}Ge \leftrightarrow {}^{72}Ge$	$22.8 \pm 0.2 \pm 0.8$
$^{76}Ge \leftrightarrow {}^{74}Ge$	$9.6 \pm 0.2 \pm 0.8$
$^{77}Se \leftrightarrow {}^{76}Se$	$0.1 \pm 0.2 \pm 0.9$
$^{78}Se \leftrightarrow {}^{76}Se$	$1.9 \pm 0.2 \pm 0.9$
$^{80}Se \leftrightarrow {}^{78}Se$	$-0.5 \pm 0.1 \pm 0.8$
$^{82}Se \leftrightarrow {}^{80}Se$	$0.1 \pm 0.2 \pm 0.7$
$^{81}Br \leftrightarrow {}^{79}Br$	$-3.9 \pm 0.2 \pm 0.7$
$^{80}Kr \leftrightarrow {}^{78}Kr$	$-7.1 \pm 0.3 \pm 0.9$
$^{82}Kr \leftrightarrow {}^{80}Kr$	$-7.0 \pm 0.3 \pm 0.8$
$^{83}Kr \leftrightarrow {}^{82}Kr$	$-8.1 \pm 0.3 \pm 0.7$
$^{84}Kr \leftrightarrow {}^{82}Kr$	$-5.1 \pm 0.3 \pm 0.7$
$^{86}Kr \leftrightarrow {}^{84}Kr$	$-5.7 \pm 0.2 \pm 0.7$
$^{87}Rb \leftrightarrow {}^{85}Rb$	$-6.4 \pm 0.1 \pm 0.6$
$^{86}Sr \leftrightarrow {}^{84}Sr$	$-13.5 \pm 0.2 \pm 0.7$
$^{87}Sr \leftrightarrow {}^{86}Sr$	$-8.9 \pm 0.3 \pm 0.6$
$^{88}Sr \leftrightarrow {}^{86}Sr$	$-9.2 \pm 0.1 \pm 0.6$

Isotope Pair	$\Delta R^{\mu}_{k\alpha}[am]$
$^{91}Zr \leftrightarrow {}^{90}Zr$	$19.1 \pm 0.2 \pm 0.5$
$^{92}Zr \leftrightarrow {}^{90}Zr$	$45.5 \pm 0.1 \pm 0.5$
$^{94}Zr \leftrightarrow {}^{92}Zr$	$32.4 \pm 0.1 \pm 0.5$
$^{96}Zr \leftrightarrow {}^{94}Zr$	$23.9 \pm 0.2 \pm 0.5$
$^{94}Mo \leftrightarrow {}^{92}Mo$	$45.7 \pm 0.1 \pm 0.6$
$^{95}Mo \leftrightarrow {}^{94}Mo$	$12.8 \pm 0.1 \pm 0.6$
$^{96}Mo \leftrightarrow {}^{94}Mo$	$40.2 \pm 0.1 \pm 0.6$
$^{97}Mo \leftrightarrow {}^{96}Mo$	$4.1 \pm 0.1 \pm 0.6$
$^{98}Mo \leftrightarrow {}^{96}Mo$	$30.8 \pm 0.1 \pm 0.6$
$^{100}Mo \leftrightarrow {}^{98}Mo$	$47.1 \pm 0.1 \pm 0.7$
$^{98}Ru \leftrightarrow {}^{96}Ru$	$39.4 \pm 1.0 \pm 0.6$
$^{99}Ru \leftrightarrow {}^{98}Ru$	$15.0 \pm 1.0 \pm 0.6$
$^{100}Ru \leftrightarrow {}^{98}Ru$	$39.0 \pm 1.0 \pm 0.6$
$^{101}Ru \leftrightarrow {}^{100}Ru$	$10.4 \pm 0.5 \pm 0.6$
$^{102}Ru \leftrightarrow {}^{100}Ru$	$35.8 \pm 0.3 \pm 0.7$
$^{104}Ru \leftrightarrow {}^{102}Ru$	$36.7 \pm 0.2 \pm 0.7$
$^{104}Pd \leftrightarrow {}^{102}Pd$	$32.0 \pm 0.6 \pm 0.6$
$^{105}Pd \leftrightarrow {}^{104}Pd$	$9.4 \pm 0.8 \pm 0.7$

TABLE V. Differences of Barrett Radii for Isotopes, $6 \leq Z \leq 82$

See page 194 for Explanation of Tables

Isotope Pair	$\Delta R_{k\alpha}^{\mu}[am]$
$^{106}Pd \leftrightarrow {}^{104}Pd$	$30.5 \pm 0.5 \pm 0.6$
$^{108}Pd \leftrightarrow {}^{106}Pd$	$30.7 \pm 0.3 \pm 0.7$
$^{110}Pd \leftrightarrow {}^{108}Pd$	$27.7 \pm 0.4 \pm 0.7$
$^{109}Ag \leftrightarrow {}^{107}Ag$	$27.2 \pm 0.1 \pm 0.6$
$^{108}Cd \leftrightarrow {}^{106}Cd$	$25.3 \pm 0.3 \pm 0.6$
$^{110}Cd \leftrightarrow {}^{108}Cd$	$25.5 \pm 0.2 \pm 0.6$
$^{111}Cd \leftrightarrow {}^{110}Cd$	$6.4 \pm 0.2 \pm 0.6$
$^{112}Cd \leftrightarrow {}^{110}Cd$	$24.7 \pm 0.2 \pm 0.6$
$^{113}Cd \leftrightarrow {}^{112}Cd$	$6.2 \pm 0.1 \pm 0.6$
$^{114}Cd \leftrightarrow {}^{112}Cd$	$22.5 \pm 0.1 \pm 0.6$
$^{116}Cd \leftrightarrow {}^{114}Cd$	$19.1 \pm 0.1 \pm 0.6$
$^{115}In \leftrightarrow {}^{113}In$	$20.9 \pm 1.2 \pm 0.7$
$^{114}Sn \leftrightarrow {}^{112}Sn$	$20.9 \pm 0.3 \pm 0.5$
$^{116}Sn \leftrightarrow {}^{114}Sn$	$20.9 \pm 0.3 \pm 0.5$
$^{117}Sn \leftrightarrow {}^{116}Sn$	$6.2 \pm 0.3 \pm 0.5$
$^{118}Sn \leftrightarrow {}^{116}Sn$	$19.8 \pm 0.4 \pm 0.5$
$^{119}Sn \leftrightarrow {}^{118}Sn$	$3.7 \pm 0.4 \pm 0.5$
$^{120}Sn \leftrightarrow {}^{118}Sn$	$18.0 \pm 0.4 \pm 0.6$
$^{122}Sn \leftrightarrow {}^{120}Sn$	$15.7 \pm 0.5 \pm 0.6$
$^{124}Sn \leftrightarrow {}^{122}Sn$	$13.4 \pm 0.5 \pm 0.5$

Isotope Pair	$\Delta R_{k\alpha}^{\mu}[am]$
$^{123}Sb \leftrightarrow {}^{121}Sb$	$10.5 \pm 0.2 \pm 0.6$
$^{123}Te \leftrightarrow {}^{122}Te$	$3.3 \pm 1.1 \pm 0.6$
$^{124}Te \leftrightarrow {}^{122}Te$	$12.2 \pm 1.1 \pm 0.6$
$^{125}Te \leftrightarrow {}^{124}Te$	$2.2 \pm 0.1 \pm 0.5$
$^{126}Te \leftrightarrow {}^{124}Te$	$10.5 \pm 0.1 \pm 0.5$
$^{128}Te \leftrightarrow {}^{126}Te$	$10.1 \pm 0.1 \pm 0.5$
$^{130}Te \leftrightarrow {}^{128}Te$	$9.5 \pm 0.1 \pm 0.5$
$^{126}Xe \leftrightarrow {}^{124}Xe$	$10.5 \pm 0.3 \pm 0.4$
$^{128}Xe \leftrightarrow {}^{126}Xe$	$6.8 \pm 0.4 \pm 0.5$
$^{129}Xe \leftrightarrow {}^{128}Xe$	$1.0 \pm 0.3 \pm 0.5$
$^{130}Xe \leftrightarrow {}^{128}Xe$	$10.0 \pm 0.6 \pm 0.5$
$^{131}Xe \leftrightarrow {}^{130}Xe$	$-2.6 \pm 0.6 \pm 0.5$
$^{132}Xe \leftrightarrow {}^{130}Xe$	$4.4 \pm 0.6 \pm 0.5$
$^{134}Xe \leftrightarrow {}^{132}Xe$	$7.2 \pm 0.1 \pm 0.5$
$^{136}Xe \leftrightarrow {}^{134}Xe$	$9.4 \pm 0.1 \pm 0.5$
$^{135}Ba \leftrightarrow {}^{134}Ba$	$-2.9 \pm 0.1 \pm 0.5$
$^{136}Ba \leftrightarrow {}^{134}Ba$	$4.3 \pm 0.1 \pm 0.5$
$^{137}Ba \leftrightarrow {}^{136}Ba$	$-0.7 \pm 0.2 \pm 0.5$
$^{138}Ba \leftrightarrow {}^{136}Ba$	$8.1 \pm 0.1 \pm 0.5$

TABLE V. Differences of Barrett Radii for Isotopes, $6 \leq Z \leq 82$

See page 194 for Explanation of Tables

Isotope Pair	$\Delta R^{\mu}_{k\alpha}[am]$
$^{142}Ce \leftrightarrow {}^{140}Ce$	$38.2 \pm 0.2 \pm 0.5$
$^{143}Nd \leftrightarrow {}^{142}Nd$	$13.9 \pm 0.3 \pm 0.5$
$^{144}Nd \leftrightarrow {}^{142}Nd$	$35.5 \pm 0.1 \pm 0.5$
$^{145}Nd \leftrightarrow {}^{144}Nd$	$15.4 \pm 0.3 \pm 0.6$
$^{146}Nd \leftrightarrow {}^{144}Nd$	$34.9 \pm 0.1 \pm 0.5$
$^{148}Nd \leftrightarrow {}^{146}Nd$	$38.4 \pm 0.2 \pm 0.4$
$^{148}Sm \leftrightarrow {}^{147}Sm$	$19.9 \pm 0.1 \pm 0.4$
$^{149}Sm \leftrightarrow {}^{148}Sm$	$12.9 \pm 0.1 \pm 0.4$
$^{152}Sm \leftrightarrow {}^{150}Sm$	55.2 ± 0.8*
$^{154}Sm \leftrightarrow {}^{152}Sm$	31.3 ± 1.7*
$^{153}Eu \leftrightarrow {}^{151}Eu$	$72.9 \pm 0.1 \pm 0.4$
$^{155}Gd \leftrightarrow {}^{154}Gd$	$15.3 \pm 0.7 \pm 0.7$
$^{156}Gd \leftrightarrow {}^{154}Gd$	$28.5 \pm 0.7 \pm 0.8$
$^{157}Gd \leftrightarrow {}^{156}Gd$	$4.7 \pm 0.3 \pm 0.8$
$^{158}Gd \leftrightarrow {}^{156}Gd$	$20.0 \pm 0.1 \pm 0.8$
$^{160}Gd \leftrightarrow {}^{158}Gd$	$21.2 \pm 0.2 \pm 0.8$
$^{162}Dy \leftrightarrow {}^{161}Dy$	$14.3 \pm 0.4 \pm 0.8$
$^{163}Dy \leftrightarrow {}^{162}Dy$	$5.9 \pm 0.2 \pm 0.8$
$^{164}Dy \leftrightarrow {}^{162}Dy$	$19.4 \pm 0.2 \pm 0.8$

* Total error including uncertainties in calculating nuclear polarization corrections and experimental errors is given.

Isotope Pair	$\Delta R^{\mu}_{k\alpha}[am]$
$^{167}Er \leftrightarrow {}^{166}Er$	$7.5 \pm 0.3 \pm 0.6$
$^{168}Er \leftrightarrow {}^{166}Er$	$18.4 \pm 0.3 \pm 0.6$
$^{170}Er \leftrightarrow {}^{168}Er$	$19.9 \pm 0.3 \pm 0.6$
$^{172}Yb \leftrightarrow {}^{170}Yb$	18.0 ± 0.6†
$^{172}Yb \leftrightarrow {}^{171}Yb$	9.8 ± 0.6†
$^{174}Yb \leftrightarrow {}^{172}Yb$	14.8 ± 0.4†
$^{174}Yb \leftrightarrow {}^{173}Yb$	8.6 ± 0.7†
$^{176}Yb \leftrightarrow {}^{174}Yb$	13.5 ± 0.5†
$^{177}Hf \leftrightarrow {}^{176}Hf$	$3.9 \pm 0.4 \pm 0.6$
$^{178}Hf \leftrightarrow {}^{176}Hf$	$11.6 \pm 0.4 \pm 0.6$
$^{179}Hf \leftrightarrow {}^{178}Hf$	$5.5 \pm 0.5 \pm 0.6$
$^{180}Hf \leftrightarrow {}^{178}Hf$	$12.7 \pm 0.5 \pm 0.6$
$^{184}W \leftrightarrow {}^{182}W$	$13.5 \pm 0.3 \pm 0.6$
$^{186}W \leftrightarrow {}^{184}W$	$12.1 \pm 0.3 \pm 0.6$
$^{188}Os \leftrightarrow {}^{186}Os$	$12.3 \pm 0.5 \pm 0.6$
$^{190}Os \leftrightarrow {}^{188}Os$	$10.6 \pm 0.4 \pm 0.6$
$^{192}Os \leftrightarrow {}^{190}Os$	$10.0 \pm 0.1 \pm 0.6$

† The shifts of the 1s state - taken from [Ze75] - are given. The quoted error includes only experimental uncertainties.

TABLE V. Differences of Barrett Radii for Isotopes, $6 \leq Z \leq 82$

See page 194 for Explanation of Tables

Isotope Pair	$\Delta R^{\mu}_{k\alpha}[am]$
$^{195}Pt \leftrightarrow {}^{194}Pt$	$3.5 \pm 0.3 \pm 0.9$
$^{196}Pt \leftrightarrow {}^{194}Pt$	$9.5 \pm 0.3 \pm 0.8$
$^{198}Pt \leftrightarrow {}^{196}Pt$	$11.8 \pm 0.4 \pm 0.6$
$^{200}Hg \leftrightarrow {}^{199}Hg$	$10.0 \pm 0.8 \pm 0.3$
$^{200}Hg \leftrightarrow {}^{198}Hg$	$12.4 \pm 0.4 \pm 0.3$
$^{201}Hg \leftrightarrow {}^{200}Hg$	5.2 ± 0.5*
$^{202}Hg \leftrightarrow {}^{200}Hg$	$12.3 \pm 0.4 \pm 0.3$
$^{204}Hg \leftrightarrow {}^{202}Hg$	$14.3 \pm 0.6 \pm 0.3$
$^{205}Tl \leftrightarrow {}^{203}Tl$	$13.1 \pm 0.5 \pm 0.5$
$^{208}Pb \leftrightarrow {}^{204}Pb$	$28.0 \pm 0.2 \pm 0.4$
$^{208}Pb \leftrightarrow {}^{206}Pb$	$14.7 \pm 0.2 \pm 0.4$
$^{208}Pb \leftrightarrow {}^{207}Pb$	$9.4 \pm 0.3 \pm 0.4$

* Only the experimental error is given

TABLE VI. *Confit* Matrices for Muonic $2p \rightarrow 1s$ Energy Differences of Isotones, $10 \leqslant Z \leqslant 82$

See page 194 for Explanation of Tables

[keV]	^{19}F	^{20}Ne	^{22}Ne	^{23}Na	^{24}Mg
^{19}F		-38.767	-38.998	-81.714	-128.020
		5	5	2	3
^{20}Ne			-0.230	-42.947	-89.252
			6	5	5
^{22}Ne				-42.717	-89.022
				4	4
^{23}Na					-46.305
					2

[keV]	^{26}Mg	^{27}Al	^{28}Si	^{31}P	^{32}S	^{34}S
^{26}Mg		-50.083	-103.428	-160.055	-219.585	-219.361
		3	6	12	12	15
^{27}Al			-53.345	-109.972	-169.502	-169.278
			5	11	12	15
^{28}Si				-56.627	-116.158	-115.933
				13	13	16
^{31}P					-59.530	-59.306
					14	16
^{32}S						-0.224
						16
^{34}S						

TABLE VI. *Confit* Matrices for Muonic $2p \rightarrow 1s$ Energy Differences of Isotones, $10 \leqslant Z \leqslant 82$

See page 194 for Explanation of Tables

[keV]	^{68}Zn	^{69}Ga	^{70}Ge	^{74}Ge	^{75}As	^{76}Se	^{78}Se	^{79}Br
^{68}Zn		-89.254	-178.338	-174.208	-265.603	-355.600	-355.331	-448.225
		40	38	45	40	42	41	42
^{69}Ga	90.236		-89.084	-84.954	-176.349	-266.346	-266.077	-358.971
	33		26	28	18	24	21	24
^{70}Ge	180.273	90.037		4.130	-87.265	-177.262	-176.994	-269.888
	29	19		33	26	30	28	30
^{74}Ge	176.081	85.845	-4.192		-91.395	-181.392	-181.123	-274.017
	35	20	21		29	33	30	32
^{75}As	268.864	178.628	88.591	92.783		-89.997	-89.728	-182.622
	33	16	20	20		24	21	24
^{76}Se	359.820	269.584	179.547	183.739	90.956		0.269	-92.625
	35	19	22	23	19		25	28
^{78}Se	359.566	269.330	179.293	183.485	90.702	-0.254		-92.894
	34	17	20	21	17	18		25
^{79}Br	453.998	363.762	273.725	277.917	185.134	94.178	94.432	
	36	20	23	24	20	23	20	

[keV]	^{80}Se	^{81}Br	^{82}Kr	^{86}Kr	^{87}Rb	^{88}Sr	^{89}Y	^{90}Zr
^{80}Se		-93.354	-185.837	-187.332	-283.170	-377.814	-473.934	-568.509
		28	46	38	24	17	18	19
^{81}Br	94.857		-92.482	-93.977	-189.816	-284.459	-380.580	-475.154
	23		42	31	26	26	21	27
^{82}Kr	188.572	93.715		-1.495	-97.334	-191.977	-288.097	-382.672
	42	44		39	48	44	45	45
^{86}Kr	190.094	95.237	1.522		-95.839	-190.482	-286.602	-381.177
	36	40	33		29	36	37	37
^{87}Rb	287.500	192.643	98.928	97.406		-94.644	-190.764	-285.338
	18	24	42	37		22	22	23
^{88}Sr	383.788	288.931	195.216	193.694	96.288		-96.120	-190.695
	14	21	41	35	15		11	13
^{89}Y	481.658	386.801	293.086	291.564	194.158	97.870		-94.575
	15	22	41	35	16	8		13
^{90}Zr	578.096	483.239	389.524	388.002	290.596	194.308	96.438	
	15	22	41	36	16	10	10	

TABLE VI. *Confit* Matrices for Muonic $2p \rightarrow 1s$ Energy Differences of Isotones, $10 \leq Z \leq 82$

See page 194 for Explanation of Tables

[keV]	^{92}Zr	^{93}Nb	^{94}Mo	^{100}Mo	^{102}Ru	^{103}Rh	^{104}Pd
^{92}Zr		-96.191	-190.438	-166.795	-357.177	-454.067	-550.377
		26	28	30	39	35	140
^{93}Nb	98.412		-94.247	-70.605	-260.986	-357.876	-454.186
	19		29	31	40	36	141
^{94}Mo	194.472	96.060		23.642	-166.740	-263.629	-359.939
	19	21		33	42	38	141
^{100}Mo	170.687	72.275	-23.784		-190.382	-287.272	-383.582
	20	22	22		43	40	142
^{102}Ru	365.639	267.227	171.167	194.952		-90.890	-193.200
	31	33	33	34		46	143
^{103}Rh	464.878	366.466	270.407	294.191	99.240		-96.310
	26	27	28	28	35		142
^{104}Pd	563.884	465.472	369.412	393.197	198.245	99.006	
	121	121	121	122	123	122	

[keV]	^{108}Pd	^{109}Ag	^{110}Cd	^{114}Cd	^{115}In	^{123}Sb	^{124}Te
^{108}Pd		-97.510	-195.198	-182.301	-280.452	-452.010	-539.937
		78	85	77	82	106	77
^{109}Ag	100.278		-97.688	-84.791	-182.942	-354.500	-442.427
	52		56	43	47	84	40
^{110}Cd	200.832	100.554		12.897	-85.255	-256.813	-344.740
	61	46		55	61	91	54
^{114}Cd	187.853	87.575	-12.979		-98.152	-269.709	-357.637
	52	33	46		49	84	39
^{115}In	289.766	189.489	88.934	101.913		-171.558	-259.485
	58	37	52	41		87	47
^{123}Sb	467.400	367.122	266.568	279.547	177.634		-87.927
	73	60	69	61	65		82
^{124}Te	557.597	457.319	356.765	369.744	267.831	90.197	
	52	32	46	32	41	60	

TABLE VI. *Confit* Matrices for Muonic $2p \rightarrow 1s$ Energy Differences of Isotones, $10 \leqslant Z \leqslant 82$

See page 194 for Explanation of Tables

[keV]	^{126}Te	^{127}I	^{128}Xe	^{132}Xe	^{133}Cs	^{134}Ba
^{126}Te		-88.364	-176.589	-171.740	-261.706	-347.789
		43	105	65	46	40
^{127}I	92.864		-88.225	-83.376	-173.342	-259.424
	39		108	71	47	47
^{128}Xe	183.456	90.592		4.849	-85.117	-171.199
	104	107		118	109	107
^{132}Xe	178.408	85.544	-5.048		-89.966	-176.048
	45	52	109		72	69
^{133}Cs	271.757	178.894	88.302	93.350		-86.083
	37	36	106	50		50
^{134}Ba	361.805	268.942	178.349	183.398	90.048	
	31	40	105	48	38	

[keV]	^{138}Ba	^{139}La	^{140}Ce	^{141}Pr
^{138}Ba		-89.368	-175.200	-263.719
		39	35	27
^{139}La	93.420		-85.832	-174.352
	33		43	45
^{140}Ce	182.946	89.526		-88.520
	32	32		41
^{141}Pr	275.607	182.187	92.661	
	25	40	39	

TABLE VII. Differences of Barrett Radii for Isotones, $8 \leq Z \leq 126$

See page 194 for Explanation of Tables

Isotone Pair			$\Delta R^{\mu}_{k\alpha}[am]$
^{16}O	$\leftrightarrow$	$^{14}C^{*}$	$242.1 \pm 12.6 \pm 1.1$
^{20}Ne	$\leftrightarrow$	^{19}F	$136.5 \pm 3.2 \pm 1.0$
^{20}Ne	$\leftrightarrow$	^{18}O	$297.6 \pm 14.0 \pm 1.0$
^{23}Na	$\leftrightarrow$	^{22}Ne	$50.6 \pm 1.8 \pm 0.9$
^{24}Mg	$\leftrightarrow$	^{22}Ne	$130.5 \pm 1.6 \pm 1.0$
^{27}Al	$\leftrightarrow$	^{26}Mg	$36.2 \pm 0.7 \pm 1.1$
^{28}Si	$\leftrightarrow$	^{26}Mg	$112.0 \pm 1.2 \pm 1.4$
^{32}S	$\leftrightarrow$	^{31}P	$92.3 \pm 1.5 \pm 1.0$
^{32}S	$\leftrightarrow$	$^{30}Si^{*}$	$164.2 \pm 6.7 \pm 0.8$
^{36}Ar	$\leftrightarrow$	^{34}S	$133.4 \pm 1.0 \pm 1.1$
^{40}Ca	$\leftrightarrow$	^{39}K	$55.1 \pm 2.0 \pm 0.7$
^{42}Ca	$\leftrightarrow$	$^{40}Ar^{*}$	$103.2 \pm 1.9 \pm 1.0$
^{45}Sc	$\leftrightarrow$	^{44}Ca	$35.3 \pm 1.3 \pm 0.9$
^{46}Ti	$\leftrightarrow$	^{44}Ca	$111.7 \pm 1.3 \pm 0.8$
^{51}V	$\leftrightarrow$	^{50}Ti	$36.0 \pm 1.0 \pm 0.7$
^{52}Cr	$\leftrightarrow$	^{50}Ti	$89.1 \pm 0.8 \pm 0.7$
^{55}Mn	$\leftrightarrow$	^{54}Cr	$24.8 \pm 0.6 \pm 0.8$
^{56}Fe	$\leftrightarrow$	^{54}Cr	$63.8 \pm 0.7 \pm 0.9$
^{59}Co	$\leftrightarrow$	^{58}Fe	$16.4 \pm 0.8 \pm 0.8$
^{60}Ni	$\leftrightarrow$	^{58}Fe	$47.2 \pm 0.8 \pm 0.7$
^{63}Cu	$\leftrightarrow$	^{62}Ni	$52.0 \pm 0.4 \pm 0.8$

Isotone Pair			$\Delta R^{\mu}_{k\alpha}[am]$
^{64}Zn	$\leftrightarrow$	^{62}Ni	$109.2 \pm 0.4 \pm 0.7$
^{69}Ga	$\leftrightarrow$	^{68}Zn	$40.0 \pm 0.4 \pm 0.7$
^{70}Ge	$\leftrightarrow$	^{68}Zn	$93.5 \pm 0.3 \pm 0.8$
^{75}As	$\leftrightarrow$	^{74}Ge	$29.2 \pm 0.2 \pm 0.8$
^{76}Se	$\leftrightarrow$	^{74}Ge	$84.4 \pm 0.2 \pm 1.0$
^{79}Br	$\leftrightarrow$	^{78}Se	$28.7 \pm 0.2 \pm 0.8$
^{81}Br	$\leftrightarrow$	^{80}Se	$25.3 \pm 0.2 \pm 0.7$
^{82}Kr	$\leftrightarrow$	^{80}Se	$65.7 \pm 0.3 \pm 0.8$
^{87}Rb	$\leftrightarrow$	^{86}Kr	$18.2 \pm 0.3 \pm 0.6$
^{88}Sr	$\leftrightarrow$	^{86}Kr	$49.7 \pm 0.2 \pm 0.7$
^{89}Y	$\leftrightarrow$	^{88}Sr	$23.4 \pm 0.1 \pm 0.6$
^{90}Zr	$\leftrightarrow$	^{88}Sr	$58.4 \pm 0.1 \pm 0.6$
^{93}Nb	$\leftrightarrow$	^{92}Zr	$23.2 \pm 0.1 \pm 0.6$
^{94}Mo	$\leftrightarrow$	^{92}Zr	$59.2 \pm 0.1 \pm 0.7$
^{102}Ru	$\leftrightarrow$	^{100}Mo	$46.4 \pm 0.2 \pm 0.8$
^{103}Rh	$\leftrightarrow$	^{102}Ru	$15.7 \pm 0.2 \pm 0.7$
^{104}Pd	$\leftrightarrow$	^{102}Ru	$34.4 \pm 0.5 \pm 0.7$
^{109}Ag	$\leftrightarrow$	^{108}Pd	$10.1 \pm 0.2 \pm 0.7$
^{110}Cd	$\leftrightarrow$	^{108}Pd	$21.0 \pm 0.2 \pm 0.7$
^{115}In	$\leftrightarrow$	$^{114}Cd^{*}$	$4.9 \pm 0.2 \pm 0.7$

TABLE VII. Differences of Barrett Radii for Isotones, $8 \leq Z \leq 126$

See page 194 for Explanation of Tables

Isotone Pair			$\Delta R^{\mu}_{k\alpha}[am]$
^{116}Sn	$\leftrightarrow$	$^{114}Cd^{*}$	$18.2 \pm 0.2 \pm 0.6$
^{124}Te	$\leftrightarrow$	^{123}Sb	$38.0 \pm 0.2 \pm 0.6$
^{124}Te	$\leftrightarrow$	$^{122}Sn^{*}$	$66.1 \pm 0.4 \pm 0.6$
^{127}I	$\leftrightarrow$	^{126}Te	$27.9 \pm 0.1 \pm 0.5$
^{128}Xe	$\leftrightarrow$	^{126}Te	$61.1 \pm 0.3 \pm 0.5$
^{133}Cs	$\leftrightarrow$	^{132}Xe	$22.0 \pm 0.1 \pm 0.5$
^{134}Ba	$\leftrightarrow$	^{132}Xe	$53.8 \pm 0.1 \pm 0.5$
^{139}La	$\leftrightarrow$	^{138}Ba	$19.7 \pm 0.1 \pm 0.5$
^{140}Ce	$\leftrightarrow$	^{138}Ba	$47.9 \pm 0.1 \pm 0.5$
^{141}Pr	$\leftrightarrow$	^{140}Ce	$18.7 \pm 0.1 \pm 0.5$
^{142}Nd	$\leftrightarrow$	^{140}Ce	$45.7 \pm 0.1 \pm 0.5$
^{144}Sm	$\leftrightarrow$	^{142}Nd	$42.9 \pm 0.2 \pm 0.5$
^{153}Eu	$\leftrightarrow$	^{152}Sm	$36.6 \pm 0.1 \pm 0.8$
^{154}Gd	$\leftrightarrow$	^{152}Sm	$43.0 \pm 0.7 \pm 0.8$
^{162}Dy	$\leftrightarrow$	^{160}Gd	$36.0 \pm 0.4 \pm 0.8$
^{166}Er	$\leftrightarrow$	^{164}Dy	$35.7 \pm 0.4 \pm 0.7$
^{176}Hf	$\leftrightarrow$	^{174}Yb	$25.5 \pm 0.9 \pm 0.7$
^{181}Ta	$\leftrightarrow$	^{180}Hf	$12.4 \pm 0.3 \pm 0.7$
^{182}W	$\leftrightarrow$	^{180}Hf	$22.5 \pm 0.3 \pm 0.7$
^{188}Os	$\leftrightarrow$	$^{186}W^{*}$	$20.6 \pm 1.0 \pm 0.8$
^{194}Pt	$\leftrightarrow$	$^{192}Os^{*}$	$20.9 \pm 0.8 \pm 0.8$
^{197}Au	$\leftrightarrow$	^{196}Pt	$5.7 \pm 0.2 \pm 0.8$
^{198}Hg	$\leftrightarrow$	$^{196}Pt^{*}$	$19.1 \pm 0.5 \pm 0.5$
^{203}Tl	$\leftrightarrow$	$^{202}Hg^{*}$	$6.1 \pm 1.1 \pm 0.5$
^{206}Pb	$\leftrightarrow$	$^{204}Hg^{*}$	$17.6 \pm 0.6 \pm 0.3$
^{209}Bi	$\leftrightarrow$	$^{208}Pb^{*}$	$18.8 \pm 3.0 \pm 0.5$

TABLE VIII. Charge Density Distribution Parameters from Elastic Electron Scattering

See page 194 for Explanation of Tables

Nucleus	model	$\langle r^2 \rangle^{1/2}$ [fm]	c [fm]	a [fm]	w	q-range [fm^{-1}]	Ref.
^{12}C	FB	2.4776 (55)				1.0 - 2.3	[Of91]
^{15}N	FB	2.612 (9)				0.4 - 3.2	[Vr88]
^{26}Mg	FB	2.960 (4)				0.6 - 3.0	[So88]
^{30}Si	FB	3.193 (13)				0.27 - 2.64	[We93]
^{31}P	FB	3.191 (5)				0.27 - 2.83	[We93]
^{32}S	FB	3.230 (5)				0.32 - 3.67	[We93]
$^{70}Ge^{\star}$	2pF	4.055 (8)	4.430 (8)	0.5807 (30)		0.59 - 1.50	[Kh90]
$^{72}Ge^{\star}$	2pF	4.088 (8)	4.446 (8)	0.5921 (30)		0.59 - 1.50	[Kh90]
$^{74}Ge^{\star}$	2pF	4.126 (8)	4.454 (8)	0.6085 (30)		0.59 - 1.44	[Kh90]
$^{76}Ge^{\star}$	2pF	4.127 (8)	4.547 (8)	0.5780 (30)		0.59 - 1.44	[Kh90]
^{74}Se	2pF	4.07 (2)	4.387 (22)	0.6078 (7)		0.42 - 1.47	[Kh88]
	3pF	4.05 (2)	4.488 (67)	0.5933 (9)	-0.09 (6)	0.42 - 1.47	[Kh88]
	2pG	4.00 (2)	4.278 (29)	2.493 (16)		0.42 - 1.47	[Kh88]
	3pG	4.04 (1)	3.838 (185)	2.536 (21)	0.534 (101)	0.42 - 1.47	[Kh88]
^{76}Se	2pF	4.162 (10)	4.471 (11)	0.6208 (39)		0.42 - 1.6	[Kh88]
	3pF	4.152 (9)	4.512 (34)	0.6189 (43)	-0.039 (31)	0.42 - 1.6	[Kh88]
	2pG	4.088 (5)	4.350 (16)	2.554 (10)		0.42 - 1.6	[Kh88]
	3pG	4.133 (7)	3.682 (93)	2.608 (10)	0.645 (38)	0.42 - 1.6	[Kh88]
^{78}Se	2pF	4.138 (14)	4.581 (18)	0.5729 (41)		0.42 - 1.68	[Kh88]
	3pF	4.123 (9)	4.634 (34)	0.5673 (53)	-0.058 (33)	0.42 - 1.68	[Kh88]
	2pG	4.077 (5)	4.503 (14)	2.451 (9)		0.42 - 1.68	[Kh88]
	3pG	4.111 (7)	4.099 (73)	2.512 (13)	0.559 (48)	0.42 - 1.68	[Kh88]
^{80}Se	2pF	4.124 (10)	4.667 (10)	0.5339 (42)		0.42 - 1.68	[Kh88]
	3pF	4.137 (9)	4.614 (33)	0.5410 (58)	0.061 (37)	0.42 - 1.68	[Kh88]
	2pG	4.076 (5)	4.622 (13)	2.365 (9)		0.42 - 1.68	[Kh88]
	3pG	4.122 (7)	4.139 (68)	2.405 (14)	0.657 (44)	0.42 - 1.68	[Kh88]

$\star$ For the Ge isotopes measurements with an extended q range are given by Mallot [Ma85]

TABLE VIII. Charge Density Distribution Parameters from Elastic Electron Scattering
See page 194 for Explanation of Tables

Nucleus	model	$\langle r^2 \rangle^{1/2}$ [fm]	c [fm]	a [fm]	w	q-range [fm^{-1}]	Ref.
^{82}Se	2pF	4.118 (11)	4.718 (11)	0.5102 (49)		0.42 - 1.6	[Kh88]
	3pF	4.134 (9)	4.642 (37)	0.5225 (72)	0.089 (43)	0.42 - 1.6	[Kh88]
	2pG	4.076 (10)	4.694 (13)	2.307 (11)		0.42 - 1.6	[Kh88]
	3pG	4.122 (8)	4.212 (73)	2.429 (17)	0.675 (49)	0.42 - 1.6	[Kh88]
^{90}Zr	FB	4.280 (10)				0.5 - 2.5	[Ma89]
^{92}Zr	FB	4.312 (11)				0.5 - 2.5	[Ma89]
^{94}Zr	FB	4.332 (11)				0.5 - 2.5	[Ma89]
^{92}Mo	FB	4.306 (10)				0.56 - 1.96	[Ma89]
^{94}Mo	FB	4.346 (10)				0.56 - 1.96	[Ma89]
^{96}Mo	FB	4.377 (10)				0.56 - 1.96	[Ma89]
^{98}Mo	FB	4.408 (10)				0.56 - 1.96	[Ma89]
^{100}Mo	FB	4.447 (10)				0.56 - 1.96	[Ma89]
^{188}Os	SOG	5.4001 (13)				0.6 - 3.2	[Bo88]
^{190}Os	SOG	5.4062 (14)				0.6 - 3.2	[Bo88]
^{192}Os	SOG	5.410 (1)				0.6 - 3.2	[Bo88]
^{194}Pt	SOG	5.369 (9)				0.6 - 3.2	[Bo88]
^{196}Pt	SOG	5.370 (3)				0.6 - 3.2	[Bo88]
^{198}Hg	FB	5.439 (4)				0.43 - 2.93	[La86]
^{204}Hg	FB	5.4717 (16)				0.42 - 2.88	[Bu89]
^{204}Pb	FB	5.4603 (40)				0.51 - 2.24	[Ma92a]
^{206}Pb	FB	5.4742 (41)				0.51 - 2.24	[Ma92a]
^{207}Pb	FB	5.4838 (41)				0.51 - 2.24	[Ma92a]
^{208}Pb	FB	5.4785 (41)				0.51 - 2.24	[Ma92a]

TABLE IX. Fourier–Bessel Coefficients from Elastic Electron Scattering

See page 194 for Explanation of Tables

Nucleus	^{12}C	^{15}N	^{26}Mg	^{30}Si	^{31}P
$\langle r^2\rangle^{1/2}$ (fm)	2.4777	2.6130	2.9610	3.1932	3.1913
$\langle r^4\rangle^{1/4}$ (fm)	2.7722	2.9689	3.2339	3.5507	3.5241
$\langle r^6\rangle^{1/6}$ (fm)	3.0397	3.3164	3.4594	3.8977	3.8251
R^e_{ka} (fm)	3.1915		3.8103	4.0994	4.0983
a1	1.5709e-2	2.5490e-2	2.9280e-2	2.8322e-2	3.5280e-2
a2	3.8610e-2	5.0630e-2	5.5520e-2	5.3722e-2	5.9545e-2
a3	3.6418e-2	2.9840e-2	2.3910e-2	2.4661e-2	1.7241e-2
a4	1.4293e-2	-5.5300e-3	-1.3940e-2	-1.2888e-2	-1.9338e-2
a5	-4.4628e-3	-1.5900e-2	-1.5840e-2	-1.7112e-2	-1.3171e-2
a6	-9.8420e-3	-7.7000e-3	-3.5680e-3	-4.4233e-3	1.4065e-3
a7	-6.6518e-3	-2.3000e-3	1.9670e-3	3.2357e-3	3.6747e-3
a8	-2.7066e-3	-4.0000e-4	1.4470e-3	2.2195e-3	6.3926e-4
a9	-5.6697e-4		-8.6820e-5	4.0898e-4	-3.2297e-4
a10	-2.7453e-4		-1.4000e-4	2.0363e-4	1.8286e-4
a11	-1.7093e-4		7.0000e-5	-2.6112e-4	-1.0781e-4
a12	1.2433e-4		-2.0000e-5	2.3104e-4	6.6628e-5
a13	-4.8496e-5		3.0000e-6	-1.8855e-4	-4.2991e-5
a14	1.5675e-5		1.0000e-7		2.8800e-5
a15	-4.5194e-6		-2.0000e-7		-1.9932e-5
a16	1.1920e-6				
a17	-2.9065e-7				
a18	6.5845e-8				
R_{cut} (fm)	8.0	7.0	8.0	8.5	8.0
Ref.	[Of91]	[Vr88]	[So88]	[We93]	[We93]

TABLE IX. Fourier–Bessel Coefficients from Elastic Electron Scattering

See page 194 for Explanation of Tables

Nucleus	^{32}S	^{90}Zr	^{92}Zr	^{94}Zr	^{92}Mo
$\langle r^2\rangle^{1/2}$ (fm)	3.2295	4.2796	4.3118	4.3319	4.3058
$\langle r^4\rangle^{1/4}$ (fm)	3.5439	4.6035	4.6399	4.6619	4.6253
$\langle r^6\rangle^{1/6}$ (fm)	3.8086	4.8695	4.9091	4.9313	4.8884
R^c_{ka} (fm)	4.1483	5.4808	5.5212	5.5465	5.5149
a1	3.7359e-2	1.4655e-0	1.4585e-0	1.4541e-0	1.4087e-0
a2	6.0918e-2	-4.8451e-1	-4.7274e-1	-4.6543e-1	-3.8490e-1
a3	1.5029e-2	-4.5590e-2	-4.8662e-2	-4.9800e-2	-8.1355e-2
a4	-1.8758e-2	7.3069e-2	6.9795e-2	6.6551e-2	5.3179e-2
a5	-1.0174e-2	2.7921e-3	3.6133e-3	4.6089e-3	1.3497e-2
a6	3.1107e-3	-1.3480e-2	-1.2283e-2	-1.1399e-2	-7.3112e-3
a7	3.9209e-3	-3.6792e-4	-4.4525e-4	-9.2051e-4	-2.7433e-3
a8	1.2556e-3	3.0278e-3	2.6520e-3	2.8621e-3	7.0109e-4
a9	-1.1683e-4	-1.4165e-5	-2.3637e-4	-3.5979e-4	1.0278e-4
a10	-6.6587e-4	-3.1561e-4	-1.2070e-4	-1.3554e-4	9.3746e-5
a11	-1.7395e-4	-1.3736e-4	-7.1995e-5	-7.2113e-5	4.5421e-5
a12	5.6504e-5	-2.2203e-5	-2.1952e-5	-1.8146e-5	1.8367e-5
a13	-1.1374e-4	1.1254e-5	-1.8051e-6	1.9590e-6	6.7518e-6
a14	9.9554e-5	1.2484e-5	2.6161e-6	5.0940e-6	2.3267e-6
a15	-6.2021e-5	7.3383e-5	2.2102e-6	3.5240e-6	7.6142e-6
R_{cut} (fm)	8.0	10.0	10.0	10.0	9.5
Ref.	[We93]	[Ma89]	[Ma89]	[Ma89]	[Ma89]

TABLE IX. Fourier–Bessel Coefficients from Elastic Electron Scattering

See page 194 for Explanation of Tables

Nucleus	^{94}Mo	^{96}Mo	^{98}Mo	^{100}Mo	^{198}Hg
$\langle r^2\rangle^{1/2}$ (fm)	4.3462	4.3766	4.4077	4.4466	5.4369
$\langle r^4\rangle^{1/4}$ (fm)	4.6719	4.7061	4.7417	4.7852	5.7615
$\langle r^6\rangle^{1/6}$ (fm)	4.9407	4.9765	5.0167	5.0657	6.0079
R^c_{ha} (fm)	5.5651	5.6032	5.6420	5.6911	6.9616
a1	1.3993e-0	1.3921e-0	1.3847e-0	1.3755e-0	0.7763e-0
a2	-3.7117e-1	-3.6096e-1	-3.5036e-1	-3.3662e-1	5.0020e-1
a3	-8.2942e-2	-8.2924e-2	-8.4221e-2	-8.7092e-2	-7.0634e-1
a4	4.9823e-2	4.6040e-2	4.3079e-2	4.0659e-2	-0.7791e-1
a5	1.3324e-2	1.3252e-2	1.3505e-2	1.3770e-2	4.0512e-1
a6	-6.7303e-3	-5.9623e-3	-4.7350e-3	-4.3166e-3	-1.0145e-1
a7	-2.5153e-3	-2.4484e-3	-2.5760e-3	-2.1707e-3	-1.3954e-1
a8	7.6567e-4	7.9107e-4	3.7381e-4	2.9343e-4	0.7129e-1
a9	1.0129e-4	6.7532e-5	9.9915e-5	3.0507e-6	0.1619e-1
a10	5.1645e-5	4.2222e-5	6.4032e-5	1.0859e-5	-0.2056e-1
a11	2.2401e-5	2.0117e-5	2.8547e-5	7.1838e-6	
a12	8.7445e-6	8.2364e-6	1.1104e-5	3.3711e-6	
a13	3.1709e-6	3.0688e-6	3.9917e-6	1.3520e-6	
a14	1.0863e-6	1.0694e-6	1.3559e-6	4.9322e-7	
a15	3.5460e-6	3.5305e-6	4.3927e-6	1.6799e-7	
R_{cut} (fm)	9.5	9.5	9.5	9.5	11.0
Ref.	[Ma89]	[Ma89]	[Ma89]	[Ma89]	[La86]

TABLE IX. Fourier–Bessel Coefficients from Elastic Electron Scattering

See page 194 for Explanation of Tables

Nucleus	^{204}Hg	^{204}Pb	^{206}Pb	^{207}Pb	^{208}Pb
$\langle r^2\rangle^{1/2}$ (fm)	5.4717	5.4603	5.4742	5.4838	5.4785
$\langle r^4\rangle^{1/4}$ (fm)	5.8157	5.8034	5.8173	5.8280	5.8224
$\langle r^6\rangle^{1/6}$ (fm)	6.0975	6.0721	6.0852	6.0978	6.0909
R^c_{ka} (fm)	6.9974	6.9787	6.9966	7.0088	7.0018
a1	5.0880e-2	1.4429e-0	1.4403e-0	1.4386e-0	1.4396e-0
a2	5.0679e-2	-4.2429e-1	-4.1971e-1	-4.1663e-1	-4.1850e-1
a3	-3.9771e-2	-9.5671e-2	-9.7085e-2	-9.8583e-2	-9.7163e-2
a4	-3.1403e-2	7.0018e-2	6.8671e-2	6.8752e-2	6.8006e-2
a5	2.8120e-2	2.6037e-2	2.6342e-2	2.6388e-2	2.6476e-2
a6	1.0580e-2	-1.6179e-2	-1.5755e-2	-1.5632e-2	-1.5307e-2
a7	-1.6402e-2	-6.9630e-3	-6.9078e-3	-6.8570e-3	-7.1246e-3
a8	-3.1958e-3	2.8872e-3	2.9708e-3	2.5973e-3	2.7987e-3
a9	6.9355e-3	2.4712e-3	2.4830e-3	2.4401e-3	2.3767e-3
a10	7.0777e-4	-1.0106e-3	-1.3911e-3	-9.4205e-4	-1.0125e-3
a11	-1.4961e-4	-2.5467e-4	1.5425e-4	-2.2020e-4	-2.5836e-4
a12	2.4032e-4	2.2412e-5	1.3471e-4	8.2610e-6	6.4297e-5
a13	-2.9939e-4	4.8363e-5	7.5187e-5	3.9685e-5	6.5528e-5
a14	2.0003e-4	1.9367e-5	3.0809e-6	1.7911e-5	1.4523e-5
a15	-1.5870e-4	-2.3405e-6	-2.4780e-5	-1.0828e-6	-1.4430e-5
R_{cut} (fm)	12.0	12.5	12.5	12.5	12.5
Ref.	[Bu89]	[Ma92a]	[Ma92a]	[Ma92a]	[Ma92a]

TABLE X. King Plots: Optical versus Combined Muonic and Elastic Electron Scattering Data

See page 194 for Explanation of Tables

20 CALCIUM			
$R^{\mu}_{k\alpha}(40)$ = 4.4628 fm	λ_{proj} = 2 · 599 nm (2-phot.trans.)	$F_{2x599nm}$ = -93.7(1.6) $\frac{MHz}{fm^2}$	
C_2/C_1 = $-2.14\cdot10^{-4}$ fm^{-2}	FS^{42-40} = -18.8(.5) MHz	NMS^{42-40} = 652.6 MHz	
C_3/C_1 = $1.37\cdot10^{-6}$ fm^{-4}	MS^{42-40} = 625.9(.1) MHz	SMS^{42-40} = -26.7(.1) MHz	
	χ^2/D.F. = 0.84	SMS/NMS = -0.0409(.0002)	

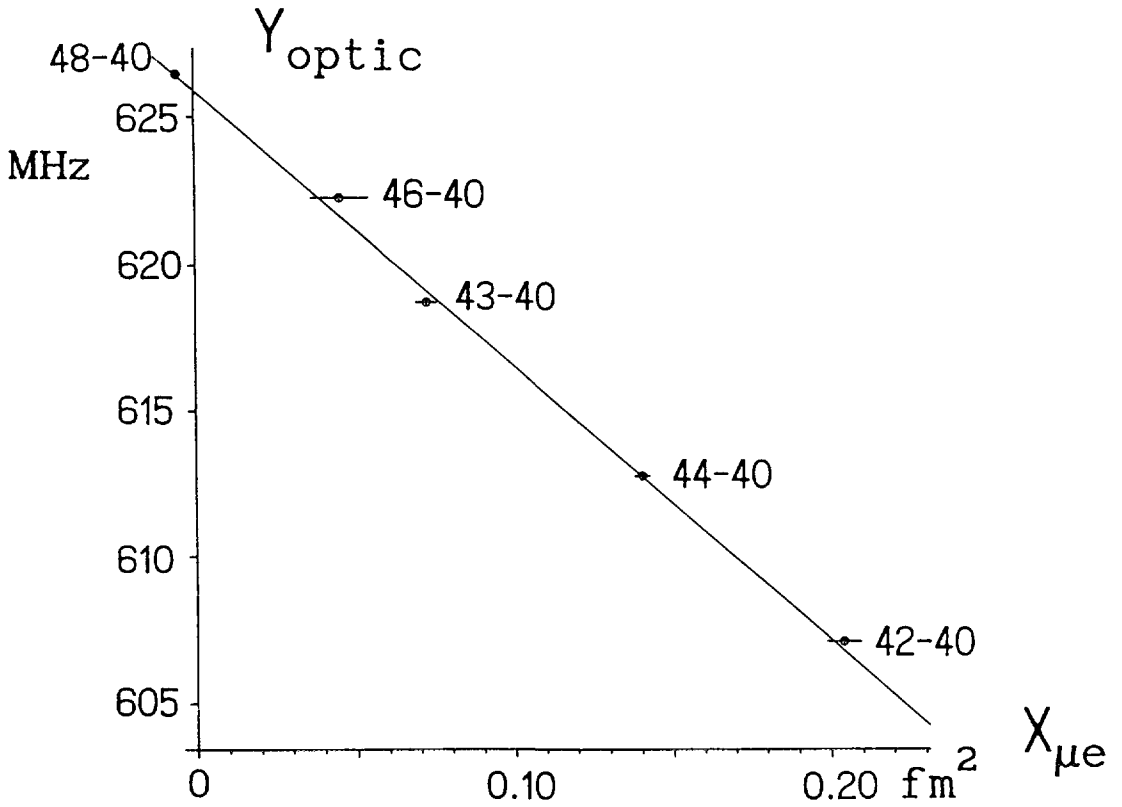

Isotope	V_2	V_4	V_6
40[e]	1.28364	1.1776	1.101
42	1.28400	1.1799	1.105
43	1.28410	1.1811	1.107
44	1.28430	1.1823	1.109
46	1.28460	1.1846	1.113
48[e]	1.28493	1.1870	1.117

Isotope pair	$\delta\langle r^2\rangle_{0\mu e}$ [fm^2]	HM [%]
42-40	0.202(4)	-0.50
43-40	0.113(3)	-0.32
44-40	0.269(5)	-0.45
46-40	0.107(4)	-0.14
48-40	-0.021(3)	-4.47

Note: The V values for ^{40}Ca and ^{48}Ca are taken from elastic electron scattering [Em83]. The V values for the other isotopes are interpolated.

TABLE X. King Plots: Optical versus Combined Muonic and Elastic Electron Scattering Data

See page 194 for Explanation of Tables

36 KRYPTON			
$R^{\mu}_{k\alpha}(80)$	= 5.3773 fm		
C_2/C_1	= $-4.11\cdot10^{-4}$ fm^{-2}		
C_3/C_1	= $1.47\cdot10^{-6}$ fm^{-4}		

λ_{proj}	= 810.7 nm	$F_{810.7nm}$	= -438(86) MHz/fm^2
FS^{80-78}	= 20.1(7.7) MHz	NMS^{80-78}	= 65.2 MHz
MS^{80-78}	= 59.9(3.9) MHz	SMS^{80-78}	= -5.2(3.9) MHz
χ^2/D.F.	= 0.20	SMS/NMS	= -0.08(.06)

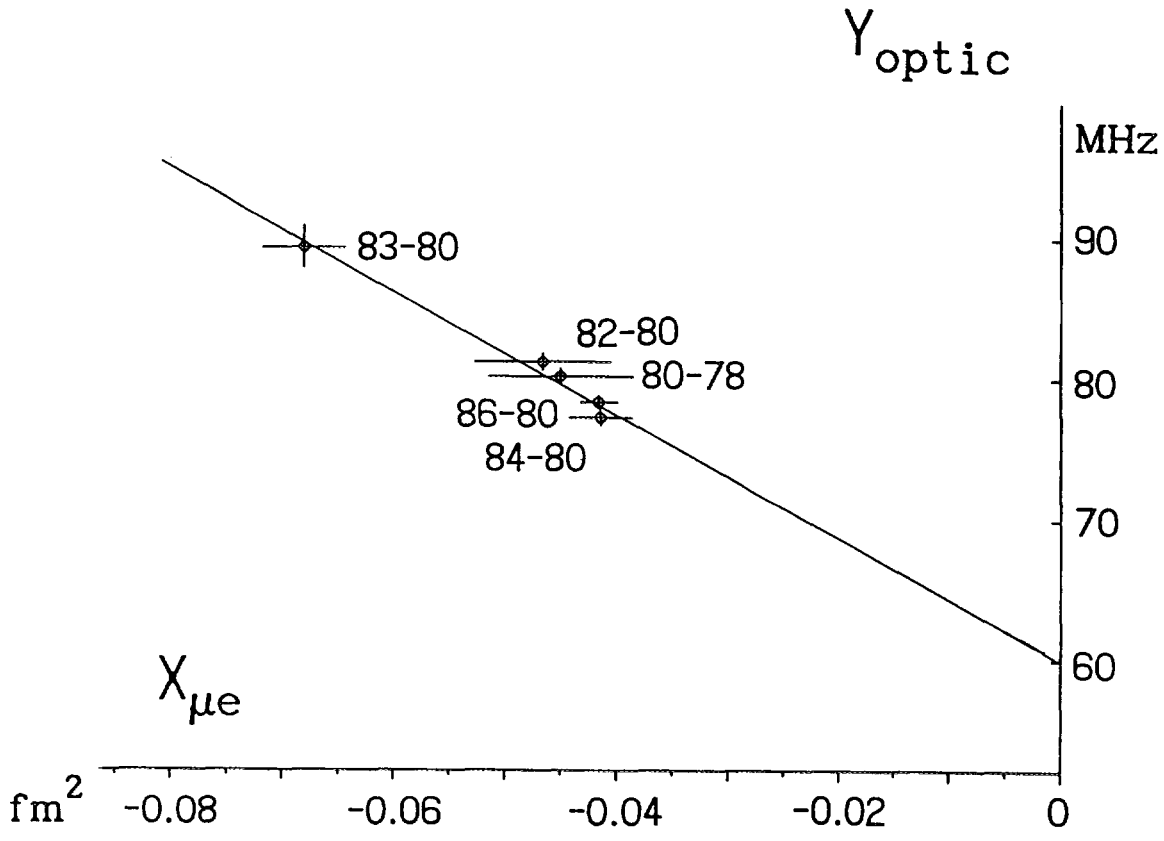

Isotope	V_2	V_4	V_6
78	1.28106	1.1876	1.116
80	1.28103	1.1874	1.116
82	1.28100	1.1873	1.115
83	1.28098	1.1872	1.115
84	1.28099	1.1872	1.115
86	1.28097	1.1871	1.115

Isotope pair	$\delta\langle r^2\rangle_{0\mu e}$ [fm^2]	HM [%]
80-78	-0.047(9)	-1.60
82-80	-0.047(9)	-1.58
83-80	-0.096(19)	-1.57
84-80	-0.075(15)	-1.58
86-80	-0.116(23)	-1.58

Note: The V values are calculated with a two parameter Fermi distribution with the parameters taken from Table III-A.

TABLE X. King Plots: Optical versus Combined Muonic and Elastic Electron Scattering Data

See page 194 for Explanation of Tables

38 STRONTIUM			
$R^{\mu}_{k\alpha}(88)$	= 5.4092 fm	λ_{proj} = 293.2 nm	$F_{293.2nm}$ = -611(81) $\frac{MHz}{fm^2}$
C_2/C_1	= $-4.45\cdot10^{-4}$ fm^{-2}	FS^{88-86} = 37.2(9.7) MHz	NMS^{88-86} = 148.4 MHz
C_3/C_1	= $1.56\cdot10^{-6}$ fm^{-4}	MS^{88-86} = 187.8(5.5) MHz	SMS^{88-86} = 39.5(5.5) MHz
		χ^2/D.F. = 0.07	SMS/NMS = 0.27(0.04)

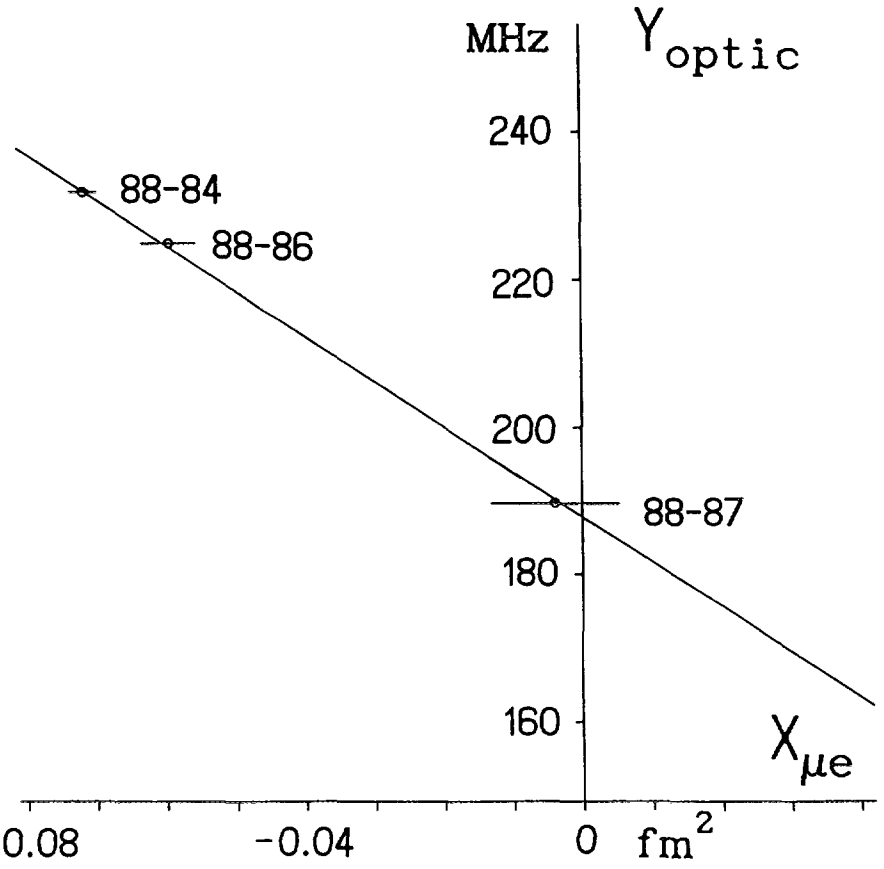

Isotope	V_2	V_4	V_6
84	1.28215	1.1952	1.134
86	1.28215	1.1952	1.134
87	1.28215	1.1952	1.134
88[e]	1.28215	1.1952	1.134

Isotope pair	$\delta\langle r^2\rangle_{0\mu e}$ [fm^2]	HM [%]
88-84	-0.149(20)	-1.83
88-86	-0.062(8)	-1.82
88-87	-0.0016(2)	-1.87

Note: The V values for ^{88}Sr are taken from elastic electron scattering [Vr87]. The same V values have been used for the other isotopes.

TABLE X. King Plots: Optical versus Combined Muonic and Elastic Electron Scattering Data

See page 194 for Explanation of Tables

40 ZIRCONIUM			
$R^{\mu}_{k\alpha}(90)$	= 5.4676 fm		
C_2/C_1	= $-4.79\cdot10^{-4}$ fm^{-2}		
C_3/C_1	= $1.67\cdot10^{-6}$ fm^{-4}		

λ_{proj}	= 613.46 nm	$F_{613.46}$	= -566(28) $\frac{MHz}{fm^2}$
FS^{92-90}	= -172(17) MHz	NMS^{92-90}	= 64.9 MHz
MS^{92-90}	= -39.0(7.2) MHz	SMS^{92-90}	= -103.9(7.2) MHz
χ^2/D.F.	= 0.84	SMS/NMS	= -1.60(.11)

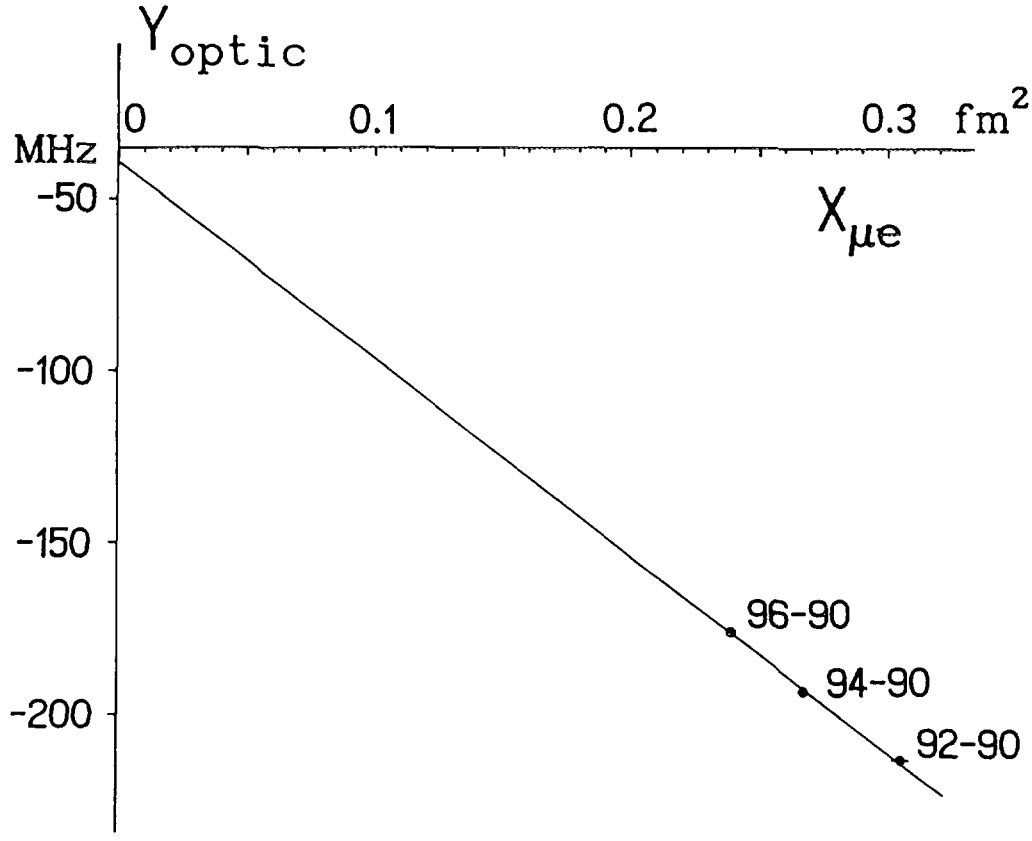

Isotope	V_2	V_4	V_6
90[e]	1.28071	1.1906	1.126
92[e]	1.28046	1.1899	1.125
94[e]	1.28031	1.1897	1.125
96	1.28010	1.1891	1.124

Isotope pair	$\delta\langle r^2\rangle_{o\mu e}$ [fm^2]	HM [%]
92-90	0.310(16)	-2.12
94-90	0.537(27)	-2.11
96-90	0.702(35)	-2.14

Note: The V values for ^{90,92,94}Zr are taken from elastic electron scattering [Ma89].
The V values for ^{96}Zr are extrapolated.

TABLE X. King Plots: Optical versus Combined Muonic and Elastic Electron Scattering Data
See page 194 for Explanation of Tables

42 MOLYBDENUM			
$R^{\mu}_{k\alpha}(96)$	= 5.6125 fm		
C_2/C_1	= $-5.07\cdot10^{-4}$ fm^{-2}		
C_3/C_1	= $1.72\cdot10^{-6}$ fm^{-4}		
λ_{proj}	= 550.6 nm	$F_{550.6nm}$	= -932(42) $\frac{MHz}{fm^2}$
FS^{96-94}	= -254(23) MHz	NMS^{96-94}	= 66.3 MHz
MS^{96-94}	= 66(12) MHz	SMS^{96-94}	= -0.4(11.5) MHz
χ^2/D.F.	= 0.55	SMS/NMS	= 0.01(.17)

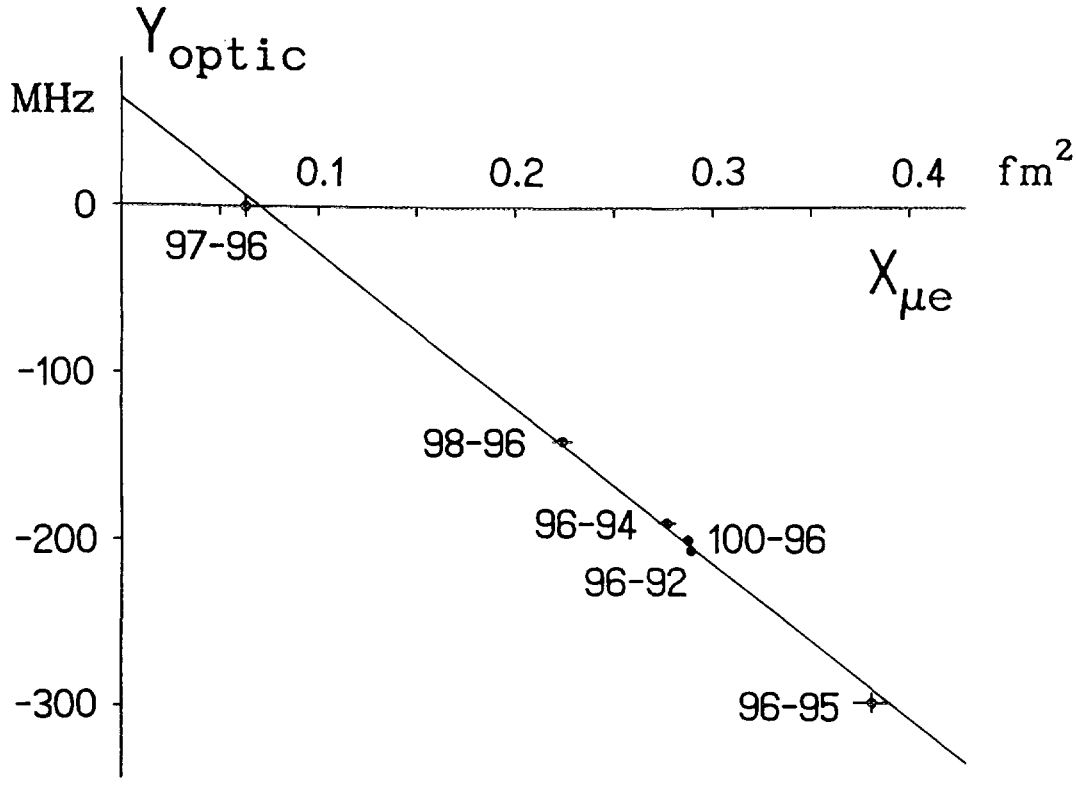

Isotope	V_2	V_4	V_6
92[e]	1.28088	1.1924	1.128
94	1.28049	1.1912	1.126
95	1.28039	1.1910	1.126
96[e]	1.28021	1.1906	1.126
97	1.28010	1.1902	1.125
98[e]	1.27994	1.1898	1.125
100	1.27971	1.1892	1.123

Isotope pair	$\delta\langle r^2\rangle_{o\mu e}$ [fm^2]	HM [%]
96-92	0.609(28)	-2.34
96-94	0.280(13)	-2.33
96-95	0.197(9)	-2.34
97-96	0.035(4)	-2.57
98-96	0.218(10)	-2.39
100-96	0.548(25)	-2.37

Note: The V values ^{92,96,98}Mo isotopes are taken from elastic electron scattering [Ma89]. The V values for the other isotopes are inter- and extrapolated.

TABLE X. King Plots: Optical versus Combined Muonic and Elastic Electron Scattering Data

See page 194 for Explanation of Tables

62 SAMARIUM			
$R^{\mu}_{k\alpha}(152)$ = 6.4891 fm	λ_{proj} = 570.68 nm	$F_{570.68nm}$ = -3860(86) $\frac{MHz}{fm^2}$	
C_2/C_1 = $-8.04\cdot10^{-4}$ fm^{-2}	$FS^{152-150}$ = -1829(80)MHz	$NMS^{152-150}$ = 25.3 MHz	
C_3/C_1 = $2.29\cdot10^{-6}$ fm^{-4}	$MS^{152-150}$ = 35(32) MHz	$SMS^{152-150}$ = 10(32) MHz	
	χ^2/D.F. = 0.88	SMS/NMS = 0.4(1.3)	

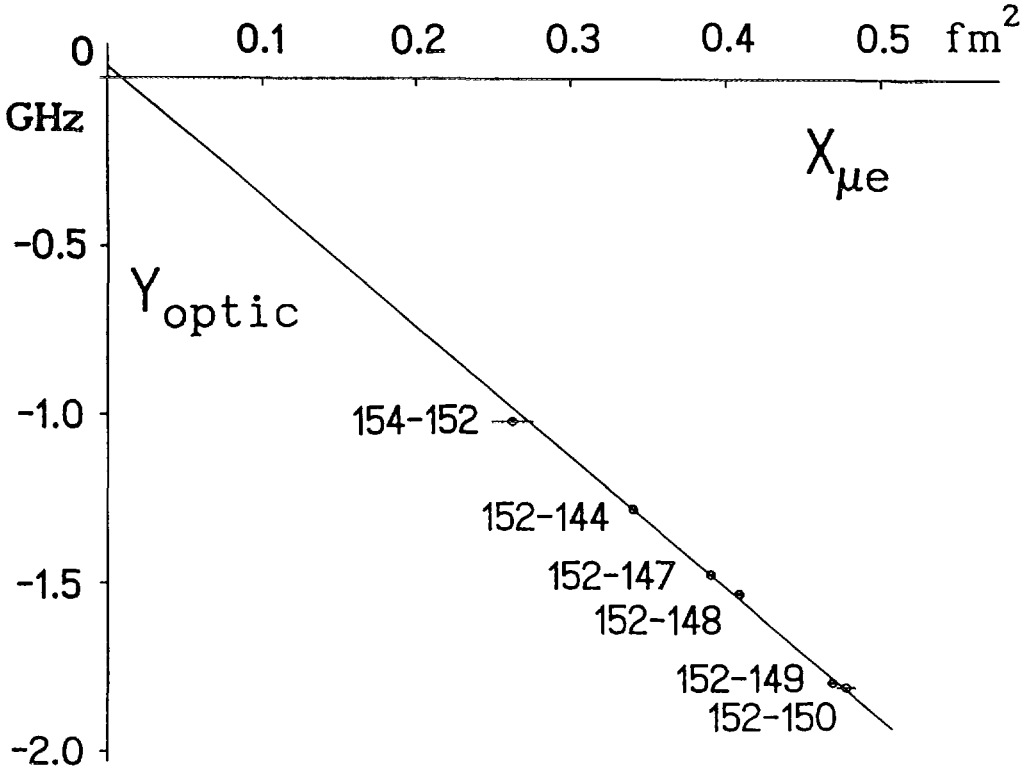

Isotope	V_2	V_4	V_6
144	1.28130	1.2049	1.152
147	1.27950	1.1997	1.143
148[e]	1.27893	1.1982	1.141
149	1.27820	1.1963	1.138
150	1.27760	1.1946	1.135
152[e]	1.27594	1.1899	1.127
154[e]	1.27549	1.1888	1.125

Isotope pair	$\delta\langle r^2\rangle_{o\mu e}$ [fm^2]	HM [%]
152-144	1.497(34)	-5.65
152-147	1.051(24)	-5.63
152-148	0.868(20)	-5.68
152-149	0.753(17)	-5.61
152-150	0.503(11)	-5.73
154-152	0.279(6)	-5.23

Note: The V values for ^{148,152,154}Sm are taken from elastic electron scattering [Vr87]. The V values for the other isotopes are inter- and extrapolated.

TABLE X. King Plots: Optical versus Combined Muonic and Elastic Electron Scattering Data

See page 194 for Explanation of Tables

64 GADOLINIUM			
$R^{\mu}_{k\alpha}(156)$ = 6.5617 fm	λ_{proj} = 575.188 nm	$F_{575.188}$ = -7.22(.75) $\frac{GHz}{fm^2}$	
C_2/C_1 = $-8.32\cdot10^{-4}$ fm^{-2}	$FS^{156-154}$ = -1.50(.30) GHz	$NMS^{156-154}$ = 23.8 MHz	
C_3/C_1 = $2.33\cdot10^{-6}$ fm^{-4}	$MS^{156-154}$ = 53(127) MHz	$SMS^{156-154}$ = 29(127) MHz	
	χ^2/D.F. = 0.98	SMS/NMS = 1.2(5.4)	

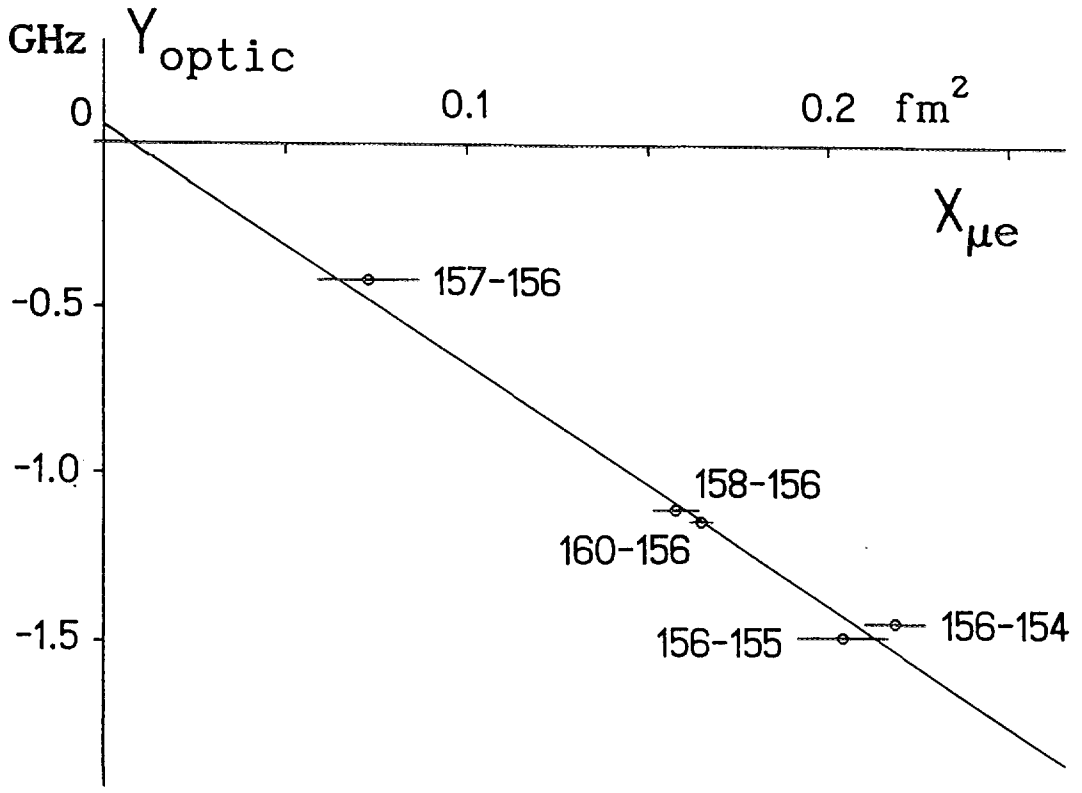

Isotope	V_2	V_4	V_6
154	1.27513	1.1884	1.125
155	1.27513	1.1884	1.125
156	1.27513	1.1884	1.125
157	1.27513	1.1884	1.125
158[e]	1.27513	1.1884	1.125
160	1.27513	1.1884	1.125

Isotope pair	$\delta\langle r^2\rangle_{o\mu e}$ [fm^2]	HM [%]
156-154	0.218(23)	-5.03
156-155	0.111(12)	-5.04
157-156	0.034(4)	-5.05
158-156	0.165(17)	-5.06
160-156	0.335(35)	-5.07

Note: The V values for ^{158}Gd are taken from elastic electron scattering [Vr87]. For the other isotopes the same V values have been used.

TABLE X. King Plots: Optical versus Combined Muonic and Elastic Electron Scattering Data

See page 194 for Explanation of Tables

82 LEAD			
$R^{\mu}_{k\alpha}(208)$ = 7.031 fm	λ_{proj} = 283.3 nm	$F_{283.3\ nm}$ = 16.5(2.5) $\frac{GHz}{fm^2}$	
C_2/C_1 = $-1.12\cdot10^{-3}$ fm^{-2}	$FS^{208-206}$ = 1.90(.51) GHz	$NMS^{208-206}$ = 27.1 MHz	
C_3/C_1 = $2.97\cdot10^{-6}$ fm^{-4}	$MS^{208-206}$ = 244(284) MHz	$SMS^{208-206}$ = 217(284) MHz	
	χ^2/D.F. = 0.00	SMS/NMS = 8(10)	

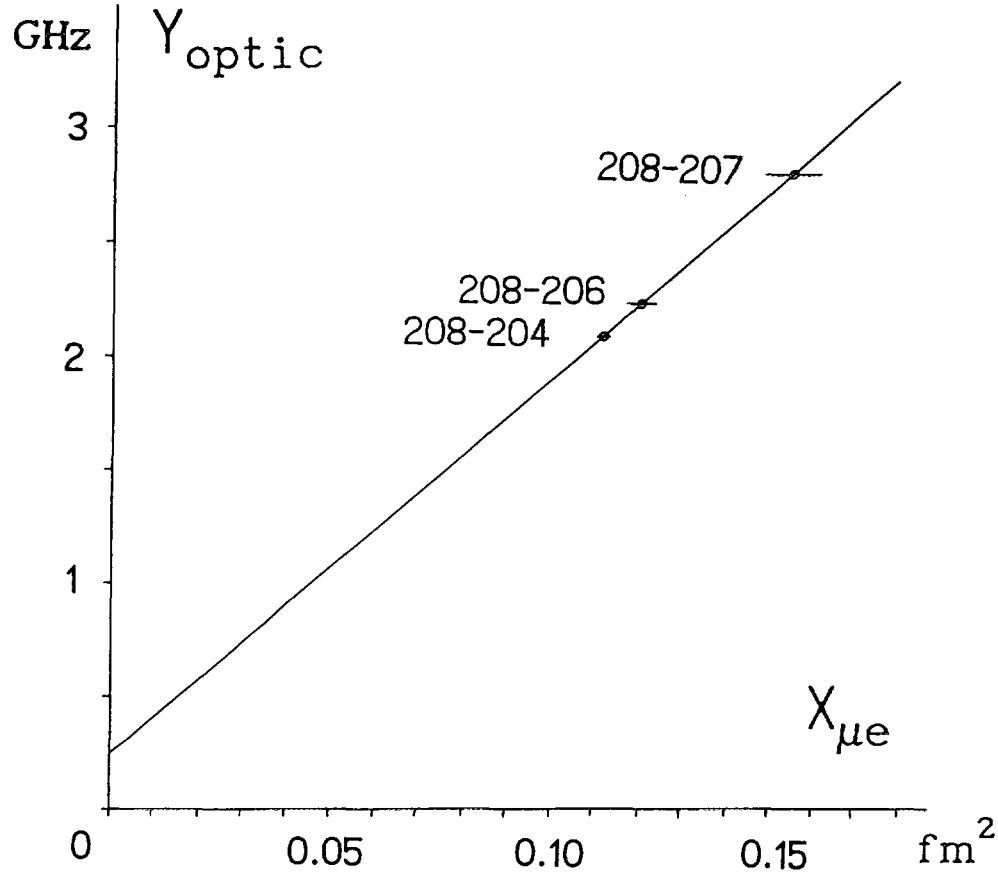

Isotope	V_2	V_4	V_6
204^e	1.27808	1.2025	1.149
206^e	1.27811	1.2027	1.150
207^e	1.27809	1.2026	1.149
208^e	1.27805	1.2026	1.149

Isotope pair	$\delta\langle r^2\rangle_{o\mu e}$ [fm^2]	HM [%]
208-204	0.240(39)	-7.55
208-206	0.128(21)	-7.91
208-207	0.080(13)	-7.89

continued

TABLE X. King Plots: Optical versus Combined Muonic and Elastic Electron Scattering Data

See page 194 for Explanation of Tables

Is.pair	$\delta\langle r^2\rangle_{o\mu e}$	Is.pair	$\delta\langle r^2\rangle_{o\mu e}$	Is.pair	$\delta\langle r^2\rangle_{o\mu e}$	Is.pair	$\delta\langle r^2\rangle_{o\mu e}$
208-196	0.65(11)	208-200	0.461(75)	208-205	0.213(35)	212-208	0.455(74)
208-197	0.65(11)	208-201	0.442(72)	209-208	0.103(17)	214-208	0.67(11)
208-198	0.560(92)	208-202	0.353(58)	210-208	0.232(38)		
208-199	0.557(91)	208-203	0.330(54)	211-208	0.329(54)		

Note: In lead the V factors for all stable have been evaluated [Ma92a] from elastic electron scattering. Taking into account their errors ($\approx 10^{-4}$) - which is in contrast to the policy of this Table X - increases the limits of error of F_i (see Table XII) by a factor of two, whereas the rms radii for lead stay unchanged. The situation for the other elements is quite different, for example in Sm (see Figs. 9 and 10).

The V values for the unstable isotopes are the average of the stable ones, namely 1.2781, 1.2026, and 1.149, respectively.

TABLE XI. Electronic Factor F and Specific to Normal Mass Shift Ratio SMS/NMS for Projected Optical Lines

See page 194 for Explanation of Tables

Element	λ [nm]	type of transition	SMS/NMS *)	F_i [GHz/fm^2] *)	calc.(MCDF)	Ref.
Ca	2·599.9	$4s^2 \rightarrow 4s5s$	-0.0409(2)	-0.0937(16)	-0.077(1)	[To85]
Kr	810.7	5s→5p	-0.08(6)	-0.438(86)		
Sr	293.2	$5s^2 \rightarrow 5s6p$	0.27(4)	-0.611(81)	-0.686(26)	[To85]
Zr	613.46	$5s^2 \rightarrow 5s5p$	-1.60(11)	-0.566(28)	-0.435(63)	[Fr93b]
Mo	550.6	5s→5p	0.01(17)	-0.932(42)	-0.93	[Fr83]
Sm	570.68	$6s^2 \rightarrow 6s6p$	0.4(13)	-3.860(86)		
Gd	575.19	$6s^2 \rightarrow 6s6p$	1.2(54)	-7.22(75)		
Pb	283.3	$6p^2 \rightarrow 6p7s$	8(10)	16.5(25)	20.6(3)	[Fr88b]

*) experimental values, taken from Table X.

TABLE XII. Root-Mean-Square Charge Radii from the Combined Analysis of Optical, Muonic, and Elastic Electron Scattering Data

See page 194 for Explanation of Tables

Isotope	$\langle r^2\rangle^{1/2}_{o\mu e}$ [fm]	$\Delta\langle r^2\rangle^{1/2}$ [am]
^{40}Ca	3.4767 (8)	0.0
^{42}Ca	3.5057 (9)	0.4
^{43}Ca	3.4928 (8)	-0.9
^{44}Ca	3.5152 (9)	0.0
^{46}Ca	3.4921 (9)	2.5
^{48}Ca	3.4736 (8)	0.2
^{78}Kr	4.2032 (12)	-0.1
^{80}Kr	4.1976 (9)	0.0
^{82}Kr	4.1921 (11)	0.2
^{83}Kr	4.1860 (14)	0.0
^{84}Kr	4.1884 (12)	-0.1
^{86}Kr	4.1839 (13)	0.0
^{84}Sr	4.2365 (13)	0.0
^{86}Sr	4.2261 (9)	-0.1
^{87}Sr	4.2190 (8)	0.1
^{88}Sr	4.2188 (8)	0.0
^{90}Zr	4.2692 (10)	0.0
^{92}Zr	4.3055 (10)	0.1
^{94}Zr	4.3314 (11)	0.1
^{96}Zr	4.3508 (12)	0.0
^{92}Mo	4.3146 (11)	0.1
^{94}Mo	4.3518 (10)	-0.1
^{95}Mo	4.3617 (9)	0.3
^{96}Mo	4.3840 (7)	0.0
^{97}Mo	4.3880 (7)	-0.4
^{98}Mo	4.4089 (10)	0.1
^{100}Mo	4.4465 (14)	0.1

Isotope	$\langle r^2\rangle^{1/2}_{o\mu e}$ [fm]	$\Delta\langle r^2\rangle^{1/2}$ [am]
^{144}Sm	4.9373 (10)	0.0
^{147}Sm	4.9824 (9)	-0.1
^{148}Sm	5.0002 (8)	-0.2
^{149}Sm	5.0129 (8)	0.1
^{150}Sm	5.0379 (9)	0.7
^{152}Sm	5.0870 (8)	-0.4
^{154}Sm	5.1143 (9)	-1.4
^{154}Gd	5.1240 (14)	-0.4
^{155}Gd	5.1353 (11)	0.2
^{156}Gd	5.1460 (9)	-0.1
^{157}Gd	5.1492 (9)	0.4
^{158}Gd	5.1618 (13)	-0.2
^{160}Gd	5.1782 (16)	0.0
^{196}Pb	5.442 (10)	
^{197}Pb	5.442 (10)	
^{198}Pb	5.450 (8)	
^{199}Pb	5.450 (8)	
^{200}Pb	5.459 (7)	
^{201}Pb	5.461 (7)	
^{202}Pb	5.469 (5)	
^{203}Pb	5.471 (5)	
^{204}Pb	5.4793 (8)	0.0
^{205}Pb	5.482 (3)	
^{206}Pb	5.4896 (7)	0.0
^{207}Pb	5.4938 (8)	0.0
^{208}Pb	5.5013 (7)	0.0
^{209}Pb	5.511 (2)	
^{210}Pb	5.523 (3)	
^{211}Pb	5.533 (5)	
^{212}Pb	5.545 (7)	
^{214}Pb	5.565 (10)	

REFERENCES FOR TABLES

[An82] A. Andl, K. Bekk, S. Göring, A. Hanser, G. Nowicki, H. Rebel, G. Schatz and R.C. Thompson
Phys. Rev. **C26** (1982) 2194

[An85] M. Anselment, S. Chongkum, S. Göring, A. Hanser, G. Meisel, H. Rebel and G. Schatz
Ann. Rep. Nucl. Phys. of KfK **3969** (1985) 63

[An86] M. Anselment, W. Faubel, S. Göring, A. Hanser, G. Meisel and G. Schatz
Nucl. Phys. **A451** (1986) 471

[An87] M. Anselment, K. Bekk, S. Chongkum, S. Göring, A. Hanser, H. Hoeffgen, W. Kälber, G. Meisel and H. Rebel
Z. Phys. **A326** (1987) 493

[As84] A. Aspect, J. Bauche, A.L.A. Fonseca, P. Grangier and G. Roger
J. Phys. **B17** (1984) 1761

[As91] A. Aspect, J. Bauche, M. Godefroid, P. Grangier, J.E. Hansen and N. Vaeck
J. Phys. **B24** (1991) 4077

[Au78] P. Aufmuth, H.P. Clieves, K. Heilig, A. Steudel, D. Wendlandt and J. Bauche
Z. Phys. **A285** (1978) 357

[Au87] P. Aufmuth, K. Heilig and A. Steudel
At. Data and Nucl. Data Tables **37** (1987) 455

[Ba72] H. Backe, R. Engfer, U. Jahnke, E. Kankeleit, R.M. Pearce, C. Petitjean, L. Schellenberg, H. Schneuwly, W.U. Schröder, H.K. Walter and A. Zehnder
Nucl. Phys. **A189** (1972) 472

[Ba81] P. Barreau, L. Roussel and R.J. Powers
Nucl. Phys. **A364** (1981) 446

[Be80] E. Bergmann, P. Bopp, Ch. Dorsch, K. Kowalski and F. Träger
Z. Physik **A294** (1980) 319

[Be88] P. Bergem, G. Piller, A. Rüetschi, L.A. Schaller, L. Schellenberg and H. Schneuwly
Phys. Rev. **C37** (1988) 2821

[Be90] C. Bernhardt, Diploma thesis
Institut für Kernphysik, **KPH 7/90** Universität Mainz 1990

[Be92] C. Bernhardt, Ph.D. thesis
Institut für Kernphysik, **KPH 6/92** Universität Mainz 1992

[Be93] C. Bernhardt, G. Fricke, C. Piller, L.A. Schaller, L. Schellenberg and E.B. Shera
private communication (Mainz/Fribourg/Los Alamos 1993)

[Bh69] S.K. Bhattacherjee, F. Boehm and P.L. Lee
Phys. Rev. **188** (1969) 1919

[Bl58] J.E. Blaise
Ann. Phys. **3** (1958) 1019

[Bo83] G.L. Borchert, O.W.B. Schult, J. Speth, P.G. Hansen, B. Jonson, H.L. Ravn and J.B. McGrory
Il Nuovo Cimento **A73** (1983) 273

[Bo88] W. Böglin, P. Egelhof, I. Sick, J.M. Cavedon, B. Frois, D. Goutte, V. Mwot, P. Leconte, X.H. Phan, S.K. Platchkov, S. Williamson and M. Girod
Nucl. Phys. **A477** (1988) 399

REFERENCES FOR TABLES continued

[Br65] R.T. Brockmeier, F. Boehm and E.N. Hatch
Phys. Rev. Lett. **15** (1965) 132

[Br79] H.W. Brandt, E. Meissner, and A. Steudel
Z. Phys. **A291** (1979) 97

[Br80] H. Brand, B. Seibert, and A. Steudel
Z. Phys. **A296** (1980) 281

[Br84] T. Brenner, S. Büttgenbach, N. Glaeser, M. Koster, H. Roeder, W. Rupprecht and F. Träber
Z. Phys. **A316** (1984) 247

[Bu85] F. Buchinger, R. Corriveau, E.B. Ramsay, D. Berdichevsky and D.W.L. Sprung
Phys. Rev. **C32** (1985) 2058

[Bu88] P. Buch, J. Nellessen, and W. Ertmer
Phys. Scr. **38** (1988) 664

[Bu89] A.J.C. Burghardt, Ph.D. thesis
University of Amsterdam 1989

[Ca90] B.D. Cannon and G.R. Janik
Phys. Rev. **A42** (1990) 397

[Ch68] R.B. Chesler and F. Boehm
Phys. Rev. **166** (1968) 1202

[Du90] S.B. Dutta, A.G. Martin, W.F. Rogers, and D.L. Clark
Phys. Rev. **C42** (1990) 1911

[Ei70a] C.W.E. Van Eijk and M.J.C. Visscher
Phys. Lett. **34B** (1970) 349

[Ei70b] C.W.E. Van Eijk and F. Schutte
Nucl. Phys. **A151** (1970) 459

[El83] E.R. Eliel, W. Hogervorst, T. Olsson and L.R. Pendrill
Z. Physik **A311** (1983) 1

[Em83] H.J. Emrich, Ph.D. thesis
Institut für Kernphysik, Universität Mainz 1983

[En74] R. Engfer, H. Schneuwly, J.L. Vuilleumier, H.K. Walter and A. Zehnder
At. Data and Nucl. Data Tables **14** (1974) 509

[En90] J.G. England, I.S. Grant, J.A.R. Griffith, D.E. Evans, D.A. Eastman, G.W.A. Newton and P.M. Walker
J. Phys. **G16** (1990) 105

[Fr82] G. Fricke, G. Mallot, H.G. Sieberling, T.Q. Phan, G. Piller, A. Rüetschi, L.A. Schaller, L. Schellenberg and H. Schneuwly
SIN Newsletter **14** (1982) 61

[Fr83] B. Fricke and G. Torbohm
private communication, Universität Kassel 1983

[Fr87] G. Fricke, T. Hack, T. Hennemann and E.B. Shera
private communication (Mainz/Los Alamos 1987)

[Fr88a] G. Fricke, T. Hack, T. Hennemann, J. Herberz, G. Mallot, L.A. Schaller and L. Schellenberg
private communication (Mainz/Fribourg 1988)

REFERENCES FOR TABLES continued

[Fr88b] B. Fricke
private communication, Universität Kassel 1988

[Fr92] G. Fricke, J. Herberz, T. Hennemann, G. Mallot, L.A. Schaller, L. Schellenberg, C. Piller and R. Jacot-Guillarmod
Phys. Rev. **C45** (1992) 80

[Fr93a] G. Fricke, C. Bernhardt, T. Hennemann, J. Herberz, G. Mallot, L.A. Schaller, L. Schellenberg and E.B. Shera
Confit, Institutsreport Kernphysik, **KPH 16/93** Universität Mainz 1993

[Fr93b] B. Fricke
private communication, Universität Kassel 1993

[Gu83] C. Günther, E.B. Shera, M.V. Hoehn, H.D. Wohlfahrt, R.J. Powers, Y. Tanaka and A.R. Kunselman
Phys. Rev. **C27** (1983) 816

[Ha67] J.E. Hansen, A. Steudel and H. Walther
Z. Phys. **203** (1967) 296

[Ha79] A.A. Hahn, J.P. Miller, R.J. Powers, A. Zehnder, A.M. Rushton, R.E. Welsh, A.R. Kunselman, P. Roberson and H.K. Walter
Nucl. Phys. **A314** (1979) 361

[Ha88] P.A. Hackett, H.D Morrison, O.L. Bourne, B. Simard, and D.M. Rayner
S. Opt. Soc. Am. **B5** (1988) 2409

[Ha89] Th. Hack, Diploma thesis
Institut für Kernphysik, **KPH 10/89** Universität Mainz 1989

[Ha92] P. Hannaford
Opt. Lett. **17** (1992) 432

[He84] T. Hennemann, Diploma thesis
Institut für Kernphysik, **KPH 2/84** Universität Mainz 1984

[He85] Th. Hennemann, G. Fricke, G. Mallot, P. Bergem, F. Bienz, N. Boschung, G. Piller, L.A. Schaller, L. Schellenberg and H. Schneuwly
SIN Newsletter **17** (1985) 31

[He86] Th. Hennemann and J. Herberz
Data [Ma83] reanalysed (Universität Mainz 1986)

[Ho81] M.V. Hoehn, E.B. Shera, H.D. Wohlfahrt, Y. Yamazaki, R.M. Steffen and R.K. Sheline
Phys. Rev. **C24** (1981) 1667

[Ho84] B. Hoffmann, G. Baur and J. Speth
Z. Phys. **A315** (1984) 57

[Ja89] J. Jansen, Diploma thesis
Institut für Kernphysik, **KPH 9/89** Universität Mainz 1989

[Ji90] W.G. Jin, H. Sakata, M. Wakasugi, T. Horiguchi and Y.Yoshizawa
Phys. Rev. **A42** (1990) 1416

[Ke75] D. Kessler, H. Mes, A.C. Thompson, H.L. Anderson, M.S. Dixit, C.K. Hargrove and R.J. McKee
Phys. Rev. **C11** (1975) 1719

REFERENCES FOR TABLES continued

[Kh88] A.A. Khomich, N.G. Shevchenko, E.O. Babichev, A.Yu. Buki, V.I. Polishchuk, B.V. Mazanko and V.P. Sergienko
Sov. J. Nucl. Phys. **47** (1988) 191

[Kh90] A.A. Khomich, N.G. Shevchenko, A.Yu. Buki, B.V. Mazan'ko, V.I. Polishchuk and Yu.N. Ranyuk
Sov. J. Nucl. Phys. **51** (1990) 17

[Kl88] R.M. Klein, Diploma thesis
Institut für Kernphysik, **KPH 8/88** Universität Mainz 1988

[Ko81] J. Konijn, W. van Doesburg, G.T. Ewan, T. Johansson and G. Tibell
Nucl. Phys. **A360** (1981) 187

[Kr85] J.R. Kropp, H.D. Kronfeldt, and R. Winkler
Z. Phys. **A321** (1985) 57

[Kr90] H.D. Kronfeldt, G. Klemz, and D.J. Weber
J. Phys. **B23** (1990) 1107

[Ku83] W. Kunold, M. Schneider, L.M. Simons, J. Wüest and R. Abela
Z. Phys. **A313** (1983) 11

[La83] D.B. Laubacher, Y. Tanaka, R.M. Steffen, E.B. Shera and M.V. Hoehn
Phys. Rev. **C27** (1983) 1772

[La86] J. Laksanaboonsong, Ph.D. thesis
University of Virginia (1986)

[La93] E. Langlois and J.-M. Gagnee
J. Opt. Soc Am. **B10** (1993) 774

[Le73] P.L. Lee and F. Boehm
Phys. Rev. **8** (1973) 819

[Lo83] C.-J. Lorenzen, K. Niemax and L.R. Pendrill
Phys. Rev. **28** (1983) 2051

[Ma83] G. Mallot, G. Fricke, L.A. Schaller and L. Schellenberg
private communication (Mainz/Fribourg 1983)

[Ma85] G. Mallot, Ph.D. thesis
Institut für Kernphysik, **KPH 1/85** Universität Mainz 1985

[Ma89] P. Mazanek, Diploma thesis
Institut für Kernphysik, **KPH 11/89** Universität Mainz 1989

[Ma92a] P. Mazanek, Ph.D. thesis
Institut für Kernphysik, **KPH 5/92** Universität Mainz 1992

[Ma92b] A.M. Mårtensson-Pendrill, A. Yunarmann, H. Warston, L. Vermeeren, R.E Silverans, A. Klein, R. Neugart, Ch. Schulz, P. Lievens and the ISOLDE - Collaboration
Phys. Rev. **A45** (1992) 4675

[Of91] E.A.J.M. Offermann, L.S. Cardman, C.W. de Jager, H. Miska, C. de Vries and H. de Vries
Phys. Rev. **C44** (1991) 1096

[Ol86] T. Olsson, L. Fraenkel, L. Lindgren, A. Nyberg, L. Robertsson and A. Rosén
Physica Scr. **34** (1986) 24

REFERENCES FOR TABLES *continued*

[Pa84] C.W.P. Palmer, P.E.G. Baird, S.A. Blundell, J.R. Brandenberger, C.J. Foot, D.N. Stacey and G.K. Woodgate
J. Phys. **B17** (1984) 2197

[Ph85] T.Q. Phan, P. Bergem, A. Rüetschi, L.A. Schaller and L. Schellenberg
Phys. Rev. **C32** (1985) 609

[Pi90] C. Piller, C. Gugler, R. Jacot-Guillarmod, L.A. Schaller, L. Schellenberg, H. Schneuwly, G. Fricke, Th. Hennemann and J. Herberz
Phys. Rev. **C42** (1990) 182

[Po68] R.J. Powers
Phys. Rev. **169** (1968) 1

[Po76] R.J. Powers, F. Boehm, P. Vogel, A. Zehnder, T. King, A.R. Kunselmann, P. Roberson, P. Martin, G.H. Miller, R.E Welsh and D.A. Jenkins
Nucl. Phys. **A262** (1976) 493

[Po77] R.J. Powers, F. Boehm, A. Zehnder, A.R. Kunselman and P. Roberson
Nucl. Phys. **A278** (1977) 477

[Po79] R.J. Powers, P. Barreau, B. Bihoreau, J. Miller, J. Morgenstern, J. Picard and L. Roussel
Nucl. Phys. **A316** (1979) 295

[Re87] M. Reutter, Diploma thesis
Institut für Kernphysik, **KPH 6/87** Universität Mainz 1987

[Ri76] G.A. Rinker
L.A.N.L., Los Alamos, NM, private communication 1976

[Ri78] G.A. Rinker and J. Speth
Nucl. Phys. **A306** (1978) 397

[Ru84a] W. Ruckstuhl, B. Aas, W. Beer, I. Beltrami, K. Bos, P.F.A. Goudsmit, H.J. Leisi, G. Strassner, A. Vacchi, F.W.N. de Boer, U. Kiebele and R. Weber
Nucl. Phys. **A430** (1984) 685

[Ru84b] A. Rüetschi, L. Schellenberg, T.Q. Phan, G. Piller, L.A. Schaller, and H. Schneuwly
Nucl. Phys. **A422** (1984) 461

[Ry72] A.S. Rylnikov, A.I. Egorov, G.A. Ivanov, V.I. Marushenko, A.F. Mezentsev A.I. Smirnov, O.I. Sumbaev and V.V. Fyodorov
Zh. Eksp. Teor. Fiz. **63** (1972) 53

[Sc80a] L.A. Schaller, L. Schellenberg, A. Ruetschi and H. Schneuwly
Nucl. Phys. **A343** (1980) 333

[Sc80b] L. Schellenberg, B. Robert-Tissot, K. Käser, L.A. Schaller, H. Schneuwly, G. Fricke, S. Glückert, G. Mallot and E.B. Shera
Nucl. Phys. **A333** (1980) 333

[Sc82] L.A. Schaller, L. Schellenberg, T.Q. Phan, G. Piller, A. Rüetschi and H. Schneuwly
Nucl. Phys. **A379** (1982) 523

[Sc85] L.A. Schaller, D.A. Barandao, P. Bergem, M. Boschung, T.Q. Phan, G. Piller, A. Rüetschi, L. Schellenberg, H. Schneuwly, G. Fricke, G. Mallot and H.G. Sieberling
Phys. Rev. **C31** (1985) 1007

REFERENCES FOR TABLES continued

[Se69] E.C. Seltzer
Phys. Rev. **188** (1969) 1916

[Sh76] E.B. Shera, E.T. Ritter, R.B. Perkins, G.A. Rinker, L.K. Wagner, H.D. Wohlfahrt, G. Fricke and R.M. Steffen
Phys. Rev. **C14** (1976) 731

[Sh82] E.B. Shera, H.D. Wohlfahrt, M.V. Hoehn and Y. Tanaka
Phys. Lett. **B112** (1982) 124

[Sh89] E.B. Shera, M.V. Hoehn, G. Fricke and G. Mallot
Phys. Rev. **C39** (1989) 195

[Si82a] H.G. Sieberling, Diploma thesis
Institut für Kernphysik, **KPH 16/82** Universität Mainz 1982

[Si82b] H.G. Sieberling, G. Fricke, L.A. Schaller and L. Schellenberg
private communication (Mainz/Fribourg 1982)

[So88] R. Soundranayagam, A. Saha, K.K. Seth, C.W. de Jager, H. de Vries, H. Blok and G. van der Steenhoven
Phys. Lett. **B212** (1988) 13

[St52] A. Steudel
Z. Phys. **133** (1952) 438

[Su67] O.I. Sumbaev, Symposium on Nuclear Structure, Dubna 1968
IAEA, Vienna, 1968, p.527
O.I. Sumbaev, E.V. Petrovich, V.S. Sykor, A.S. Rylnikov and A.I. Grushko
Sov. J. Nucl. Phys. **5** (1967) 387

[Su69] O.I. Sumbaev, A.F. Mezentsev, V.I. Marushenko, A.S. Rylnikov, G.A. Ivanov and A.I. Egorov
Int. Conf. Prop. Nucl. States, Montreal, Canada, 1969 (Contrib. 2.67)

[Ta84a] Y. Tanaka, R.M. Steffen, E.B. Shera, W. Reuter, M.V. Hoehn and J.D. Zumbro
Phys. Rev. **C29** (1984) 1830

[Ta84b] Y. Tanaka, R.M. Steffen, E.B. Shera, W. Reuter, M.V. Hoehn and J.D. Zumbro
Phys. Rev. **C29** (1984) 1897

[Ta84c] Y. Tanaka, R.M. Steffen, E.B. Shera, W. Reuter, M.V. Hoehn and J.D. Zumbro
Phys. Rev. **C30** (1984) 350

[Th83] R.C. Thompson, M. Anselment, K. Bekk, S. Göring, A. Hanser, G. Meisel, H. Rebel, G. Schatz and B.A. Brown
J. Phys. **G9** (1983) 443

[To85] G. Torbohm, B. Fricke and A. Rosén
Phys. Rev. **A31** (1985) 2038

[Vr87] H. de Vries, C.W. de Jager and C. de Vries
ATOMIC DATA AND NUCLEAR DATA TABLES **36** (1987) 495

[Vr88] J.W. de Vries, D. Doornhof, C.W. de Jager, R.P. Singhal, S. Salem, G.A. Peterson and R.S. Hicks
Phys. Lett. **B205** (1988) 22

REFERENCES FOR TABLES continued

[Wa90] M. Wakasugi, T. Horiguchi, W.G. Jin, H. Sakata and Y. Yoshizawa
J. Phys. Soc. Japan **59** (1990) 2700

[We93] J. Wesseling, C.W. de Jager, L. Lapikas, H. de Vries, M.N. Harakeh, N. Kalantar-Nayestanaki, L.W. Fagg, R.A. Lindgren, E. Moya De Guerra and P. Sarriguren
to be published

[Wo81] H.D. Wohlfahrt, E.B. Shera, M.V. Hoehn, Y. Yamazaki and R.M. Steffen
Phys. Rev. **C23** (1981) 533

[Ya78] Y. Yamazaki, E.B. Shera, M.V. Hoehn and R.M. Steffen
Phys. Rev. **C18** (1978) 1474

[Ze75] A. Zehnder, F. Boehm, W. Dey, R. Engfer, H.K. Walter and J.L. Vuilleumier
Nucl. Phys. **A254** (1975) 315

[Zu84] J.D. Zumbro, R.A. Naumann, M.V. Hoehn, W. Reuter, E.B. Shera, C.E. Bemis Jr. and Y. Tanaka
Phys. Rev. Lett. **20** (1984) 1888

[Zu86] J.D. Zumbro, R.A. Naumann, M.V. Hoehn, W. Reuter, E.B. Shera, C.E. Bemis Jr. and Y. Tanaka
Phys. Lett. **167B** (1986) 383